

**STUDY OF HUMAN BRAIN
METABOLITES USING MAGNETIC
RESONANCE SPECTROSCOPY
METHODS AT 7 TESLA**

Dissertation

zur Erlangung des akademischen Grades

doctor rerum naturalium

(Dr. rer. nat.)

genehmigt durch die Fakultät für Naturwissenschaften
der Otto-von-Guericke-Universität Magdeburg

von **M.Sc. Mohammed Abdelsalam Mohammed Elywa**

geb. am 27.03.1973 in Sharkia Ägypten

Gutachter: **Prof. Dr. Oliver Speck**

Gutachter: **Prof. Dr. Ewald Moser**

eingereicht am: 24.11.2011

verteidigt am: 11.04.2012

Acknowledgement

I would like to express my profound gratitude and sincere appreciation to Prof. Dr. Oliver Speck for his inspiration, indispensable guidance and for teaching me invaluable knowledge throughout the course of my study. With his initial support, this great dream can finally turn to reality, and with his unending guidance throughout the study, I was able to navigate the arduous path down to the very end. I am sure that whatever I have learned while working with him will be very useful in my future endeavors. He has been a great mentor.

My deep thanks to my wife and my children.

I am very thankful to all members in the biomedical magnetic resonance (BMMR) group. I would also like to express my gratitude to Dr. Samir mulla Osmain. Also, my deep thanks to Dr. F. Godenschweger, Dr. Med. M. Walter, Dr. J. Kaufmann, Dr. K. Zhong, Myung-Ho In, R. Yakupov and O. Khorkhordin for their help.

I thank very much the Axel Springer Foundation for helping me to finish this Thesis.

I am deeply indebted to my country EGYPT for accepting and supporting me to do my Ph.D. in Germany.

M.Sc. Mohammed Elywa

Contents

Acknowledgement	II
List of Contents	VI
Abbreviations	VII
Summary	IX
Zusammenfassung	XI
1 Introduction	1
2 Magnetic Resonance Spectroscopy	4
2.1 1H -MR Spectroscopy Phenomenon	4
2.2 Macroscopic Rotational Angular Momentum	4
2.3 Microscopic Rotational Angular Momentum	5
2.3.1 Spin Angular Momentum	6
2.3.2 Nuclear Spin Quantum Number I	6
2.3.3 Nuclear State Splitting	6
2.3.4 Nuclear Magnetic Momentum μ	6
2.4 Magnetization Vector	7
2.5 Larmor Frequency	7
2.6 Relaxation Times T_1 , T_2 and T_2^*	9
2.7 Sequence Times TR, TE and Received Signal	11
2.7.1 Repetition Time (TR)	11
2.7.2 Received Signal	12
2.7.3 Echo Time (TE)	12

2.8	Chemical Shift	12
2.8.1	Chemical Shift Displacement	14
2.8.2	J-Coupling	15
2.8.3	Multiplicity (m)	16
2.9	Localized Spectroscopy and MRS Techniques	16
2.10	DATA Processing in Frequency Domain	17
2.10.1	Eddy Current Correction(ECC)	18
2.10.2	Fourier Transformation	18
2.10.3	Baseline Correction	18
2.10.4	Phase Correction	18
2.10.5	Curve Fitting	19
3	Materials and Methods	20
3.1	Experimental Set Up	20
3.2	Materials	21
3.2.1	Preparation of the Model Solutions	22
3.2.2	Reference Peaks	22
3.2.3	Compatibility Requirement	23
3.3	Human Subjects	23
3.4	Methods	23
3.4.1	Acquiring the Basis Spectra	24
3.4.2	Introduction to LCMgui and Makebasis.in File	24
3.5	Shimming	24
3.6	Water Suppression	25
3.7	RF Pulse Sequences	25
3.8	PRESS, STEAM, and VERSE	28
3.8.1	Point Resolved Spectroscopy (PRESS)	28
3.8.2	Stimulated Echo Acquisition Mode (STEAM)	28
3.8.3	Variable Rate Selective Excitation (VERSE)	29
3.9	Simulation Database	30
3.10	Instruments	32
3.10.1	Magnet System	32

3.10.2	Gradient System	32
3.10.3	Shimming Coil	33
3.10.4	Single Volume Coil	33
3.10.4.1	CP Coil	34
3.10.5	24 Channels Volume Coil)	34
4	Results	36
4.1	<i>RF</i> -Flip Angle Optimization at 3T and 7T	36
4.2	Comparison between STEAM and STEAM with VERSE Pulses	40
4.3	Database Spectra Measured at 7T	43
4.4	Comparison between Measured and Simulated Glutamate Spectrum	43
4.5	Comparison between Experimental and Simulated Basis Sets	44
4.6	Human Acquisition Time Optimization	50
4.7	Analysis of Human Brain Data using Short and Long TE Database	50
4.8	Comparison between the 3T and 7T Human Spectra	52
4.8.1	Using PRESS at 3T and STEAM with VERSE Pulses at 7T	52
4.8.2	Using STEAM with VERSE Pulses at 7T and JPRESS at 3T	55
4.9	Human Brain Spectra Measured in Five Different Locations	56
4.9.1	Parietal Region	57
4.9.2	Pregenual Anterior Cingulate Cortex (pgACC)	57
4.9.2.1	NAAG Detection using Simulated Database with Long TE	62
4.9.3	Posterior Cingulate Cortex (PCC)	64
4.9.4	Anterior Middle Cingulate Cortex (AMCC)	66
4.9.5	Brodmann 23C region (23C)	68
4.10	Human Brain Metabolites Correlation	70
4.10.1	Grey Matter and Glutamine Concentrations Correlation	70
4.10.2	Gln and Glu Correlation using Short and Long TE	70
4.11	Fifteen Human Brain Metabolites Detection in the Different Brain Areas	71
4.11.1	Metabolites Detection in WM and GM using TE = 20 ms	73
4.11.2	Human Brain Metabolites Detected in GM using Short and Long TE	73

5	Discussion	74
5.1	Optimization of 90° Flip Angle	74
5.2	Reduction of the Applied Voltage of 90° Flip Angle	75
5.3	SNR Increase at 7T Compared to 3T	75
5.4	GABA, Gln and Glu Quantification using Short <i>TE</i> at 7T	76
5.5	Comparison between GM pgACC and WM Parietal Regions	77
5.6	Human Brain Metabolites Quantification	77
6	Conclusions	79
	Appendix	80
A		81
B		92
C		95
	Bibliography	97
	List of Tables	108
	List of Figures	117
	Erklärung	118
	Curriculum Vitae	119
	List of Publications	120

Abbreviations

<i>Subscript</i>	<i>Meaning</i>	<i>Subscript</i>	<i>Meaning</i>
1H	Hydrogen proton	<i>Ala</i>	L-Alanine
<i>ADC</i>	Analog digital convertor	<i>Act</i>	Acetate
N_H	Number of protons	<i>Asp</i>	Aspartate
<i>CHESS</i>	Chemical shift suppression	<i>Cit</i>	Citrate
<i>CP</i>	Circular polarization	<i>Cr</i>	Creatine
<i>CSI</i>	Chemical shift imaging	<i>GABA</i>	γ -Aminobutric acid
<i>FID</i>	Free induction decay	<i>Glc</i>	Glucose
LCModel	Linear combination model	<i>Gln</i>	L-Glutamine
<i>MR</i>	Magnetic resonance	<i>Glu</i>	Glutamate
<i>MRI</i>	Magnetic resonance imaging	<i>Gly</i>	Glycine
<i>MRS</i>	Magnetic resonance spectroscopy	<i>GPC</i>	Glycerophosphocholine
<i>NMR</i>	Nuclear magnetic resonance	<i>GSH</i>	Glutathione
<i>OVS</i>	Outer volume suppression	<i>Ins</i>	myo-Inositol
<i>PRESS</i>	Point resolved spectroscopy	<i>Lac</i>	L-Lactate
<i>RF</i>	Radiofrequency	<i>NAA</i>	N-acetylaspartate
<i>ROI</i>	Region of interest	<i>PCh</i>	Phosphocholine
<i>SE</i>	Spin echoes	<i>PCr</i>	Phosphocreatine
<i>SNR</i>	Signal to noise ratio	<i>PE</i>	Phosphorylethanolamine
<i>STEAM</i>	Stimulated echo acquisition mode	<i>Suc</i>	Succinate
<i>STE</i>	Stimulated echo	<i>Tau</i>	Taurine
<i>SVS</i>	Single volume spectroscopy	<i>HCOONa</i>	Sodium Formate
<i>WS</i>	Water suppression	<i>KH2PO4</i>	Monopotassium phosphate
<i>TMSP</i>	Trimethylsilyl propionate	<i>K2HPO4</i>	Dipotassium phosphate
<i>VERSE</i>	Variable rate selective excitation	<i>VOI</i>	Volume of interest
<i>FFT</i>	Fast Fourier transform	<i>1D</i>	One dimension
M_0	Net magnetization	<i>ACC</i>	Anterior cingulate cortex
<i>pgACC</i>	Pregenual anterior cingulate cortex		
<i>AMCC</i>	Anterior middle cingulate cortex		

<i>Symbol</i>	<i>Meaning</i>	<i>Symbol</i>	<i>Meaning</i>
$\gamma/2\pi$	Gyromagnetic ratio	I	Spin quantum number
h	Planck's constant	T	Absolute temperature
ν	Linear frequency	m	Multiplicity
G_i	Magnetic field gradient	BW	Band width
T_1	Longitudinal relaxation time	B_0	Magnetic field strength
ω_0	Larmor frequency	T_2	Transverse relaxation time
μ_0	Permeability of free space	B_1	RF magnetic field intensity
K	Boltzmann's constant	σ	Electrons shield constant
δ	Chemical shift	Δx	Spatial displacement
B_i	Induced magnetic field	V_i	Localized volume of interest
μ	Nuclear magnetic moment	$\Delta\nu$	RF bandwidth
μ_r	Relative permeability	χ_v	Bulk magnetic susceptibility
μ_m	Permeability of material	$\Delta\omega$	Spectral bandwidth
M	Magnetization vector	TR	Repetition time
L_t	Total angular momentum	S	Spin angular momentum
TM	Mixing time	TE	Echo time

Summary

Over the last decades, proton magnetic resonance spectroscopy (1H -MRS) has been used in several studies in order to detect human brain metabolites. The signal to noise ratio (SNR) and spectral resolution are important quality measurements of MRS. Therefore, many MR spectroscopy techniques have been proposed to achieve improvements. One of the major localization techniques is single volume spectroscopy (SVS) which employs pulse sequences based on spin echoes (PRESS) or stimulated echoes (STEAM). It was shown that low magnetic field strengths leads to peak overlaps of human brain metabolites such as Glutamate with Glutamine and NAA with NAAG. Moreover, at high field strength the limited available RF transmitter power causes difficulty in achieving a true 90° excitation or 180° refocusing flip angle in standard sequences such as STEAM or PRESS.

In this work, a 24 channel volume coil has been used to acquire spectra from deep brain areas. To reduce the required RF peak power and to decrease the pulse duration to be available for human studies, variable-rate selective excitation (VERSE) has been applied to the standard spectroscopy RF sequence (STEAM).

The aim of this thesis was to establish a proton magnetic resonance spectroscopy method to obtain accurate quantification of in vivo metabolites such as Gln, GABA and NAAG, which will benefit from the increased sensitivity at ultra high magnetic field strength (7 Tesla). This 1H -MRS method should be used to investigate human brain metabolites in deep human brain regions.

For this project an adapted MRS sequence for 7T (STEAM with VERSE) was developed. Twenty metabolite solutions had been prepared and then measured at 7T. These build an experimental basis set for metabolite quantification. Moreover, a simulated basis set was calculated using NMR-SIM software and compared to the

experimental results.

The results show for the first time the detection and quantification of fifteen human brain metabolites in deep brain regions such as the pregenual anterior cingulate cortex (pgACC), anterior middle cingulate cortex (AMCC), posterior cingulate cortex (PCC) and Brodmann area 23 C.

Finally, we have succeeded to measure Gln, GABA and NAAG levels by using 1H -MRS at 7T, which could not be separated at lower field strengths using standard MRS sequences (STEAM or PRESS). It is tempting to conclude that separating Gln and Glu may be useful for patients who suffer from major depressive disorder (MDD).

Zusammenfassung

Magnetresonanzspektroskopie an Wasserstoffkernen (1H -MRS) ist in den letzten Jahrzehnten von vielen Arbeitsgruppen zur Erforschung verschiedener Erkrankungen eingesetzt worden. Als wichtige Qualitätskriterien einer 1H -MRS sind die Messung des Signal-zu-Rausch-Verhältnisses (SNR) und der spektralen Auflösung dokumentiert.

Dafür wird üblicherweise Single-Voxel-Spektroskopie (SVS) mit Pulssequenzen, die auf Spin Echos (PRESS) oder auf stimulierten Echos (STEAM) basieren, benutzt. Es wurde bereits gezeigt, dass es bei niedrigeren Feldstärken als 7T zu Überlappungen (im gemessenen Spektrum) der im menschlichen Hirn vorhandenen Metaboliten, wie z.B. Glu mit Gln oder NAA mit NAAG, kommen kann. Andererseits führt die bei 7T vorhandene B_1 Inhomogenität und die (durch SAR-Grenzen) eingeschränkte verfügbare Senderleistung zu großen Schwierigkeiten bezüglich des Erreichens eines genauen 90° Hochfrequenz-Sendepulses mittels der bisher als Standard verwendeten PRESS und STEAM Sequenzen. Verschiedene frühere Studien konnten zeigen, dass die Erhöhung der magnetischen Feldstärke vorteilhaft für die Separation der Metaboliten im gemessenen Spektrum der 1H -MRS ist. Ebenso konnte ein höheres SNR und gleichzeitig eine höhere Sensitivität im Vergleich zu niedrigeren Feldstärken nachgewiesen werden.

Bei den vorangehenden Hochfeld-MRS-Studien wurden Oberflächenspulen verwendet; dadurch konnten tiefere Hirnregionen nicht untersucht werden. In dieser Arbeit wurde für die Erfassung von Spektren tieferer Hirnareale mittels 1H -MRS eine 24-Kanal-Spule verwendet. Weiterhin wurde zur Reduzierung der benötigten HF-Sendeleistung und damit zur Verkürzung der Pulsdauer "Variable-Rate-Selective-Excitation" (VERSE) in der Standardsequenz für Spektroskopie, STEAM, implementiert. Ein Ziel dieser Arbeit ist die genaue

Mengenbestimmung von Metaboliten wie Gln, GABA und NAAG *in vivo* unter Nutzbarmachung der höheren Sensitivität bei Ultra-Hochfeld-MRS (7 Tesla). Außerdem erfolgt in dieser Arbeit die Untersuchung einer tieferen Hirnregion (nahe dem Corpus Callosum) unter Verwendung einer 24-Kanal-Spule. Dafür wurde ebenfalls die speziell für Ultra-Hochfeld-MRS modifizierte Sequenz (STEAM mit VERSE) benutzt. Insgesamt zwanzig Proben von Metaboliten des menschlichen Hirns wurden vorbereitet und an einem 7 Tesla Magnetresonanztomografen vermessen. Basissätze von Spektren wurden experimentell erhoben und verarbeitet. Weiterhin wurden zwanzig Spektren-Datensätze mittels NMR-SIM simuliert.

Die Resultate zeigen erstmalig die Erkennung von 15 verschiedenen Hirn-Metaboliten in tieferen Hirnregionen (anterior cingulate cortex (pgACC), anterior middle cingulate cortex (AMCC), posterior cingulate cortex (PCC) and Brofmann area 23 C). Die Konzentration dieser Metaboliten wurde mittels LCModel Basissets (experimentell und simuliert, kurze und lange Echozeiten) für 7T bestimmt. Schlussendlich konnten die Anteile von Gln, GABA und NAAG mittels 1H -MRS bei 7T erfolgreich bestimmt werden. Dies war bisher bei niedrigeren Feldstärken nicht möglich. Die durch die Separation von Gln und Glu bei Ultra-Hochfeld-MRS entstehenden Möglichkeiten der Untersuchung von Patienten, die an Depressionen (Major Depressive Disorder, MDD) leiden, erscheinen viel versprechend.

Chapter 1

Introduction

Proton magnetic resonance spectroscopy 1H -MRS is an effective way to study the human brain metabolites non-invasively and provides markers for specific diseases [1, 2]. Signal to noise ratio, spatial and spectral resolution as well as scan time are some of the important quality measurements of MRS. Several localization methods have been proposed. Single volume spectroscopy (*SVS*) localization techniques use pulse sequences based on spin echoes (PRESS) [3] or stimulated echoes (STEAM) [4] and provide the highest spectral quality with limited spatial information. Lower magnetic field strengths result in peak overlap of the human brain metabolites, such as Glu with Gln and NAA with NAAG. Besides, standard spectroscopic sequences such as STEAM or PRESS will suffer if limited transmitter voltage is available. This results in a reduced excitation flip angle and consequently inefficient excitation in the volume of interest (VOI). Moreover, previous studies have investigated that an increase in the magnetic field strength increases the 1H -MR spectral peak separation, signal to noise ratio (SNR) and thus provides higher sensitivity compared with lower field strengths [5, 6, 7, 8, 9, 10, 11]. With standard *RF* amplifiers and volume *RF* coils at 7T, short 180° refocusing pulses are difficult to achieve in most parts of the brain. Earlier high field MRS studies, therefore, frequently employed surface coils with locally higher B_1 field amplitude [12, 13]. However, not all brain areas can be adequately examined using surface coils. As the goal of this study was to examine the deeper areas of the human brain, the STEAM volume selection principle has been applied. The 90° -pulses require only half the peak power of the 180° -pulses in PRESS. Moreover, STEAM with

short echo times benefits from reduced signal decay due to J-evolution of the coupled spin system, thus allowing a more precise quantification of the metabolites, especially with short T_2 relaxation time [14]. Short echo times have been used in several studies [15, 16, 17, 18] as well as in this work, TE was selected to be 20 ms. Earlier studies that had employed STEAM with ultra short echo times were again limited by the surface coils which prevented detection in the deep brain regions. TEs down to 6 ms were possible and the metabolites were resolved better at 7T than at 3T [14]. A quadrature (transmit/receive) surface RF coil or a half-volume RF coil have been used for these studies [19, 20].

In this thesis, a 24-channel volume coil has been used to acquire spectra from deep brain areas. To reduce the required RF peak power and decrease the pulse duration, variable-rate selective excitation (VERSE) [21] had been applied into the standard spectroscopy RF sequence (STEAM) [22]. Therefore, the aim of this thesis was to establish a proton magnetic resonance spectroscopic method to obtain an accurate quantification of *in vivo* metabolites such as Gln, GABA and NAAG, which will benefit from the increased sensitivity at ultra high magnetic field strength (7 Tesla). After that, this 1H -MRS method will be used to investigate human brain metabolites in deep human brain regions, around the corpus callosum using a 24-channel volume coil. Throughout this project an adapted MRS sequence especially suited for 7T application (STEAM with VERSE) was used. Twenty human brain metabolite solutions had been prepared and then measured at 7T. The spectra of the experimental basis set were acquired and processed. Twenty spectra have been simulated using *NMR – SIM* software. Our results show for the first time the detection of 15 human brain metabolites in the deep parts of the brain (pgACC, AMCC, PCC and Brodmann 23 C region). At the same time, the concentration of these brain metabolites was calculated using the LCModel basis sets (experimental and simulated, using short and long echo times) at 7T. This method proved to be successful to measure Gln, GABA and NAAG levels by using 1H -MRS at 7T, which could not be earlier separated at lower field strengths. It, therefore, becomes tempting to conclude that separating Gln and Glu can be helpful, especially when scanning patients suffering with Major Depressive Disorder (MDD) [23, 24].

This was achieved by following five stages of investigations; selection and

optimization of the sequence parameters resulting in high spectral resolution spectra, measurement of 20 human brain metabolite solutions using short and long echo times, simulation of the same 20 metabolite spectra using the *NMR-SIM* program, creation of experimental and simulated basis sets using 20 *in vitro* spectra and 20 simulated spectra respectively, creation of LCModel basis sets which were used in the analysis of the acquired human spectra.

More than 80 human brain spectra from 30 healthy subjects (age 23-35 years) were measured in 5 brain regions at 7T. Further, the metabolite concentrations have been quantified by the LCModel program.

Chapter 2

Magnetic Resonance Spectroscopy

In this chapter, the following sections will be explained in detail: 1H -MR spectroscopy phenomenon, spin quantum numbers, magnetization vector, Larmor frequency, relaxation times T_1 , T_2 and T_2^* , chemical shift, localized spectroscopy, MRS techniques and MRS data analysis in frequency domains.

2.1 1H -MR Spectroscopy Phenomenon

Proton magnetic resonance spectroscopy (1H -MRS) is a non-invasive tool used to investigate human brain metabolites from brain structures [25]. The phenomenon of 1H -MRS can be described as follows: when the proton of hydrogen atom (1H) is exposed to an external magnetic field B_0 , certain amount of energy is absorbed. This absorbed energy is released as electromagnetic waves at a resonant frequency (Larmor frequency) in the range of radiofrequency waves [26].

2.2 Macroscopic Rotational Angular Momentum

Any rotating particle possesses a rotational angular momentum. The orientation of it can be described by the right hand rule, where, if the fingers wrap in the direction of the rotation, the thumb points along the angular momentum orientation [27].

2.3 Microscopic Rotational Angular Momentum

Atoms have been documented to consist of subatomic particles like electrons, protons and neutrons which are always rotating [28]. In quantum mechanics, their angular momenta are quantized. Moreover, a rotating molecule (e.g, H₂O) has several stable rotational states denoted by (J). The total angular momentum (L_t) can be calculated by the following Equation [27].

$$L_t = \sqrt{J(J+1)}\hbar \quad (2.1)$$

where $J = 0, 1, 2, \dots$ and $\hbar = 1.054 \times 10^{-34}$ J s (the reduced Planck constant, $h/2\pi$).

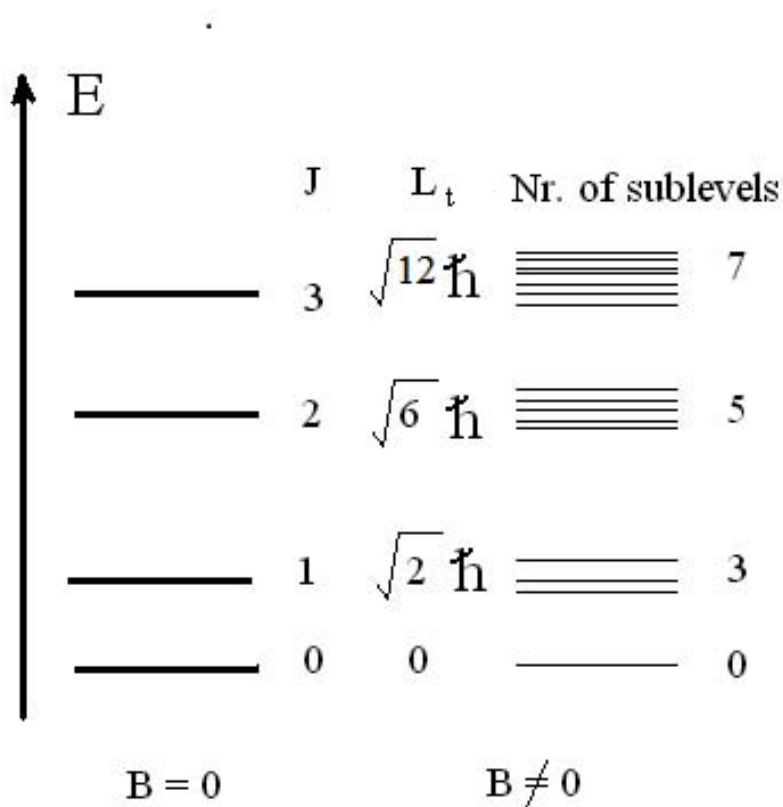


Figure 2.1: The rotational energy states of a molecule such as H₂O in the absence of magnetic field and on applying it.

As seen in Fig. 2.1, the molecule can be in a stable energy state i.e., with total angular momentum $L_t = 0$ or $\sqrt{2}\hbar$, or $\sqrt{6}\hbar$, etc. Further information on molecule rotation is given by the quantum number (M_J) where, $M_J = 2J + 1$ integer values. Moreover, M_J sometimes refers to the number of sublevels.

2.3.1 Spin Angular Momentum

The electron of the hydrogen atom has two motions; a circulating motion around the nucleus (angular momentum, L) and an intrinsic motion (spin angular momentum, S). Particles with spin S have $(2S + 1)$ sublevels on applying an external magnetic field [26].

2.3.2 Nuclear Spin Quantum Number I

Spin is an intrinsic property of the particle itself. It is also a form of angular momentum. The nuclear spin quantum number (I) of any given nucleus depends on the proton number Z and neutron number N . Nuclei whose Z and N are even-even numbers, have a nuclear spin quantum number $I = 0$ and they are inactive in NMR spectroscopy. The elements whose Z and N are even-odd or odd-even numbers, have nuclear spin quantum numbers I , with the values ($I = 1/2, 3/2, \dots$). Add to this, the nuclei whose Z and N are odd-odd numbers ($I = 1, 2, 3, \dots$).

The spin of a system, therefore, consists of two particles and is a combination of their spin i.e., $I = (I_1 - I_2)$ or $(I_1 + I_2)$. If $I_1 = 1/2$ and $I_2 = 1/2$, $I = 0$ (antiparallel spin orientations, high energy state) and $I = 1$ (parallel spin orientations, low energy state) [29].

2.3.3 Nuclear State Splitting

Consider a nucleus of spin I , with $(2I + 1)$ energy states. These states have the same energy in the absence of an external magnetic field (the degeneracy case). As seen in Fig. 2.1 the magnetic field breaks the degeneracy to $2I + 1$ sublevels. This process is called nuclear Zeeman splitting [30].

2.3.4 Nuclear Magnetic Momentum μ

The motion of a proton around its rotational axis generates a magnetic moment μ , which depends upon spin angular momentum S , along the axis of rotation [29]. The

relation between these quantities is explained by the following Equation.

$$\vec{\mu} = \gamma \vec{S} \quad (2.2)$$

2.4 Magnetization Vector

The vector of summation of the magnetic momentums is nonzero when an external magnetic field is applied. Moreover, the orientation of this vector points parallel to the field direction, as seen in Fig. 2.2. In other words, the tissue gets polarized or magnetized in the presence of the external magnetic field with a value of net magnetization (M_0). At equilibrium, the spins are in the stable state. Moreover, Equation 2.3 indicates that the magnitude of M_0 is proportional to the magnetic field strength B_0 [31].

$$\vec{M}_0 = \chi_v \vec{B}_0 \quad (2.3)$$

where M_0 is the net magnetization vector of the material (the magnetic dipole moment per unit volume) and is measured in amperes per meter. B_0 is the magnetic field intensity measured in Tesla while χ_v is the volume magnetic susceptibility (no unit) and $\chi_v = \mu_r - 1$, where, $\mu_r = \frac{\mu_m}{\mu_0}$ (relative permeability, the ratio between the permeability of material (μ_m) to the permeability of free space ($\mu_0 = 4\pi 10^{-7} H/m$)).

2.5 Larmor Frequency

The nuclei with spin quantum number ($I > 0$), have their energy states split into different energy sublevels when they are localized in the external magnetic field B_0 . The exact number of protons in each energy state is governed by a distribution known as the Boltzmann distribution [32], as shown below:

$$\frac{N_{upper}}{N_{lower}} = \exp\left(-\frac{\Delta E}{KT}\right) \quad (2.4)$$

where (N_{upper}) and (N_{lower}) are the number of protons in the upper and lower energy states, respectively, and K is Boltzmann's constant, $1.381 \times 10^{-23} \text{ J k}^{-1}$.

Moreover, when the nuclei are irradiated with radiofrequency (RF) pulses, energy

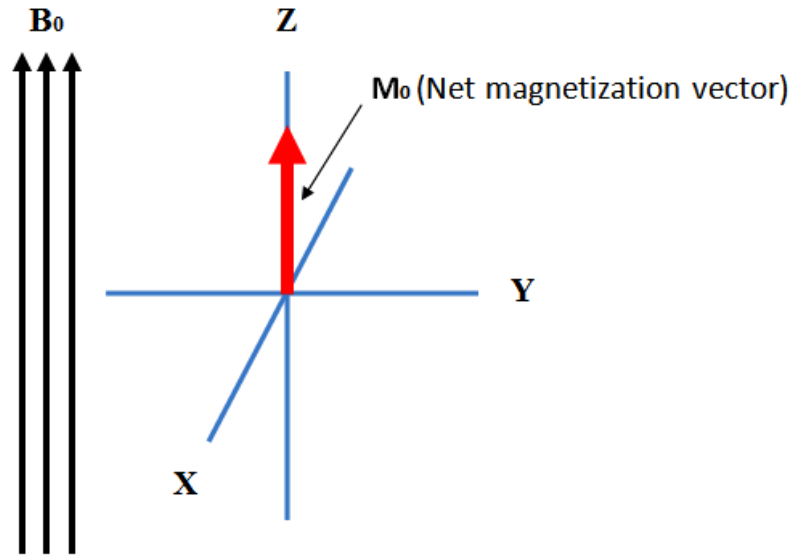


Figure 2.2: The net magnetization M_0 of a sample along the magnetic field direction B_0 , at equilibrium. The coordinates (x, y and z) are right-handed.

absorption occurs, and the spin in the lower energy state flips to the higher energy state. The difference in energy between the two energy states can be calculated using the following equation,

$$\Delta E = \gamma \frac{h}{2\pi} B_0 \quad (2.5)$$

where, (ΔE), γ , and h represent the differences in energy, gyromagnetic constant, and Planck's constant, respectively.

Besides, the introduced frequency (ν) at which the absorption energy occurs can be calculated using equation 2.6 [30].

$$\nu = \frac{\Delta E}{h} \quad (2.6)$$

where, (ΔE) is the absorbed RF energy which is equal to the energy difference between the two energy states. Substituting ΔE from equation 2.5 in equation 2.6, the resonance condition is obtained.

$$\nu = \gamma \frac{B_0}{2\pi} \quad (2.7)$$

$$\omega = \gamma B_0 \quad (2.8)$$

where $\omega = 2\pi\nu$, and is the Larmor frequency (radians per second, rad s^{-1}). Moreover ν is the linear frequency in Hz. Equation 2.8 is established as the necessary resonance condition [33]. Fig. 2.3 shows the circular and precession motions of a proton in external magnetic field B_o .

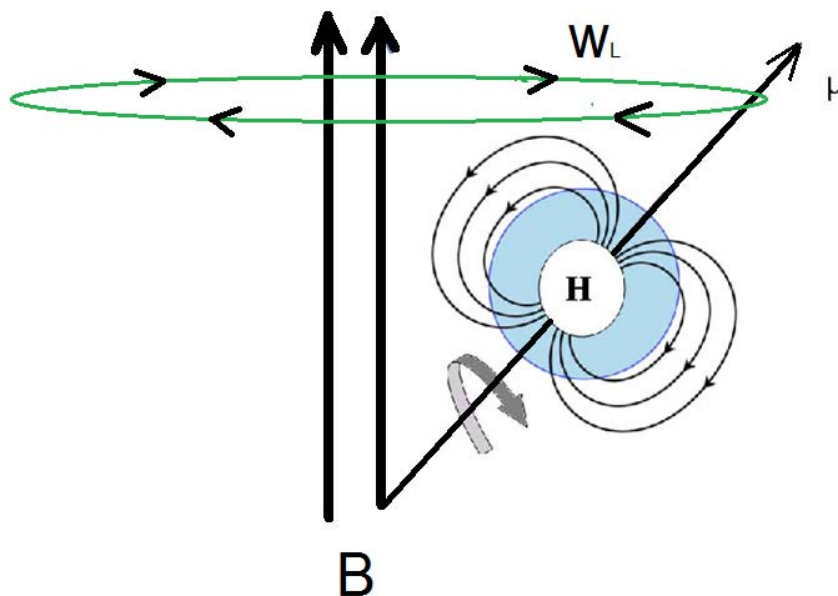


Figure 2.3: Applying an external magnetic field B_0 leads to the magnetization vector being tilted away from the z axis. The proton has two motion: one around its own axis that is denoted by the magnetic moment μ and a precession motion around the direction of B_0 . The magnetic moment sweeps by a certain angle from the B_0 direction. The vector sweeps out a cone of constant angle to the magnetic field direction. This precession frequency is known as the Larmor frequency ω_0 .

2.6 Relaxation Times T_1 , T_2 and T_2^*

It was stated that, when the nuclei absorb a certain amount of energy (equal to the energy difference between the two energy states), they are excited to a higher energy state, which occurs immediately after the excitation 90° pulse of the RF applied pulses. The return of the nuclei to the lower energy state is associated with loss of energy to the surroundings, which happens when the RF turns off. Therefore, the net magnetization returns to equilibrium during the spin-lattice or longitudinal relaxation time (T_1). Fig.

2.4 shows that T_1 can be defined as the time for $M(t)$ return to 63 % of its original value M_0 . Moreover, at time = 3 T_1 , the z-component returns to 95% of M_0 . The relation between the M_z magnetization component and T_1 can be illustrated by the following equation [34],

$$M_z(t) = M_0[1 - \exp(-\frac{t}{T_1})] \quad (2.9)$$

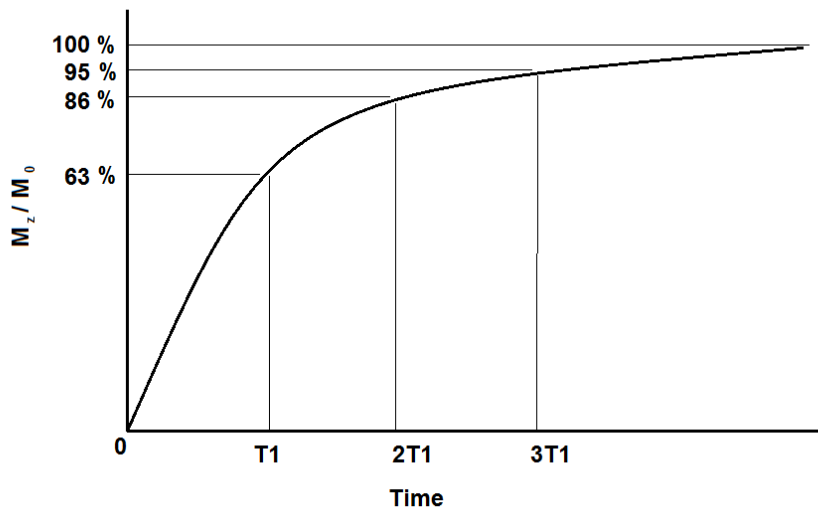


Figure 2.4: The relaxation times, the spin-lattice or longitudinal relaxation time, T_1 .

Equation 2.10 indicates the relation between the spin-spin or transverse relaxation time (T_2) and the M_{xy} magnetization component in the xy plane. During T_2 the spins in the higher and lower energy states exchange without loss to the surrounding nuclei. The transverse magnetization component M_{xy} decays at the rate of $(1/T_2)$. Within the relaxation time T_2 , the net magnetization reached to 37 % of the original value, as seen in Fig. 2.5.

$$M_{xy}(t) = M_{xy(max)}(\exp(-\frac{t}{T_2})) \quad (2.10)$$

$$Relaxation\ rate = \frac{1}{T_2} \quad (2.11)$$

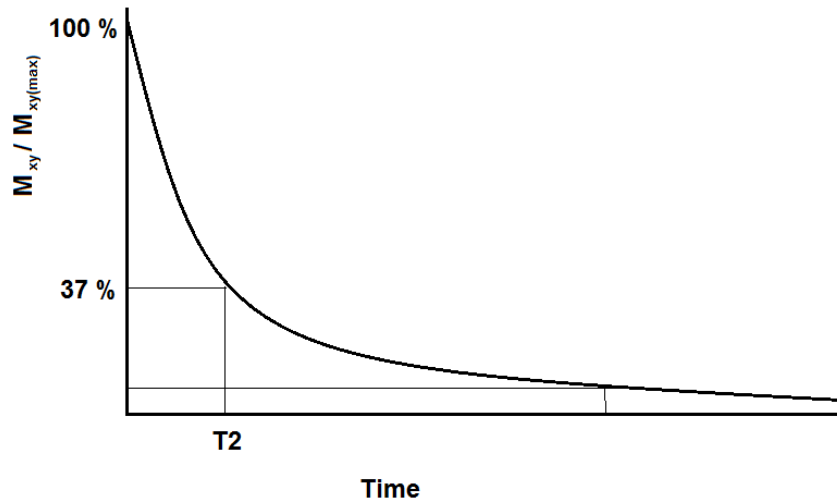


Figure 2.5: The relaxation times (spin-spin or transverse relaxation time, T_2).

$$\frac{1}{T_2^*} = \frac{1}{T_2} + \gamma \Delta B \quad (2.12)$$

Equation 2.11 shows the relaxation rate with units of s^{-1} , where in equation 2.12, the total transverse relaxation time, T_2^* , depends on the relaxation rate of tissue T_2 plus the magnetic field inhomogeneity of the external magnetic field ΔB [35].

2.7 Sequence Times TR, TE and Received Signal

The repetitions time (TR) and echo time (TE) parameters are related to the tissue relaxation times (T_1) and (T_2), respectively. However, unlike T_1 and T_2 , which represent the inherent properties of the tissue, and therefore, are fixed, TR and TE can be adjusted. Moreover, changing the values of TR and TE affects on T_1 and T_2 weighting, depending on the clinical applications.

2.7.1 Repetition Time (TR)

TR defined as the time interval between the two applications such as two 90° pulses. The magnetization vector points along the \mathbf{Z} direction where ($M_z = M_0$). At ($t = +0$), immediately after ($t = 0$), the magnetization in the $\mathbf{X-Y}$ plane has the component

($M_{xy} = M_0$). As $t = TR$, some magnetization along the Z-direction is recovered and some or all magnetization is lost in the X-Y plane. The final magnetization at $t = TR$ is shown by the following [36].

$$M_z(TR) = M_0[1 - \exp(-\frac{TR}{T_1})] \quad (2.13)$$

i.e. the magnetization (M_z) at time ($t = TR$) is smaller than the original magnetization (M_0) if the second 90° pulse is applied before recovering total (T_1).

2.7.2 Received Signal

Because the series of 90° pulses alone are applied, the signal received (S) will be a series of FIDs. The signal S is proportional to the term $(1 - \exp(-\frac{TR}{T_1}))$ and the spin density (N_H) as illustrated in equation 2.14.

$$S = N_H(1 - \exp(-\frac{TR}{T_1})) \quad (2.14)$$

2.7.3 Echo Time (TE)

The signal cannot be measured immediately after the RF pulse goes off without delay. This cannot really happen in practice. Instead of making the measurement immediately after the RF pulse, we need to wait for a short time period and then record the signal. This time is called the time of echo (TE) and related to T_2^* by the quantity $(\exp(-TE/T_2^*))$ [36]. Equation 2.15 illustrates the received signal depending on TE and TR.

$$S = N_H[\exp(-\frac{TE}{T_2^*})][1 - \exp(-\frac{TR}{T_1})] \quad (2.15)$$

2.8 Chemical Shift

The circulation of electrons around the nucleus induces a magnetic field (B_i), which is opposed to the external magnetic field. In accordance with this induced field, the total magnetic field strength is reduced. This reduction is called *magnetic shielding* [29].

The relation between B_i and B_0 can be expressed by the following relation

$$B_i = \sigma B_0 \quad (2.16)$$

The term σ (refers to the diamagnetic shielding constant) where, its value depends on the electron density of any atom. The chemical shift is interpreted relative to the increase or decrease of electron density [37]. Therefore, the effectiveness of the applied magnetic field on the atomic nucleus (B_{eff}) is

$$B_{eff} = B_0 - \sigma B_0 = B_0(1 - \sigma) \quad (2.17)$$

The chemical shift is defined as the difference between the reference frequency (ω_{ref}) in Hz and the sample frequency (ω_{sample}) in Hz.

$$\Delta \omega = \omega_{sample} - \omega_{ref} \quad (2.18)$$

As tetramethylsilane (TMS) is regarded as the reference material, the frequency difference, chemical shift, ($\Delta\omega$) will increase with the increased B_o . Further, the chemical shift in Hz must be divided by the frequency of the spectrometer in Hz and multiplied by 10^6 to negate the effect of the different magnetic field strengths. Therefore, the chemical shift is recognized by (δ) and measured in ppm instead of in Hz [37].

$$\delta = \frac{\Delta\omega}{\omega_{spectrometer}} 10^6 \quad (2.19)$$

For example, at 7T, the chemical shift between the water and fat signals was estimated using equation 2.19, where the resonance frequencies for water and fat are separated by approximately 3.5 ppm, which in turn corresponds to an absolute frequency difference of 1043 Hz.

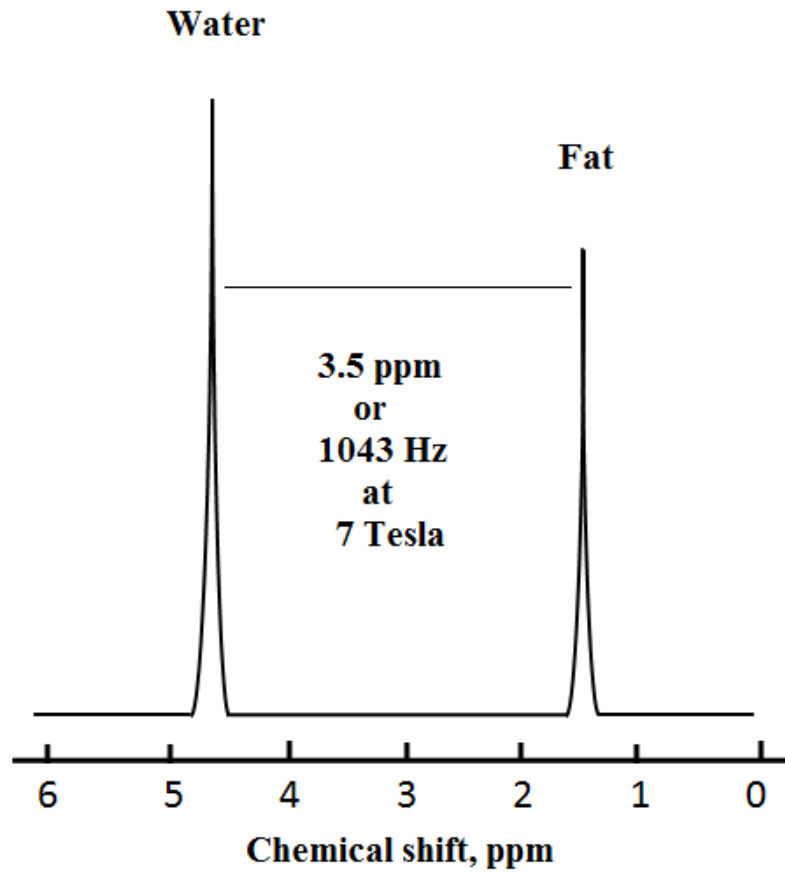


Figure 2.6: The chemical shift in ppm between water and the fat spectra at 7 T.

2.8.1 Chemical Shift Displacement

The frequency of spins with Larmor frequency (ω_0) in the presence of a magnetic field gradient (G_x) in \mathbf{x} direction is given by:

$$\begin{aligned}\omega(x) &= \omega_0 + \gamma \Delta x G_x \\ \Delta\omega &= \omega(x) - \omega_0 = \gamma \Delta x G_x\end{aligned}\tag{2.20}$$

where, $\Delta\omega = \omega(x) - \omega_0$ is the difference in the chemical shift between two different compounds, like water and fat. Δx is the chemical shift displacement in the \mathbf{x} -direction [38].

De Graaf and *et al.*, 2000 [39] illustrated that the voxel size ($V_i, i = x, y, z$) can be defined as the ratio between the *RF* bandwidth and the magnetic gradient strength.

$$V_i = \frac{RFbandwidth(Hz)}{gradientstrength(Hz/cm)} \quad (2.21)$$

Thus,

$$V_i = \frac{\Delta\nu}{\gamma G_i} \quad (2.22)$$

As the gradient field strength is defined as the change of the magnetic field relative to distance, then

$$V_i = \frac{\Delta\nu}{\gamma \frac{\Delta B}{\Delta V_i}} \quad (2.23)$$

Or,

$$V_i = \frac{\Delta\nu}{\gamma \Delta B} \Delta V_i \quad (2.24)$$

Therefore, the two voxels corresponding to their resonances will be shifted by the amount of

$$\Delta V_i = \frac{\gamma \Delta B}{\Delta\nu} V_i \quad (2.25)$$

Or,

$$\Delta x = \frac{\Delta\omega}{\Delta\nu} X \quad (2.26)$$

where, the chemical shift displacements in the y-direction and z-direction are Δy and Δz , respectively.

2.8.2 J-Coupling

Consider a system of two protons H_A and H_B which resonate as doublets. Fig. 2.7 shows the chemical shifts and coupling constant (in Hz) of the doublet lines. The two coupled protons H_A and H_B are separated by three chemical bonds. The coupling constant between H_A and H_B is J_{AB} . Moreover, the dotted lines at δ_A and δ_B show the chemical shift of H_A and H_B , respectively, before they influence each other. The spin-spin splitting refers to the number of neighboring protons. In this example, there are two peaks for each proton i.e. each proton has only one neighboring proton [40].

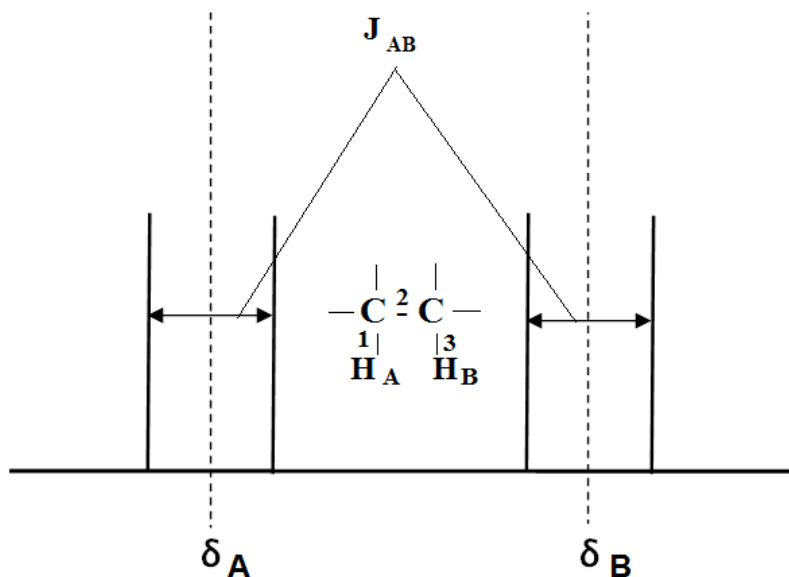


Figure 2.7: Chemical shift and J-coupling of two coupled protons H_A and H_B (spin-spin splitting). The coupling constant ${}^3J_{AB}$, (3) indicates the number of chemical bonds, and (AB) shows the coupled protons.

2.8.3 Multiplicity (m)

Multiplicity refers to the number of spectral peaks and gives the number of neighbor protons (n) where, $m = n + 1$ [41]. For example, γ -Aminobutric (GABA) compound consists of four carbon atoms bonded with hydrogen atoms as shown in Fig. 2.8 (A). The GABA spectrum (in range 0.4-4.4 ppm) has three groups of peaks; Group (A) contains five peaks (i.e., $n+1=5$ or $n=4$) or four neighbor protons. Group (B) and (C) have two neighbor protons for each one.

2.9 Localized Spectroscopy and MRS Techniques

The two common methods used in MR spectroscopy studies are single volume spectroscopy (SVS) and chemical shift imaging (CSI). By utilizing the SVS technique, when a certain volume of interest (VOI) was excited, the desired spectra were obtained. Fig. 2.9 (A) shows the examined VOI using SVS technique. As seen in Fig. 2.9 (B), several spectra were obtained from the field of view (FOV) using the CSI method [42].

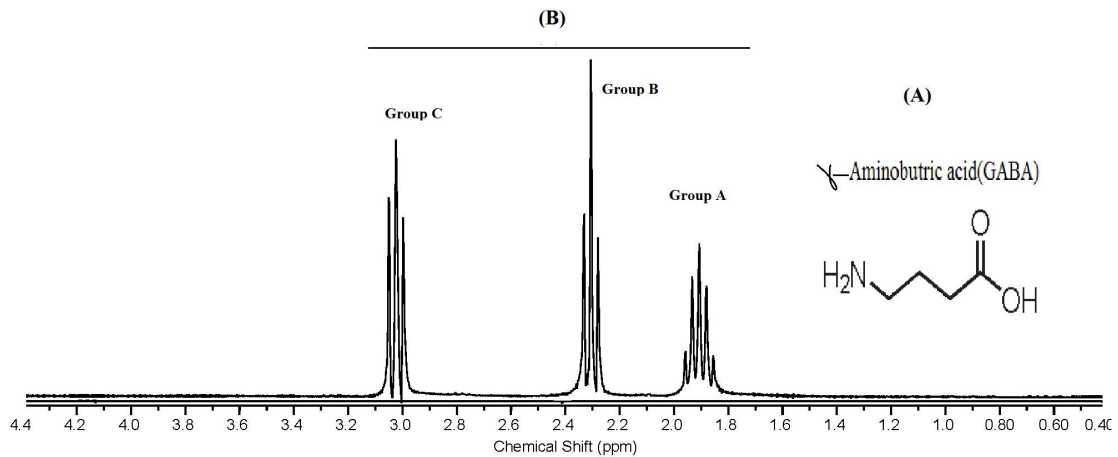


Figure 2.8: $^1\text{H MRS}$ spectrum of GABA solution measured at 7T. (A) The chemical structure of the compound and (B) The spectral peaks in the range 0.4 ppm to 4.4 ppm.

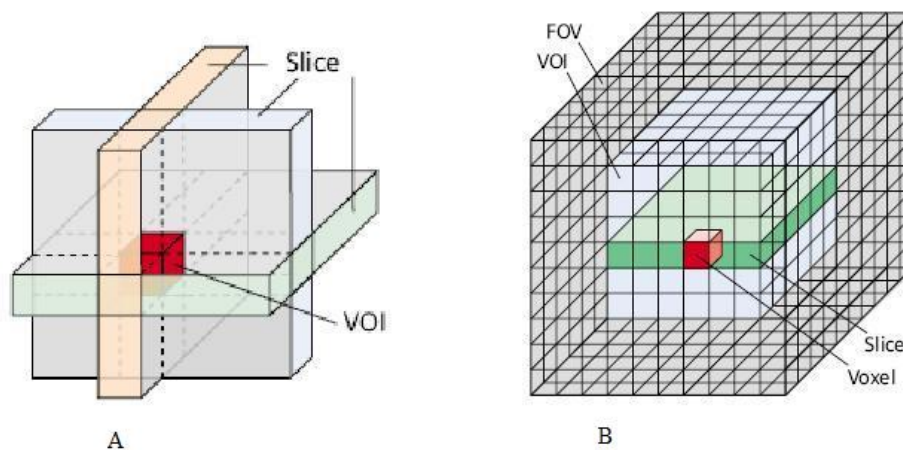


Figure 2.9: The localization techniques for MR spectroscopy applications (A) The SVS shows the intersection of three slices (VOI) (B) The CSI shows several voxels of FOV.

2.10 DATA Processing in Frequency Domain

The measured free induction decay (FID) signal is in the time domain. This signal can be converted to the frequency domain using Fourier transformation (FT). Processing in the frequency domain offers an easy way to reduce the data analysis to a limited frequency region of the MRS spectra. However, under certain conditions, frequency-selective quantitative data analysis in the time domain is also feasible [43, 44, 45].

The following post processing steps can be applied after acquiring the FID signals.

2.10.1 Eddy Current Correction(ECC)

The eddy current producing the raw data could be problematic to phase shifts. The effect of these eddy currents on the MRS spectrum can be compensated by subtracting the phase of the unsuppressed water signal from the suppressed water signal to be evaluated [46].

2.10.2 Fourier Transformation

Fourier transformation (FT) is a mathematical algorithm used to translate the measurement signals from the time domain (the measured signal) into the frequency domain (spectrum).

2.10.3 Baseline Correction

The incomplete suppression of the water signal, spectra may exhibit some degree of distortion (baseline). This distortion is often strong particularly around the water signal. The baseline can be corrected using an nth order polynomial fitting to the spectrum. This polynomial is subtracted from the original spectrum, resulting in a more horizontal baseline. A flat baseline is essential for the integration of metabolite signals which is important for metabolite quantification. The baseline can be modified manually: it can also be done automatically by using the LCModel through spline functions [47].

2.10.4 Phase Correction

A complex spectrum consists of a real part and an imaginary part. These represent the frequency-dependent x and y projections of the transverse magnetization of the spins. Phase correction can be achieved with two processes zero order phase correction and first order phase correction. The amount of phase correction is related to each individual peak in the spectrum [46, 48].

2.10.5 Curve Fitting

Spectra often contain a large number of peaks, making it difficult to assign metabolites to the individual peaks. For example, several human brain metabolite peaks can be quantified in the frequency domain in the range from 0.2 ppm to 4.2 ppm, as mentioned under Results. The linear combination of *in vitro* spectra of model solutions of human brain metabolites can be used as the basis set of a commercial program known as LCModel [47].

The human brain metabolite concentrations can be estimated in the frequency domain using this model. As the basis set and the *in vivo* data are generally not acquired under identical conditions, leading to different scaling, scaling the human brain spectra by a water scaling factor (f_{scale}) becomes important to determine the absolute concentrations [49]. With water scaling, the LCModel multiplies the data by f_{scale} to scale the data consistently with the basis set. Incidentally, f_{scale} is defined as the ratio of the normalized signal strength in the basis set to the normalized unsuppressed water signal in *in vivo* data. Further, the metabolite absolute concentrations can be calculated using the following equation,

$$Con_{met} = Ratio_{area} \times \frac{2}{N1H_{met}} \times \frac{ATT_{H2O}}{ATT_{met}} \times W_{conc} \quad (2.27)$$

where Con_{met} is the metabolite concentration. $Ratio_{area}$ is the ratio of the metabolite resonance area to the unsuppressed water resonance area. $N1H_{met}$ demonstrates the number of the equivalent proton in the metabolite groups. W_{conc} is the water concentration in the examined VOI in mM/L. ATT_{met} and ATT_{H2O} the attenuation factor of the metabolite and water, respectively.

Chapter 3

Materials and Methods

In this chapter, the preparation and measurement of 20 human brain metabolite solutions are described. The total number of healthy subjects is identified. Besides, the methods used in this research are clearly explained. Section 3.1 generally represents the context of the current chapter.

3.1 Experimental Set Up

All the *in vivo* and *in vitro* measurements were performed on a whole body 3T and 7T systems (Siemens, Erlangen, Germany). The measured data was saved in a spectroscopy raw data format. Localized proton magnetic resonance spectroscopy was used as a MRS technique [4]. The stimulated-echo acquisition mode (STEAM) was adapted and optimized by introducing variable rate selective excitation (VERSE) pulses to reduce the *RF* peak voltage at 7T.

Further, STEAM adapted with the VERSE pulses of pulse durations of 2.5 ms, TR=3000 ms, TE=20 ms, TM=15 ms and voxel size $(15 \times 15 \times 15) \text{ mm}^3$, 3600 Hz spectral band width, and 2048 sample points were optimized at 7T. A 24-channel volume coil was used for measurement of the human brain spectra, and a circular polarized coil (CP) was used to acquire the *in vitro* spectra. Thus, the simulated and experimental basis sets were achieved.

3.2 Materials

In this work, 20 model solutions of human brain metabolites were prepared. They measured at 7T and their spectra were acquired. These *in vitro* spectra were used to create the experimental basis set for the LCModel [47]. Concentration, molecular weight, and the initial mass of these 20 metabolites have been described in Table 3.1. All the chemicals were bought from Sigma-Aldrich.

Table 3.1: Twenty metabolite solutions and reference substances of LCModel basis set

Metabolite	Symbol	C (mmol)	M.W(g/mol)	I.W(g)
L-Alanine	Ala	100	89.090	0.356
Acetate	Act	200	82.040	0.656
Aspartate	Asp	40	133.100	0.213
Citrate	Cit	200	294.100	2.353
Creatine	Cr	50	149.150	0.373
γ -Aminobutric Acid	GABA	200	103.120	0.825
Glucose	Glc	200	180.160	1.441
L-Glutamine	Gln	100	146.150	0.585
Glutamate	Glu	50	187.140	0.468
Glycine	Gly	200	75.070	0.601
Glycerophosphocholine	GPC	33	440.540	0.581
Glutathione	GSH	70	307.330	0.861
myo-Inositol	Ins	200	180.160	1.441
L-Lactate	Lac	100	112.060	0.448
N-acetylaspartate	NAA	50	175.140	0.438
Phosphocholine	PCho	27	329.730	0.356
Phosphocreatine	PCr	50	155.100	0.510
phosphorylethanolamine	PE	50	141.060	0.282
Succinate	Suc	100	270.100	1.080
Taurine	Tau	200	125.150	1.001
Reference Markers				
Sodium Formate	HCOONa	200	68.010	13.602
Trimethylsilyl propionate	TMSP	10	172.280	1.723
Dipotassium phosphate	K2HPO4	72	174.180	11.287
Monopotassium phosphate	KH2PO4	28	136.090	3.429

3.2.1 Preparation of the Model Solutions

Spherical phantoms made of plastic of 40 mm diameter were used as solution containers. The standard solvent is consisted of (200 mM/L of **Na-formate** and 10 mM/L of **TMS**), was solved in one liter of distilled water. Some of the model solutions did not dissolve in the solvent, due to the phosphate content, such as (GPC) and (PCh). Therefore, 100 mL of the solvent was added to (72 mM/L of K_2HPO_4 and 28 mM/L of KH_2PO_4) to prepare these metabolites. Then 900 mL of the solvent without any additions was used to prepare all the other metabolites.

The pH values of several metabolites such as NAA, Lac and Glu, were adjusted to 7.2 using careful titration with concentrated NaOH or HCl to avoid their resonance shift.

3.2.2 Reference Peaks

Na-formate and **TMS** are the two reference substances which were used in this work. As **Na-formate** concentration was the same in all the model solutions, the **Na-formate** resonance peak was found to be around 8.44 ppm and it was used to scale the 20 *in vitro* spectra consistently with each other. **TMS** also has singlet at 0 ppm. The **Na-formate** and **TMS** singlets are also used by the LCModel for automatic phasing. Therefore, it is important to use the same reference marker for all the model metabolites. The chemical structure of the **TMS** and **Na-formate** are indicated in Fig. 3.1.

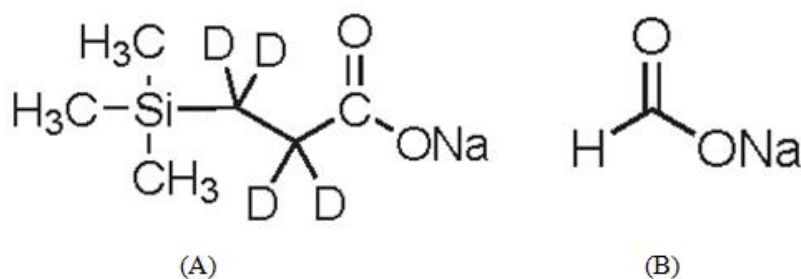


Figure 3.1: Chemical structures of (A) TMS and (B) Na-formate reference substances

The temperature of the solution is often adequate for acquiring the quality spectra at 7 T. It is best to adjust the phantom temperature closer to the room temperature.

In this work, all the metabolite solutions were left in the scanner room for three hours before beginning the measurements.

3.2.3 Compatibility Requirement

To analyze *in vivo* or *in vitro* spectra, a basis set must be obtained and some conditions need to be matched, such as the static magnetic field strength (B_0), localization sequence, TE, TM (in STEAM only). However, TR, vector size, acquisition time, and spectral bandwidth do not have to be matched.

3.3 Human Subjects

In this study, all volunteers were healthy subjects between 23 and 35 years. The number of subjects and their spectra were classified into three groups.

1. Group one was related to the parietal locations. The volunteers were in number 8 while the spectra numbered 32.
2. Group two was related to the pgACC regions. Eleven subjects were measured at 7T while three of them were measured at 3T for comparison. The total number of subjects was 11 and the acquired spectra were 14.
3. Group three includes 6 volunteers who were measured at 7T. Four positions were selected (pgACC, AMCC, Brodmann area (23C) and PCC) have been measured with short TE=20 ms. Two of them (pgACC and AMCC) were measured with long TE=74 ms. Therefore, the total number of subjects in this group was 6 and the total number spectra was 36.

Finally, the number of subjects measured was 30 and the total number of acquired spectra was 82.

3.4 Methods

Point resolved spectroscopy (PRESS) was used at 3T [3] and stimulated echoes (STEAM) at 7T [4]. Experimental basis sets of 20 model solutions were measured

at 7T using (STEAM with VERSE) pulses with different echo times and mixing times. Twenty human brain metabolite simulated spectra have been done using "WIN-SIM" NMR spectroscopy software. Creation of "BASIS" files was done for the LCMModel. In addition, a segment of the original image to gray matter (GM), white matter (WM) and cerebrospinal fluid (CSF) images was obtained using "SPM" software and the partial volume of GM was calculated using the "imageJ" software.

3.4.1 Acquiring the Basis Spectra

STEAM with VERSE pulses of (pulse durations 2.5 ms, TR=3000 ms, TE=74/30/20 ms, TM=15 ms and voxel size $15 \times 15 \times 15 \text{ mm}^3$, 3600 Hz spectral band width, and 2048 sample points) are maintained the same throughout all measurements. It is essential that the basis spectra are scaled consistently with each other, Therefore, the *in vitro* spectra were acquired under the same conditions viz., the position of the phantom in the magnet, acquisition time and spectral bandwidth. Additionally, the voxel was located in the center of the phantom in order to fix the coordinates of the VOI position in all the phantoms. Moreover, it was found best if all the spectra were acquired with the same time period.

3.4.2 Introduction to LCMgui and Makebasis.in File

LCMgui is a graphical mode used to analyze the acquired spectroscopy data. When the LCMgui processing was used, 11 files were produced. One of them was a "ps" file which included a spectral fit, concentration values, fit residual and other spectral information.

3.5 Shimming

The quality of the acquired spectra depends upon the shimming quality achieved for MRS examinations, where, by changing the shim currents, FWHM and T_2^* can be optimized. Moreover, interactive shimming compensates for inhomogeneities of the magnetic field. This has been confirmed by users. Therefore, the user can adjust the shimming currents to obtain high quality spectrum with a line width as narrow as

possible [50, 51, 52, 53]. At 3T and 7T, interactive and automatic 3D shim have been used.

3.6 Water Suppression

It is important to mention that, in *in vivo* measurements the water signal has more than 10000 times higher than the metabolite signals, as seen in Fig. 3.2 (A). Therefore, it is necessary to suppress the water signal in order to obtain sufficient signals of the human brain metabolites. The effect of the water suppression process has been shown in Fig. 3.2 (B). The method most frequently used in MR spectroscopy is selective excitation and dephasing of the water signal prior to the actual spectroscopy experiment. As seen in Fig. 3.3, the chemical shift selective suppression (CHESS) sequence consists of three 90° pulses applied before the PRESS or STEAM pulses [54, 55]. Sometimes it is good to use the manual water adjustment to optimize the flip angle, where, the flip angles are set for optimal suppression of the water signal by determining a correction factor for the transmitter amplitude of these *RF* pulses [56].

3.7 RF Pulse Sequences

Consider that an *RF* sequence consists of three 90° pulses as shown in Fig. 3.4. This pulse sequence generates five echoes and three FIDs [57, 25]. When the first two pulses are separated by a delay ($TE/2$) and the last two pulses are separated by a TM , four spin echoes (SE) are formed. Pulses 1 and 2 form the spin echo (SE_{12}), which occurs at a time TE after the initial excitation pulse. (SE_{13}) is formed at ($TE + 2TM$), (SE_{23}) at ($TE/2 + 2TM$) and (S_{123}) occurs at position ($2TM$). (S_{123}) occurs due to refocusing by pulses 2 and 3 of magnetization excited by pulse 1. Add to these four (*SEs*), a stimulated echo (*STE*) is formed at position ($TE + TM$) or after a delay ($TE/2$) following the last 90° pulse.

Moreover, the positions of the different (*SEs*) depend on the timing parameters TE and TM , while the relative amplitudes depend on the flip angles of the *RF* pulses. In MR spectroscopy measurements, (*STE*) is the signal of interest. Therefore, the *FID* and other (*SEs*) signals need to be eliminated in order to obtain only (*STE*). Those

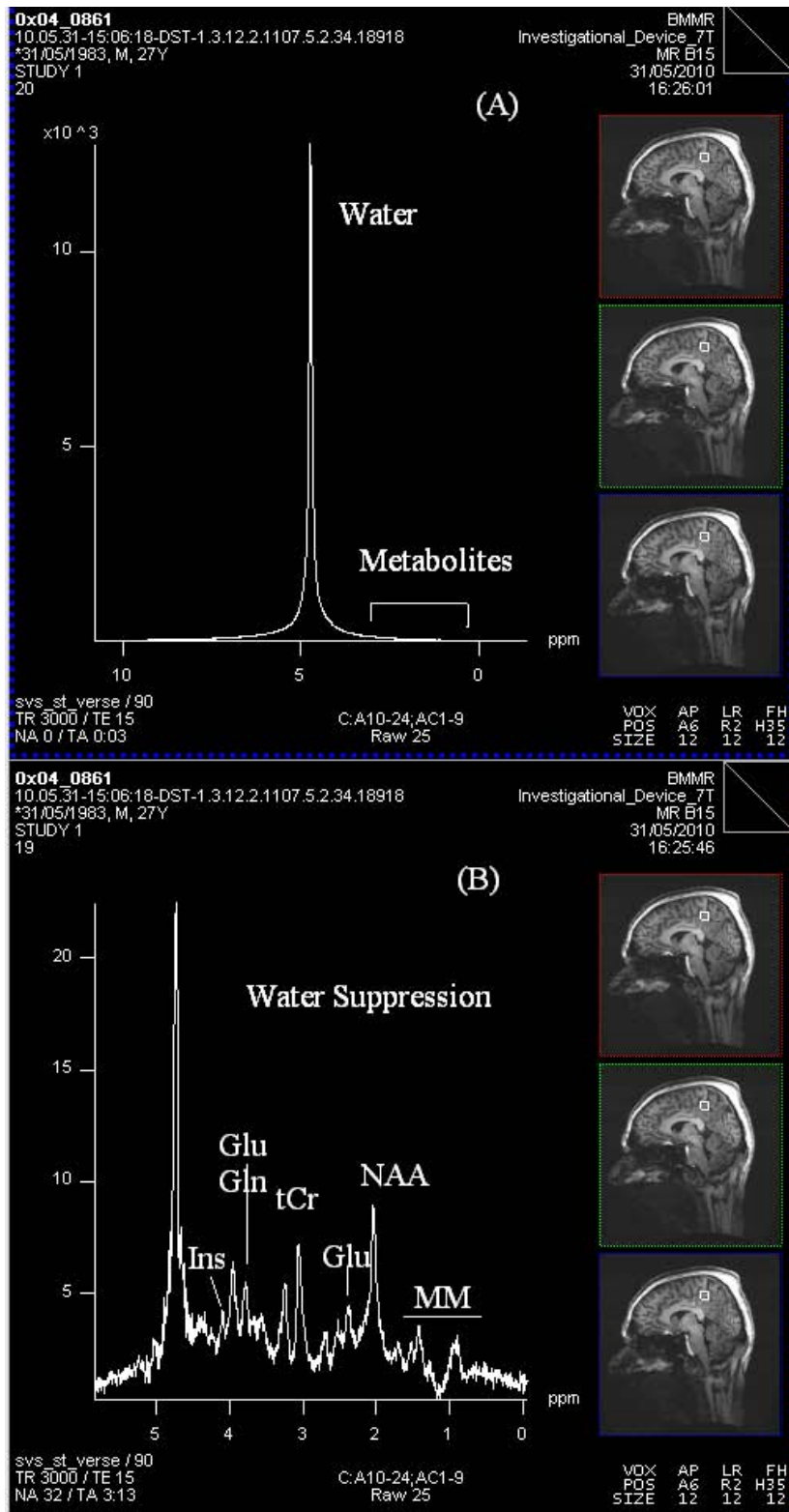


Figure 3.2: ^1H -MRS spectrum represents (A) Water signal besides the metabolite signals (unsuppressed water option). (B) The metabolite signals besides the water (after water suppression was done).

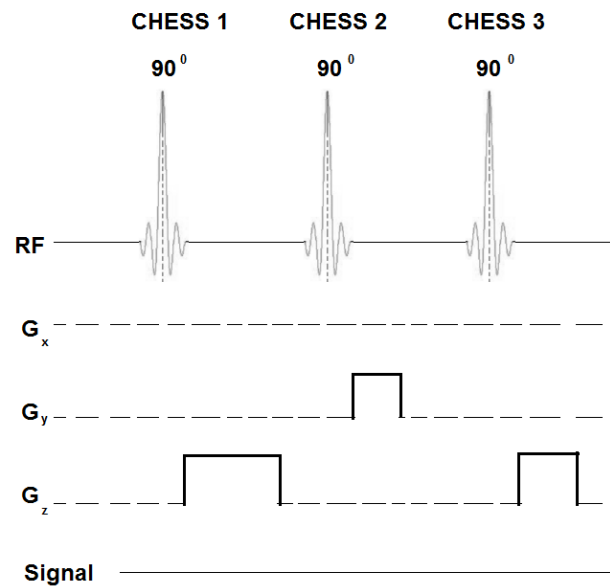


Figure 3.3: Water suppression (CHESS) pulses.

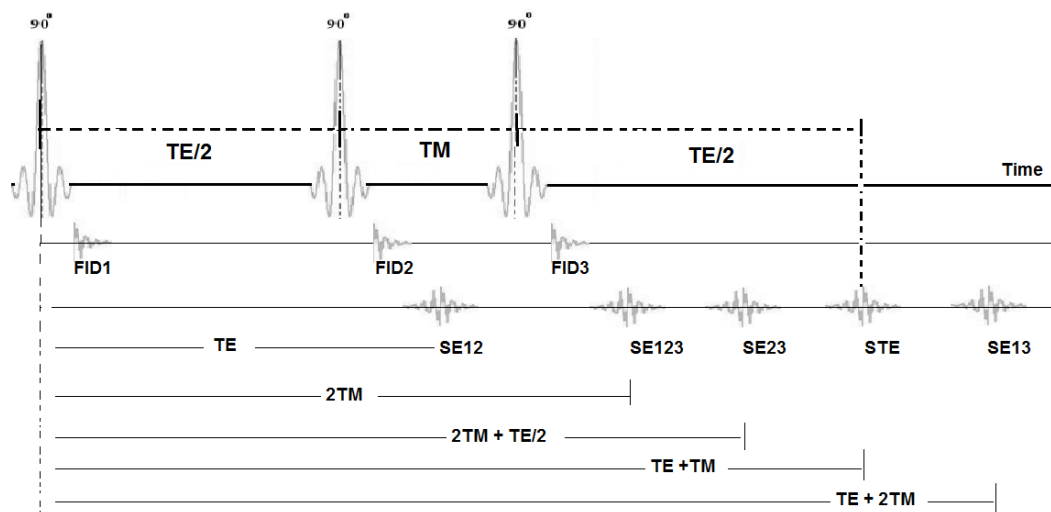


Figure 3.4: Three FIDs (FID1, FID2, and FID3) achieved for spin echoes SE_{12} , SE_{13} , SE_{23} , and SE_{123} respectively. Moreover, one stimulated echo (STE) can be generated. (A) The echoes appear at distinct temporal positions, depending on the (TE) and TM periods. (B) The (ADC) of the four echoes have been shown respect to time scale.

signals can be eliminated by using magnetic field gradients. By placing a magnetic gradient in the TM period, all SEs are eliminated leaving only the (STE). Add to

this, the *FID* component increases due to the last 90° excitation pulse [58].

3.8 PRESS, STEAM, and VERSE

Two techniques are commonly used in human magnetic resonance spectroscopy to obtain spectra from localized volumes in the brain. These are point resolved spectroscopy (PRESS) and stimulated echo acquisition mode (STEAM). PRESS gives a signal twice as large as that obtained with STEAM, but suffers from longer minimum echo times, while STEAM must be used to detect samples with short TE times. Several authors have used PRESS and STEAM sequences as excitation and selection methods [59, 25, 60, 61, 62].

3.8.1 Point Resolved Spectroscopy (PRESS)

As seen in Fig. 3.5, the PRESS sequence consisting of an 90° excitation pulse and two 180° refocusing pulses. When the first 180° pulse is executed at time $(TE_1/2)$ after the 90° pulse, a spin echo is formed at time $8TE_1$). The second 180° pulse refocuses this spin echo during the delay (TE_2) , such that the final spin echo is formed at time $(TE = TE_1 + TE_2)$. The three *RF* pulses are frequency selection and are executed in combination with the magnetic field gradients [38].

3.8.2 Stimulated Echo Acquisition Mode (STEAM)

Three slice selective 90° pulses are used in the stimulated echo acquisition method (STEAM) [4]. The first pulse flips the net magnetization vector M_0 into the **XY** plane. The second pulse flips part of the spins back into the **Z**-direction. The remaining transverse net magnetization decays through *TM* and does not contribute to the acquired MRS signal. The third pulse flips the magnetization back into the **xy** plane. After $TE/2$, a stimulated echo is produced as *FID*. During *TM*, the longitudinal magnetization is subjected to T_1 relaxation. Fig. 3.6 shows the schematic diagram of the stimulated echo *RF* pulses of the STEAM sequence with the magnetic field gradient pulses (G_x , G_y and G_z) which were used for slice selection [38].

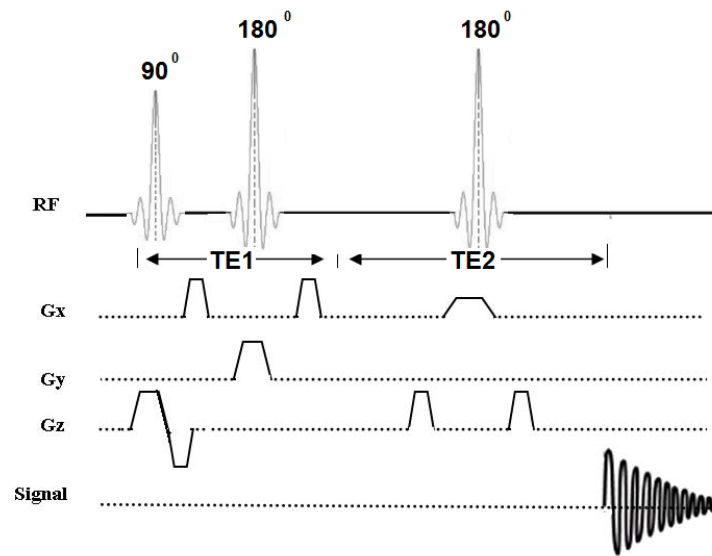


Figure 3.5: PRESS sequence with three RF pulses applied simultaneously with the field gradients along the main axes of the magnet.

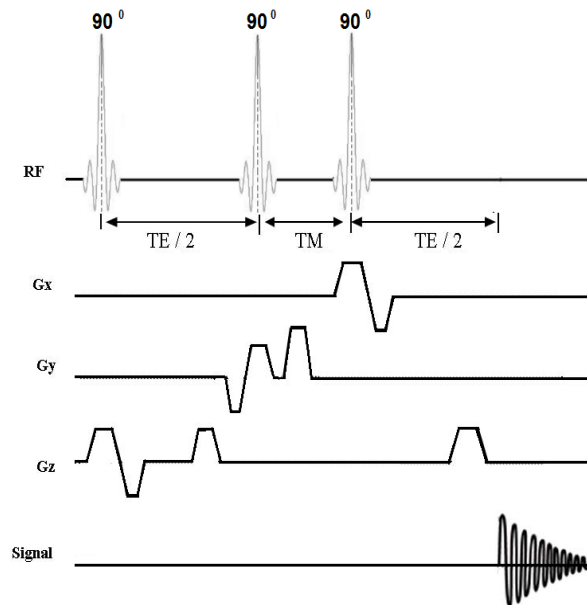


Figure 3.6: Sequence scheme for the STEAM sequence. The refocusing gradients need to be positioned before the second RF pulse and after the third RF pulse.

3.8.3 Variable Rate Selective Excitation (VERSE)

The variable rate pulse (VR) is considered a spatially selective RF pulse; it is also a time varying gradient [63]. Variable rate pulses are also known as variable rate selective

excitation (VERSE) pulses [21]. One main application of VR pulses is the RF power reduction which is placed in patients [64]. Moreover, in order to maintain the nominal flip angle when the RF amplitude is reduced, the VR pulse is stretched. This in turn reduces the RF bandwidth at any portion of the pulse. Fig. 3.7 (A) shows an example of an original pulse while Fig. 3.7 (B) shows a modified sinc pulse with an applied gradient [64].

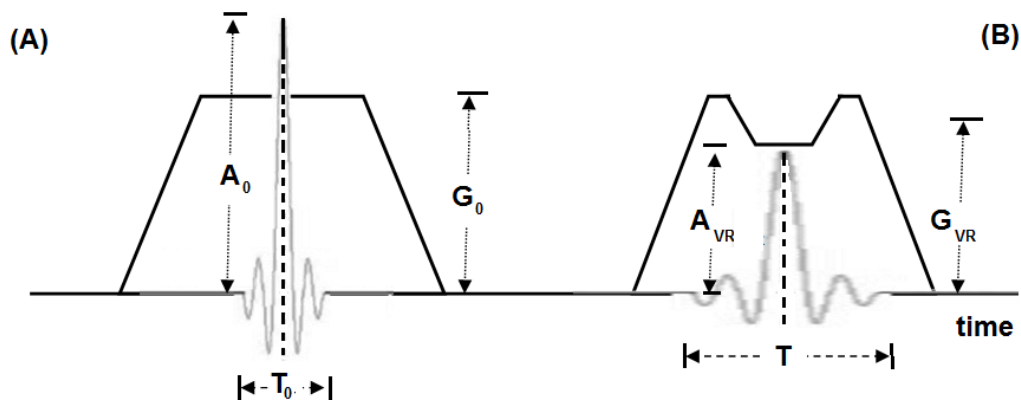


Figure 3.7: Variable-rate modification to a sinc RF pulse. (A) The original RF envelope A_0 is attenuated wherever the gradient amplitude G_0 is reduced. (B) VR-modified sinc pulse of amplitude A_{VR} with a concurrent gradient G_{VR}

3.9 Simulation Database

This section explains the data simulation using the nuclear magnetic resonance simulation program ($NMR - SIM$) to simulate metabolite spectra as they are in a real experiment. However, the calculation is based on an ideal spectrometer (i.e. ignoring the effects such as magnetic field inhomogeneity). Several parameters can be modified to study the impact of non-optimum conditions on a spectrum. The FID is calculated from the solution of the Liouville - Von Neumann equation, which is called the density operator equation. The spin system of any metabolite and the pulse sequence are explained in detail in Appendix (C). Moreover, in order to simulate the FID signal of any metabolite, two parameters should be established

1. RF pulse sequence

2. Spin system of each metabolite

The simulation of an NMR experiment is based on the density matrix approach. Relaxation phenomena are implemented using a model based on the Liouville equation. Cross-correlation and cross relaxation effects are ignored.

Furthermore, the Bloch simulator module is designed to calculate and visualize the motion of the \vec{M} through the NMR experiment. The motion of the magnetization vector is described by the equation 3.1. Fig. 3.8 shows the amplitude and phase of a simulated RF-sinc pulse using the applied frequency of 297.14 MHz. Moreover, Fig. 3.9 indicates the Fourier transform of the 90° RF profile using STEAM with VERSE pulses at 7T. Moreover, the simulated RF bandwidth was simulated and equal to 3600 Hz.

$$\frac{dM_z}{dt} = -\gamma(\vec{B} \times \vec{M}) + \frac{M_z - \vec{M}_0}{T_1} \quad (3.1)$$

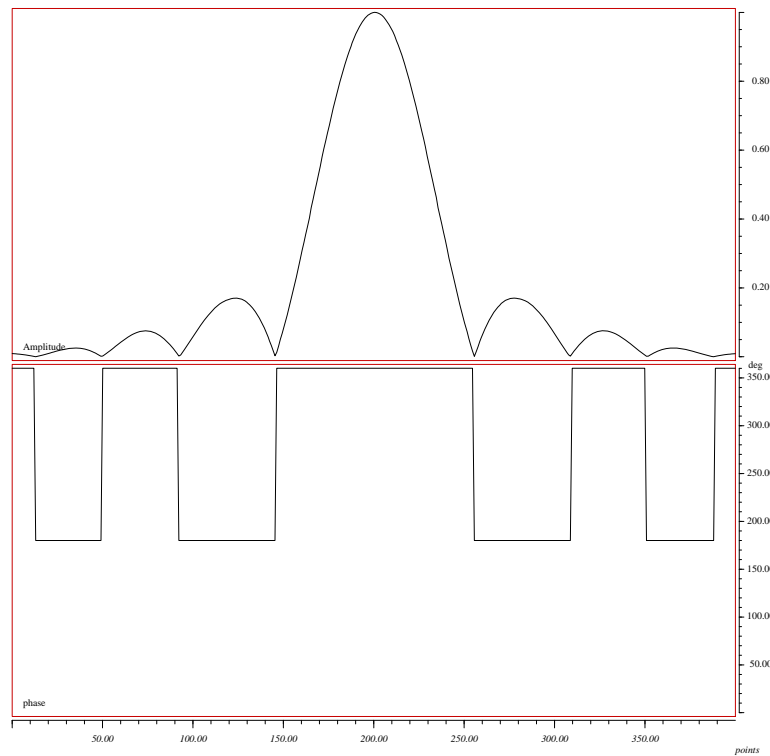


Figure 3.8: Pulse shape display in NMR-SIM

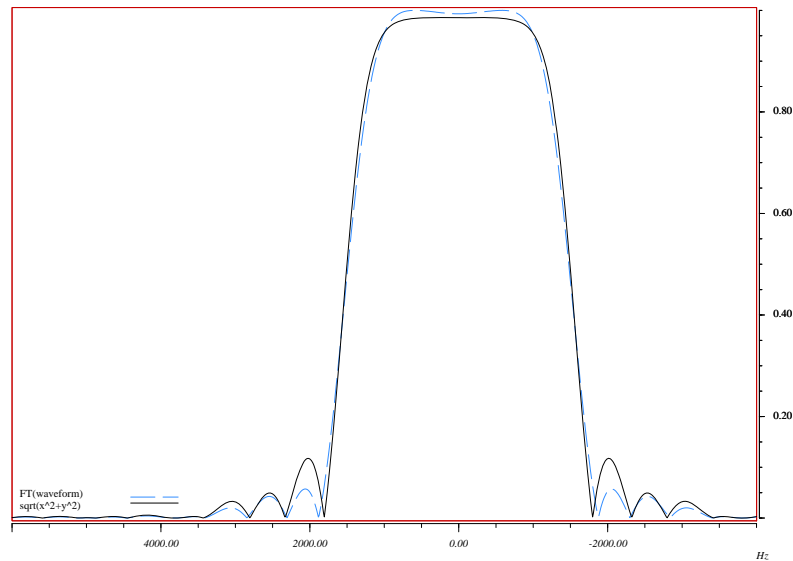


Figure 3.9: The excitation profile of the sinc 90° pulse of the STEAM with VERSE pulses.

3.10 Instruments

3.10.1 Magnet System

The magnet system generates the basic magnetic field B_0 . The magnet comprises a superconductive electrical magnet including the cooling system (interface for helium fill/refill, cold head), monitoring the magnet during the operation [42]. Moreover, the superconducting magnet produces a strong homogeneous magnetic field with strength of 7 Tesla. The magnet jacket is filled with liquid helium acting as the coolant. Fig. 3.10 shows the 7T whole body scanner.

3.10.2 Gradient System

The gradient system produces linear dynamic magnetic field gradients in three directions (\mathbf{X} , \mathbf{Y} , and \mathbf{Z}). The gradient coil and the gradient amplifier are the two components of this system. The first is comprised to the coil systems to generate the gradient field. The second is used to generate and regulate the gradient current.

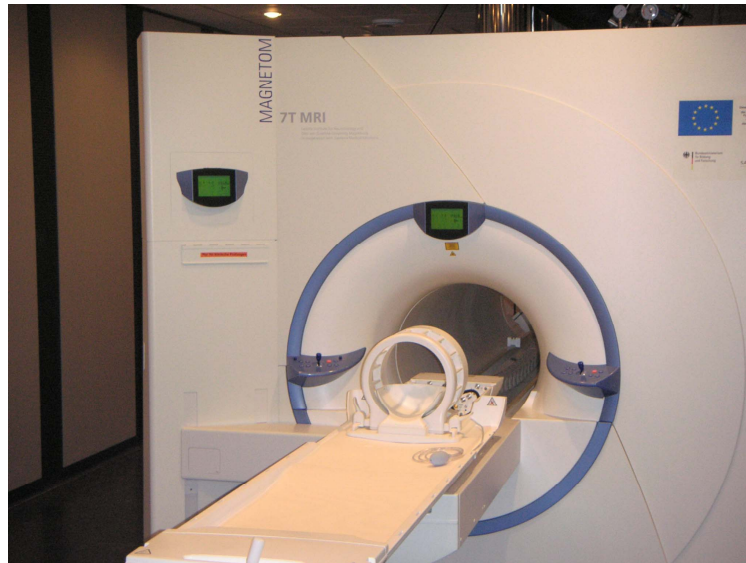


Figure 3.10: The whole body 7 Tesla system

3.10.3 Shimming Coil

The local variation of the magnetic field is different for each examined subject. The distribution of the magnetic field can be modified by varying the electric current within the shim coils, which produce additional magnetic fields of different spatial shapes. This process, called shimming, is necessary for spectroscopic measurements. The MRI scanner includes additional built-in coils known as shimming coils [58]. The current flowing in the shim coil controls the strength of the magnetic shim field.

3.10.4 Single Volume Coil

The transmitter / receiver coil excites the hydrogen atoms in the voxel and is to be examined as homogeneously as possible. All affected spins should have the same level of excitation. The receiver coil is used to receive an MR signal with as little noise as possible. The signal to noise ratio is dependent upon the excited volume in the coil and on the distance between the receiver coil and the VOI (filling factor) [65]. All the basis set spectra were acquired at 7T using the High-pass BirdCage coil. The model consists of a single tuned, highpass birdcage quadrature coil mounted in a shielded cylindrical plastic house [66].

3.10.4.1 CP Coil

The Doty quadrature coil (CP) interface is used to interface the Doty LitzCage Model to the 7T MRI whole body scanner. This device can split the RF transmission signal from the scanner into two quadrature signals that feed the volume coil. During the receipt of the acquired signal, the quadrature coil interface amplifies the MRI signal from both channels before sending them into the scanner.

Doty Litzcage coil includes the Circular-Polarization (CP) of the RF -birdcage coils, the insulated crossovers of the Doty linear Litz coil, and a novel symmetrising network to provide extraordinary B_1 homogeneity, superior SNR and exceptional simplicity in tuning to widely varying samples. The tuning of the small volume coil includes connecting the RF sweeper and adjusting the volume coil as shown in Fig. 3.11 (A). Preparing the measurement requires a connection between the two terminal connectors (right and left) of the interface box with the volume coil and a connection between the interface box with the scanner side as indicated in Fig. 3.11 (B).

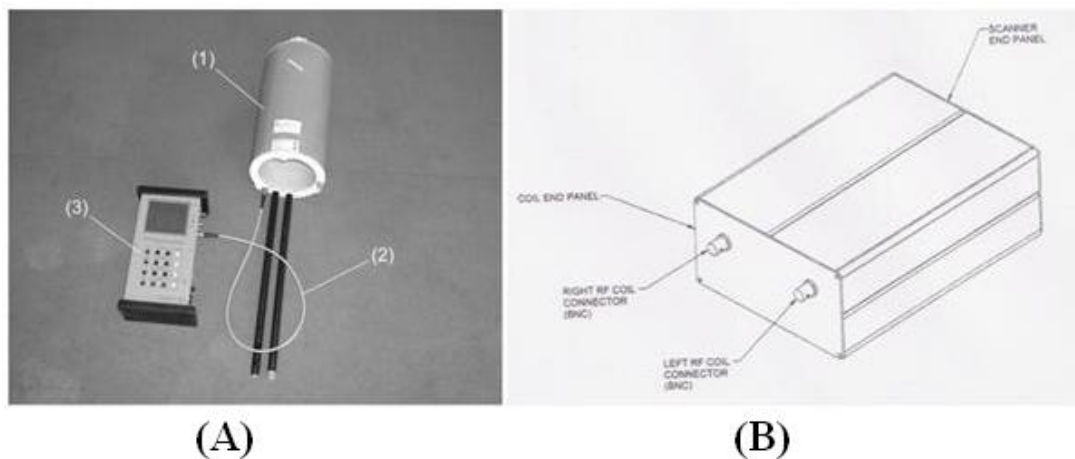


Figure 3.11: Volume coil setup (A) Tuning the coil at the 7T frequency circa 300MHz, (B) Connection of the coil with the scanner.

3.10.5 24 Channels Volume Coil)

All *in vivo* data was acquired by the 24 channels volume coil (Coil Set, Nova Medical, Inc.) at 7T MRI devices. This coil was designed for high human brain performance

imaging/spectroscopy on the 7T whole body instrument.

All the 24-channel particularly are used as receiver coils and only the volume coil is used as the transmitter coil. The volume transmit coil is based upon 30 cm diameter multiplied by the 20 cm long volume resonator enclosed within the 38 cm shield and open at both ends of the coil body.

Chapter 4

Results

The main goal of this work is to establish an 1H MRS method to detect and quantify a large number of human brain metabolites in the various brain areas, especially those that are not resolved at fields lower than 7T, such as Gln, GABA and NAAG. This study includes five stages of investigation, selection and optimization of the *RF* sequence parameters that produce good spectral resolution, measurement of 20 human brain metabolite solutions at short and long echo times, simulation of the same 20 metabolite spectra, creating the LCModel database of the *in vitro* spectra (measured and simulated databases), and finally using the created LCModel file to analyze the acquired human spectra.

4.1 *RF*-Flip Angle Optimization at 3T and 7T

The radiofrequency field B_1 is used to rotate the net magnetization vector M of a sample by a defined flip angle. The inhomogeneity of B_1 causes local variation of the flip angle in the sample. Therefore, the true flip angle depends on the position in the sample and may lead to a reduced signal and thus the efficiency. Localized adjustment of water suppression is routinely performed. However, local adjustment is time consuming. In this section, the experimental results demonstrate that the correct transmission voltage for signal generation can be calculated based on the local water suppression adjustment. Therefore, the current method optimizes the MR-spectroscopy *RF* flip angle resulting in the highest signal without additional scan time. To exploit the local water suppression (WS) adjustment for optimum signal, measurements were

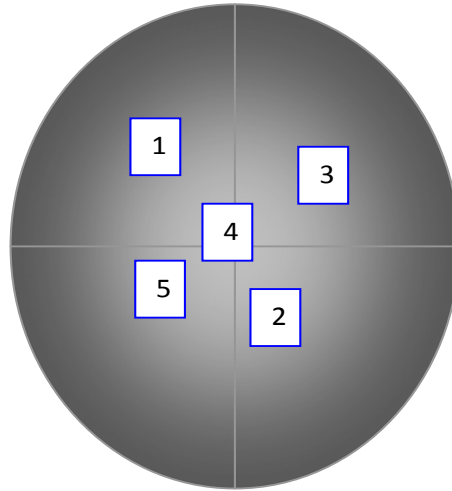


Figure 4.1: Different positions in a phantom sample (gray scale of the gradient echo image inverted)

performed on the whole body 3T and 7T systems. Single voxel proton spectra of a phantom were recorded in various positions in both scanners. A global adjustment was done for the whole sample to obtain a gradient-echo image using $TR = 100$ ms, $TE = 4$ ms, 8-channel head coil. Fig. 4.1 shows various positions, one of them at the center of the sample, where the B_1 field typically is the strongest and the other positions were distributed around the center where B_1 is lower.

Within the spectroscopy software supplied by the vendor a correction factor (Cf), defined as the ratio between the experimental WS voltage adjustment and the calculated WS voltage was present. A linear relationship exists between the correction factor and the applied WS voltage. Therefore, when the correction factor equals to one, the water suppression is correctly calculated and the true flip angle is achieved.

At 3T and 7T, PRESS and STEAM sequences have been applied respectively. In both fields, the following parameters have been used: $TR = 10$ s, $TE = 136$ ms, $VOI = 20 \times 20 \times 20$ mm³, $TM = 20$ ms (for STEAM only), flip angle = 90° , eight channel volume coil, WS-bandwidth = 35 Hz. The excitation voltage was varied from 110 V to 360 V at 3T and from 100 V to 400 V at 7T, for each voltage the maximum amplitude of water signal was determined.

A relationship between the water signal and the transmission voltage has been established for each position. Table 4.1 illustrates the data at different positions in the

Table 4.1: Correction factors and voltages at 3T and 7T scanners

At 3T(PRESS)			At 7T(STEAM)		
	position 1	position2		position1	position2
Cf	0.9454	1.0635	Cf	0.8890	1.1970
90°	296.764	296.764	90°	274.522	274.522
180°	367.733	367.733	90°	274.522	274.522
180°	367.733	367.733	90°	274.522	274.522
ws1	8.736	10.971	ws1	11.328	15.385
ws2	8.168	10.557	ws2	10.591	14.384
ws3	15.748	19.777	ws3	20.421	27.734

sample at 3T and 7T, all data are in volts, except for the correction factor which is unitless. 90° , 180° , 180° are the three spectroscopy pulses of the RF field and (ws1, ws2 and ws3) are the three water suppression pulses.

The correction factor Cf varied from one position to another due to B_1 field inhomogeneity. As shown in Table 4.1, at 3T the three RF voltages are different for the PRESS sequence ($90^\circ - 180^\circ - 180^\circ$). But at 7T the three voltages are identical for STEAM sequence ($90^\circ - 90^\circ - 90^\circ$).

At 3T, the excitation voltage which is the transmission voltage for the 90° excitation pulse (V_{exc}) was varied from 110 V to 360 V and the water signal intensity was recorded. In order to exactly determine the voltage for true 90° flip angle, the signal model $f(x) = a * \sin(b * x)$ has been used in order to fit the data points. Where $f(x)$ is the water signal intensity in (a.u.), x is applied voltage in volt and (a, b) are constants. Fig. 4.2 shows the water signal amplitude as a function of the transmitted excitation voltages at one position in the sample.

At 7T, a STEAM sequence has been used. Thus, three identical 90° pulses are employed and the voltage for all three pulses has been modified simultaneously. Fig. 4.3 shows the variation of the transmitted voltages of the STEAM sequence from 100 V to 400 V together with the measured water signal intensity at 7T. Besides, 240 V results in the highest water signal. As all three pulses have been modified in the STEAM sequence, the function $f(x) = a * \sin^3(b * x)$ has been used in order to fit

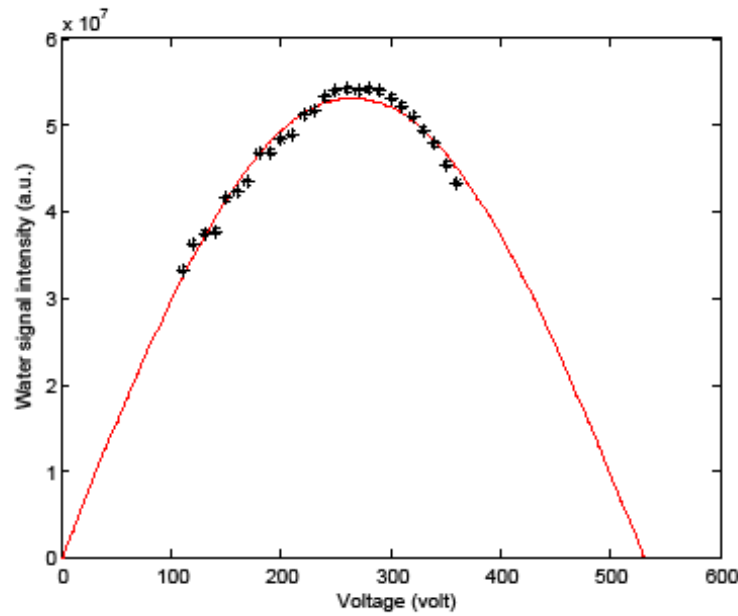


Figure 4.2: Measured data points of one position acquired at 3T while the red line is the fit using the equation $f(x) = a * \sin(b * x)$.

the data points and to calculate the voltage for the 90° flip angle. Fig. 4.2 and Fig. 4.3 refers to only one position at 3T and 7T, where V_{cal} is the calculated transmission voltage corresponding to the 90° flip angle. Fit parameters were calculated in MATLAB at both fields.

Table 4.2 shows that for each position in the sample, one flip angle corresponds to the highest signal (the experimental value) V_{exc} and the calculated voltage V_{cal} which predicted from the reference value. The ratio V_{cal}/V_{exc} is calculated and compared to the correction factor. Fig. 4.4 (A and B) illustrates the linear relationship between the ratio V_{cal}/V_{exc} and the correction factor Cf at 3T and 7T, respectively. $F(x) = a*x+b$ is a model of fit the data points where $F(x)$ is the ratio V_{cal}/V_{exc} , x represents the Cf , and a and b are the slope and y-axis intersection, respectively.

$$V_{cal} = V_{exc} * Cf \quad (4.1)$$

Finally, when the spectroscopy measurement is done at a position far from the center where B_1 is different from the nominal value the true flip angle is not achieved. This problem is solved by using Equation 4.1. V_{exc} and Cf are determined from the standard adjustment and thus the optimal transmission voltages that produce the

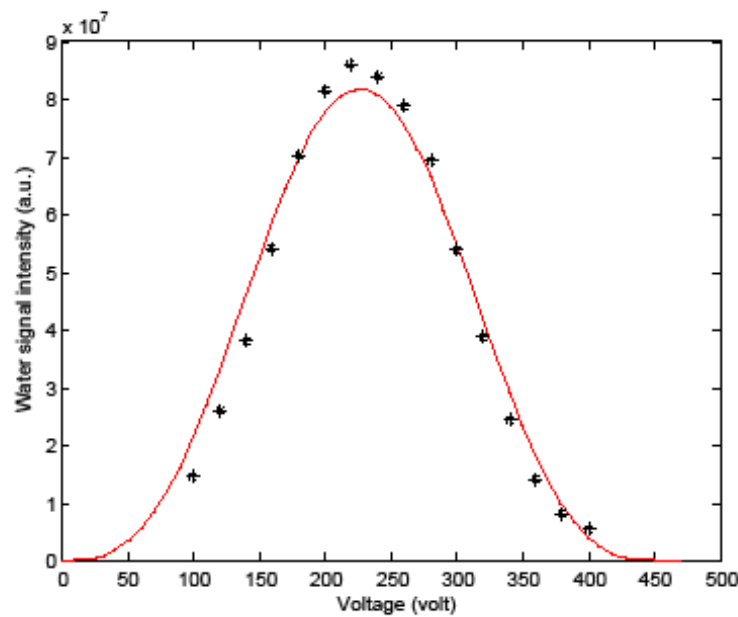


Figure 4.3: The fitting curve using $f(x) = a * \sin^3(b * x)$ for the experimental data points of one position examined at 7T

nominal true flip angle in the sample can be calculated. Therefore, based on the spectroscopy adjustments to determine the water saturation voltage and the correction factor, a new reference voltage can be calculated by multiplication of the original value with the WS correction factor. If a second water suppression adjustment is performed, the new correction factor is approximately one i.e. the correct flip angle has been achieved. Table 4.3 indicates different values of the correction factor before and after using equation 4.1.

4.2 Comparison between STEAM and STEAM with VERSE Pulses

The results of the previous section show that the required transmitted voltage for the true 90° flip angle changes as the position of the voxel changes in the sample. Also, it was clear that the standard sequences STEAM and PRESS need high power to achieve the true excitation flip angle. Therefore, STEAM adapted with variable rate selective excitation (VERSE) [22] was used in order to reduce the required power. A comparison between the standard STEAM and the STEAM with VERSE was done to estimate

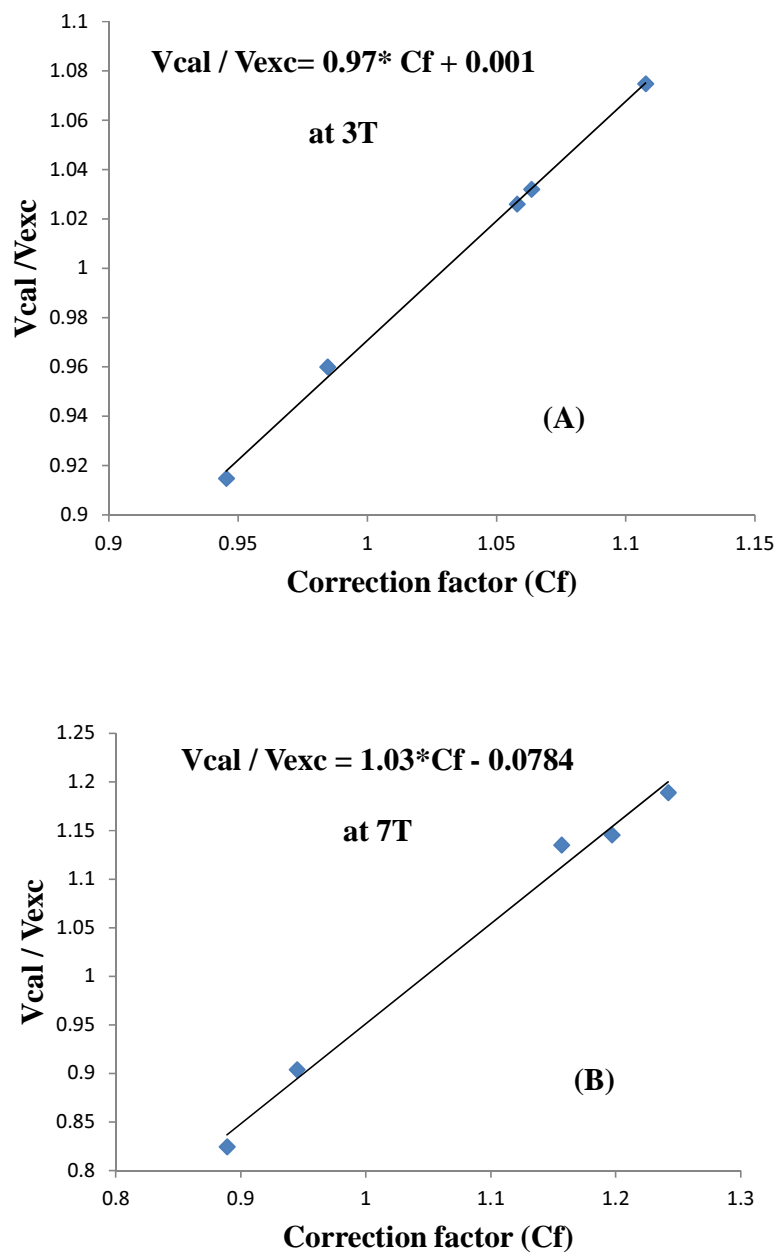


Figure 4.4: The relationship between the correction factor and the fraction V_{cal}/V_{exc} at 3T B) The relationship between the correction factor and the fraction V_{cal}/V_{exc} at 7T.

Table 4.2: The excitation voltages and the calculated voltages for different positions at 3T and 7T.

At 3T					
	Position 1	Position 2	Position 3	Position 4	Position 5
Cf	0.9454	1.0635	1.1077	0.9846	1.0579
V_{exc}	296.764	296.764	296.864	297.144	297.44
V_{cal}	271.487	306.268	319.076	285.255	305.186
$\frac{V_{cal}}{V_{exc}}$	0.9148	1.032	1.0748	0.96	1.026
At 7T					
	Position 1	Position 2	Position 3	Position 4	Position 5
Cf	0.8890	1.1970	0.9450	1.1567	1.2420
V_{exc}	274.522	274.522	274.522	262.118	262.118
V_{cal}	226.339	314.432	248.151	297.4990	311.665
$\frac{V_{cal}}{V_{exc}}$	0.8245	1.1454	0.9039	1.1350	1.1890

the degree of power reduction. Fig. 4.5 shows the relation between the required transmitted voltage and the water signal intensity. This comparison has been done in the range from 160 to 550 V. For each voltage, the water signal intensity was recorded. All data were acquired at 7T with scan parameters TR/TE/TM = 3000/20/15 ms, which remained the same during all the measurements, except that the VERSE factor changed from 1 to 1.4 for standard STEAM sequence to STEAM with VERSE pulses, respectively. The calculated transmit voltage V_{cal} in equation 4.1 can be used to adjust the voxel which is located far from the center of the sample. Moreover, Fig. 4.5 shows that the required voltage for the 90° flip angle is 320 volts using standard STEAM and is 253 using STEAM with VERSE, i.e. the voltage reduced by 28 % using STEAM with VERSE pulses. It is important that all the following measurements, either *in vitro* or *in vivo* have been done using STEAM with VERSE pulses.

Table 4.3: The resultant data at 3T and 7T.

(Cf)	V_{cal}	New (Cf)
1.308	352.7	1.003
1.102	306.4	1.000
0.925	421.6	0.968
1.058	421.6	1.031
1.327	349.6	1.085
0.913	387.1	0.989

4.3 Database Spectra Measured at 7T

All *in vivo* spectra in the experimental basis set were acquired with high S/N. Moreover, single volume spectroscopy (SVS) as localization method, STEAM with VERSE pulses, and intensive shimming were a good combination to accomplish the acquisition of high quality spectra.

STEAM with VERSE pulses has been used with short TE = 20 ms and long TE = 74 ms. All the *in vitro* measurements of 20 metabolite solutions were acquired at 7T with TR = 3000 ms and (TE = 20 ms and TM = 15 ms) and (TE = 74 ms and TM = 68 ms) as shown in Figs. 4.6 and 4.7, respectively. The advantage of using short TE is that the SNR is higher than that of the long TE. However, long TE indicates a reduction in the baseline distribution.

4.4 Comparison between Measured and Simulated Glutamate Spectrum

Although the experimental database reflects all the real conditions of the experimental measurements, the materials used cost money. In this work, the simulated database spectra have been simulated using the nuclear magnetic resonance simulation program *NMR-SIM*. This program attempts to simulate the real scan parameters, although the calculation is based on an ideal spectrometer and ignores the effect of magnetic field inhomogeneity. *NMR-SIM* (learning version) is based on a density matrix with

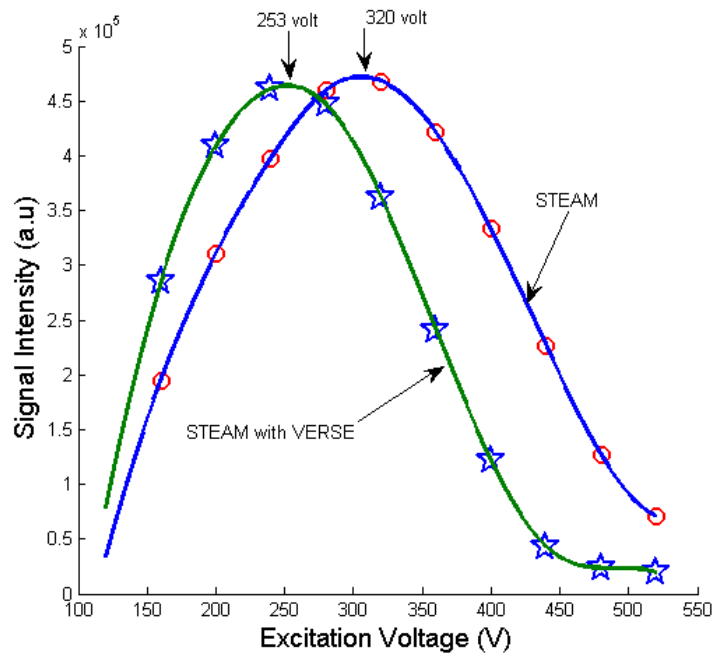


Figure 4.5: Comparison between the STEAM and STEAM with VERSE pulses.

relaxation phenomena implemented using a simple model based on Bloch equations. [67]. The spin system of 20 human brain metabolites and the pulse sequence are explained in the previous chapter and illustrated in detail in Appendix (C). Fig. 4.8 shows a simulated (red line) and measured (blue line) spectra of glutamate with 20 ms at 7T. This figure indicates the peaks of the CH₂ group at 2.35 ppm of the two databases. Therefore we can use the simulated database to create the LCModel basis set to analyze the human data.

4.5 Comparison between Experimental and Simulated Basis Sets

Figures 4.9 and 4.10 show the fit of the ¹H-MRS human brain spectrum measured in the Brodmann 23C region from a healthy volunteer using experimental and simulated basis sets, respectively. The LCModel fit is the same in both figures. Further, the SNR are the same and also the two baselines are identical. However, the absolute

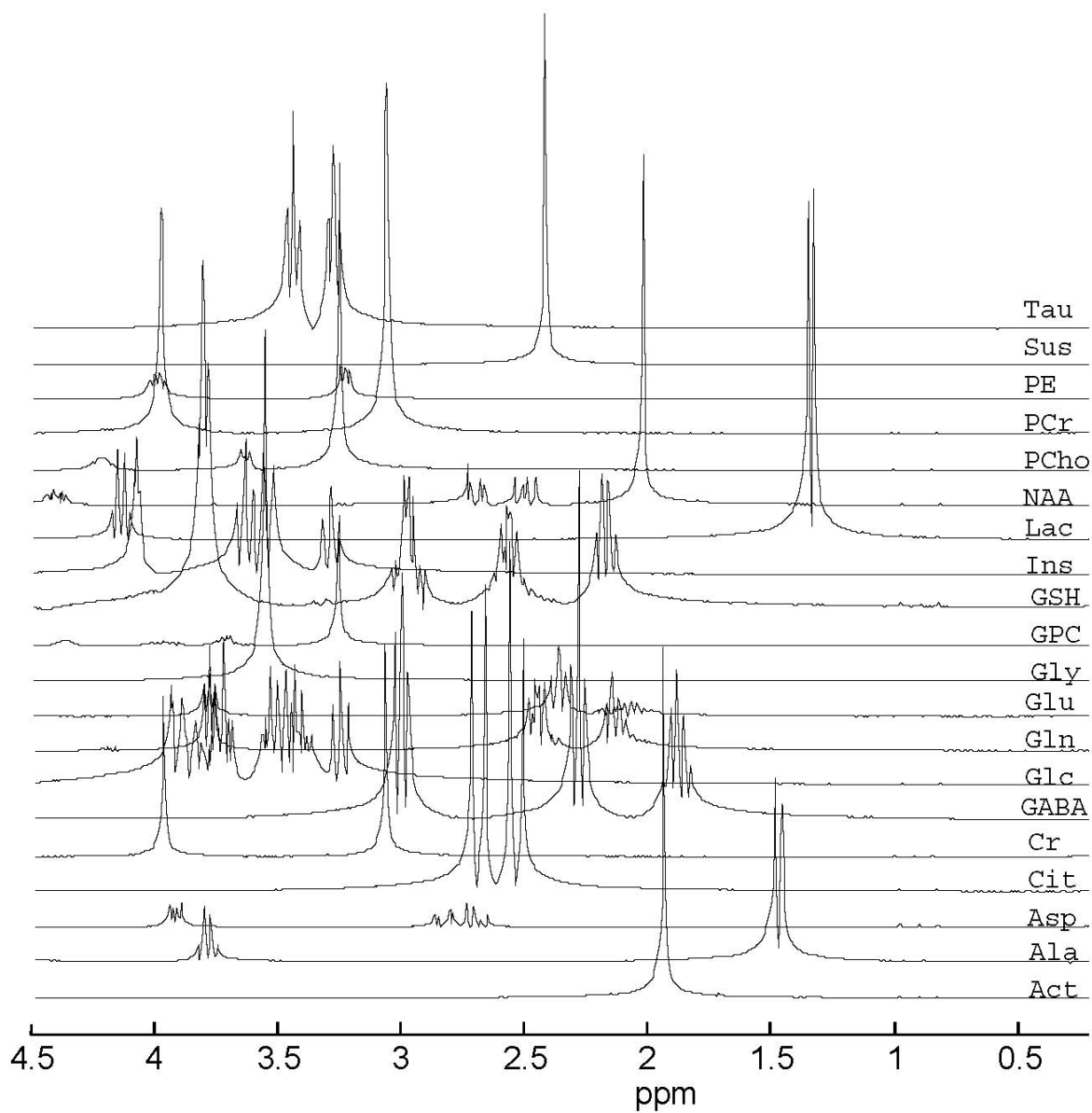


Figure 4.6: Twenty metabolite spectra of the *in vitro* database using TR = 3 s, TE = 20 ms and TM = 15 ms at 7T

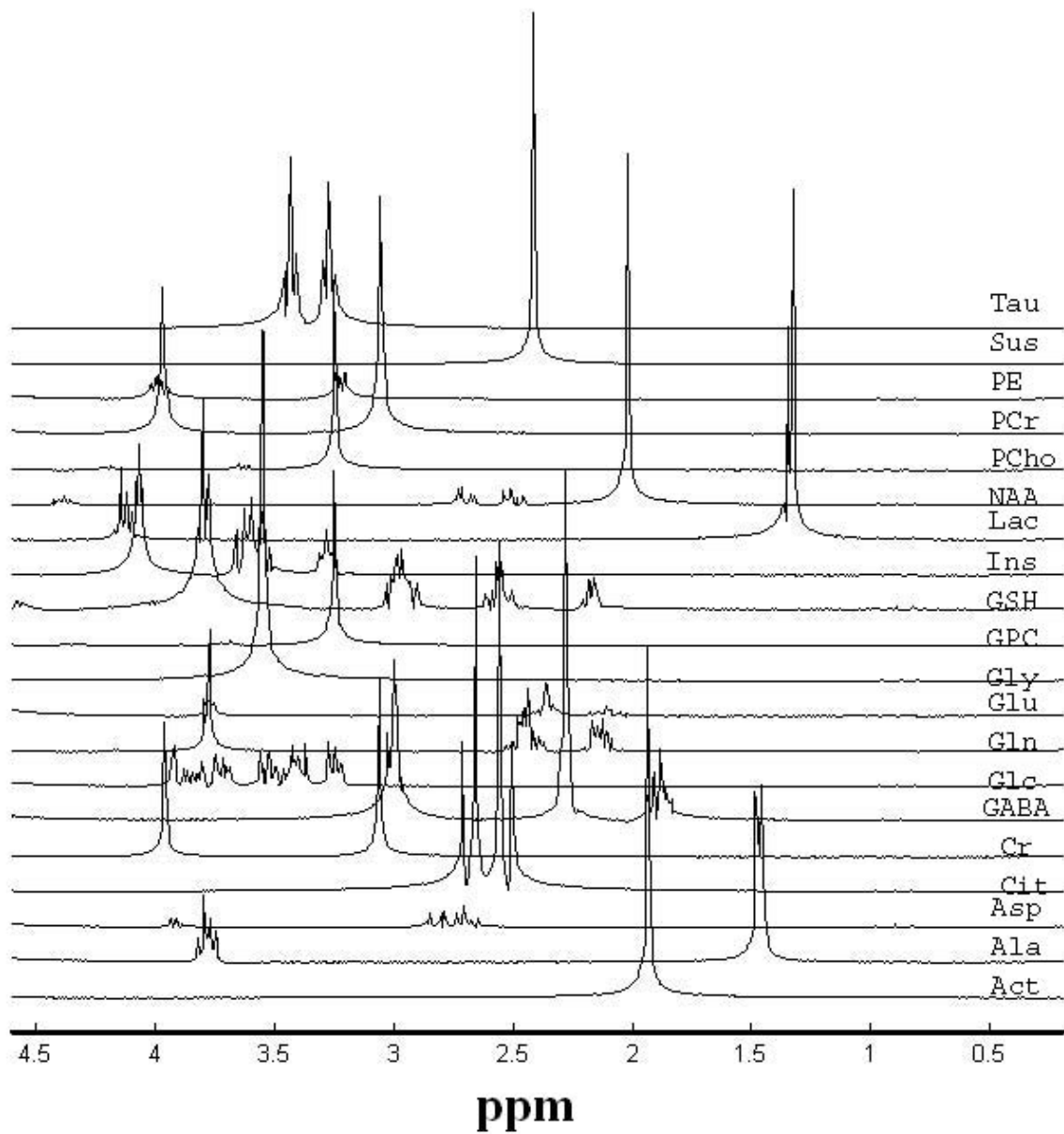


Figure 4.7: The 20 *In vitro* spectra of metabolite solutions using long TE = 74 ms and TM = 68 ms at 7T

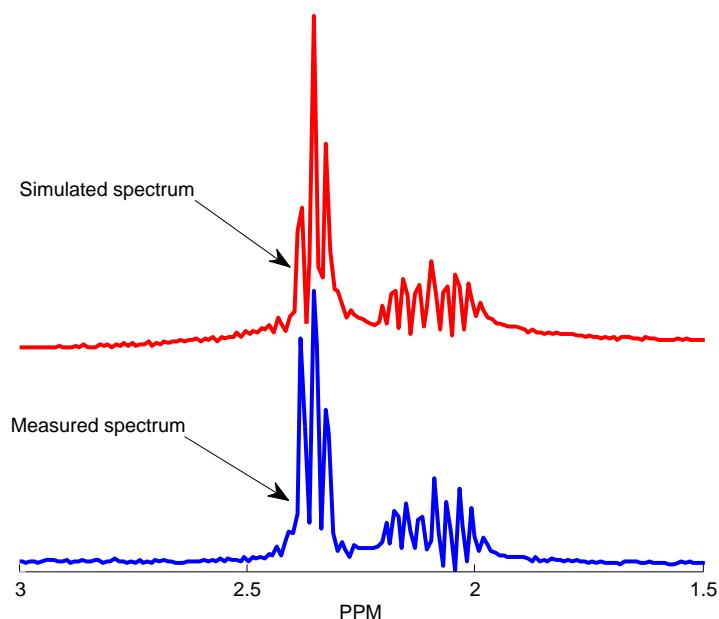


Figure 4.8: Simulated and experimental spectra of Glutamate solution using $TE = 20$ ms at 7T

concentration of the human brain metabolites in both Figs. are not well matched as the fact that in the simulation processing the real conditions are neglected. The simulation runs in the ideal condition of ideal spectrometric devices. Even though there are some differences between the concentration values in two LCModel fits, these values closely approached to values of the previous study [47].

Table 4.4 illustrated the comparison between the absolute concentration of 6 healthy subjects; (mean \pm SD) of human brain metabolites using experimental and simulated basis sets. The differences in the two quantifications are because the experimental data were acquired under real conditions; therefore, different parameters did not match with the simulation process, such as the temperature, receiving / transmitting coils and the signal noise.

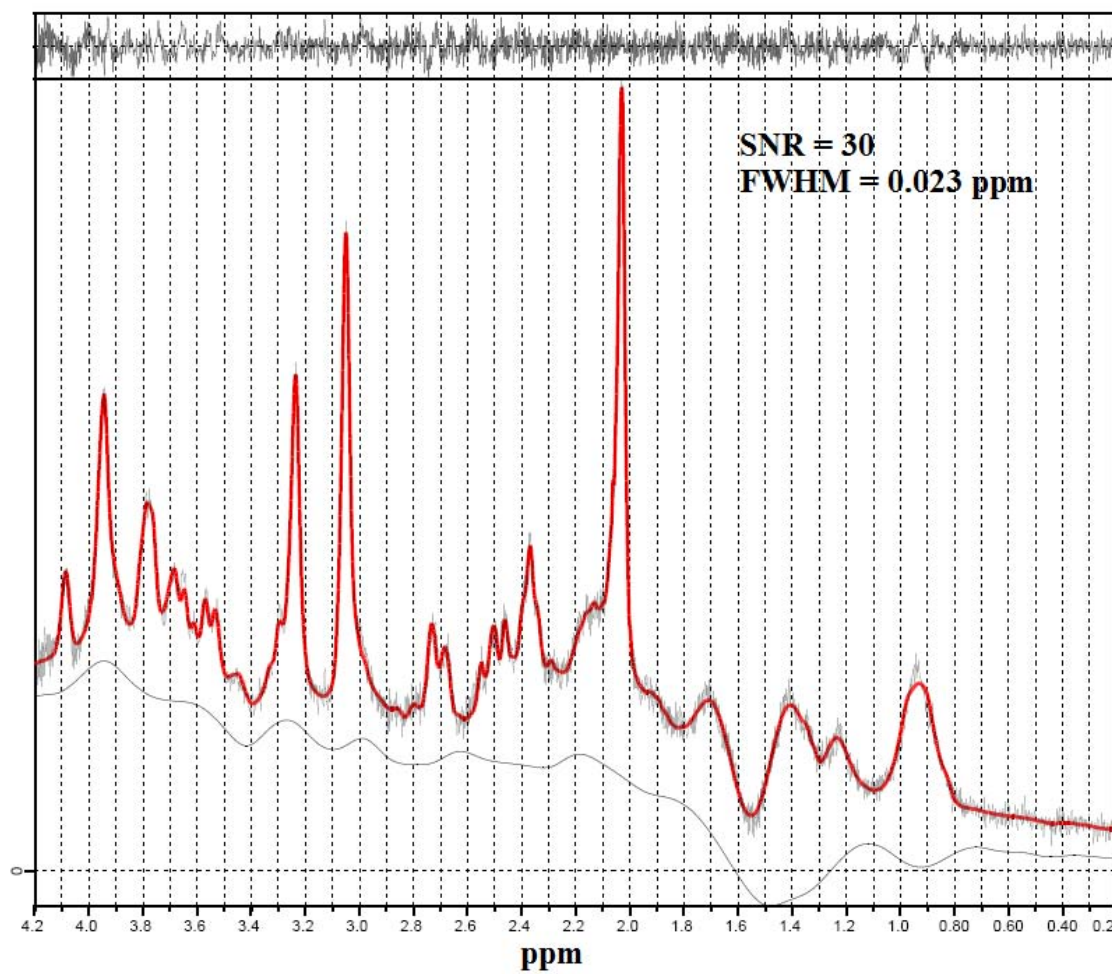


Figure 4.9: LCMdel fit of ^1H -MRS human brain spectrum measured in the Brodmann 23C region from a healthy volunteer using experimental basis set with $\text{TR} = 3$ s, $\text{TE} = 20$ ms and $\text{TM} = 15$ ms at 7T

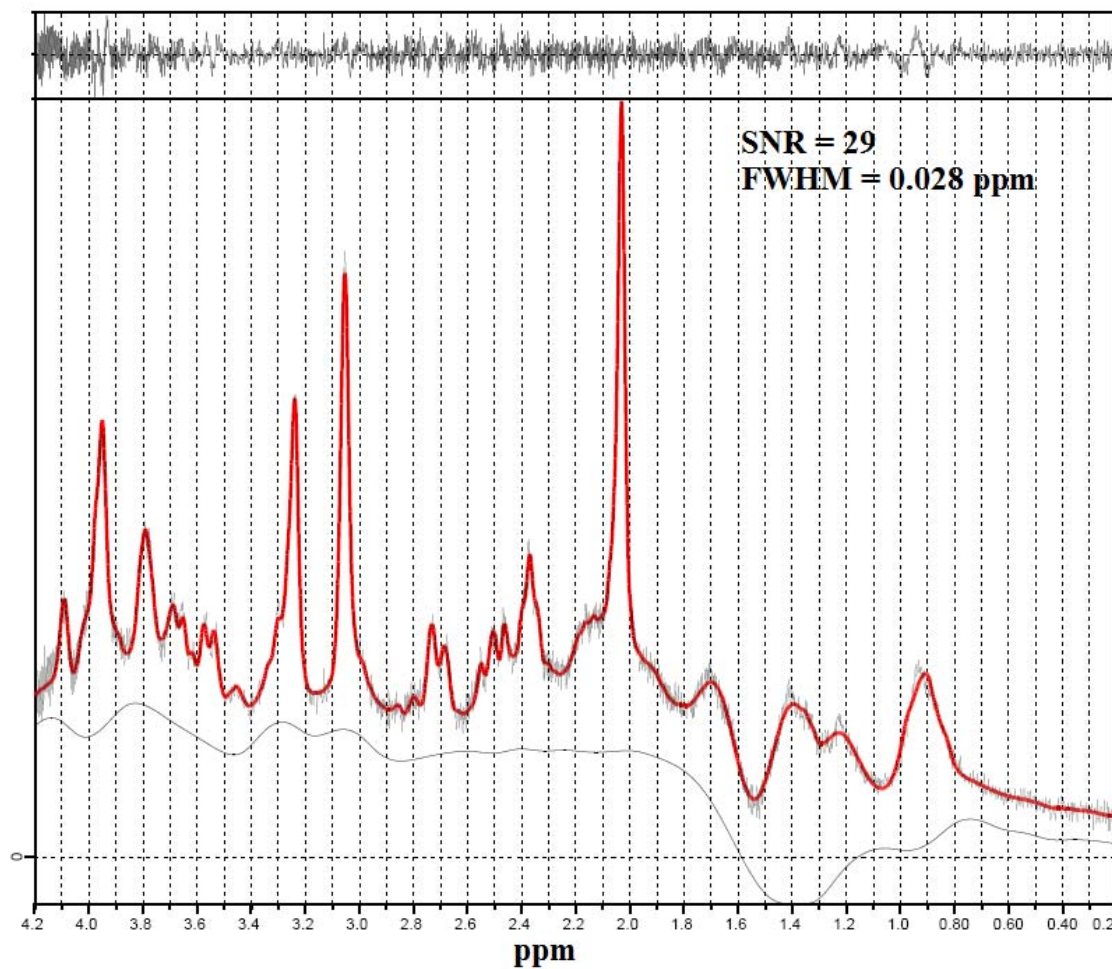


Figure 4.10: ^1H -MRS human brain spectrum measured in the Brodmann 23C area from a healthy volunteer. The red line shows the LCMoDel fit using the simulated basis set (WIN-SIM) with $\text{TR} = 3$ s, $\text{TE} = 20$ ms and $\text{TM} = 15$ ms and at 297.14 MHz (7T)

Table 4.4: Comparison between the absolute concentrations of the human brain metabolites of 6 healthy subjects at 7T using simulated and experimental basis sets

Metabolite	Experimental basis set Concentrations \pm SD	Simulation basis set Concentrations \pm SD
NAA	9.31 ± 1.90	9.43 ± 2.02
Cr	5.82 ± 1.16	5.21 ± 0.90
Glu	8.62 ± 0.85	9.58 ± 1.03
Gln	2.09 ± 0.97	1.32 ± 1.22
GABA	0.85 ± 0.21	0.94 ± 0.27

4.6 Human Acquisition Time Optimization

In the earlier studies [15], STEAM has been used under completely relaxed conditions $TR = 6000$ ms and $TE = 20$ ms in order to minimize corrections due to T_1 and T_2 attenuation, and the spectra of metabolites with strongly coupled resonances can be depicted. Moreover, errors due to the different T_1 times of protons within a metabolite are avoided by using fully relaxed *in vivo* spectra with $TR = 6$ s at 2T [68].

As a follow up of these studies, the proton MR spectra were obtained using the STEAM with VERSE pulses with $TR = 2, 2.5, 3$ s and $TE = 20$ ms has been used to optimize the TR and number of averages, where the signal to noise ratio is a function of TR and the number of average (Av) together. Fig. 4.11 shows three spectra acquired from a human brain. The acquisition time (At) is selected to be constant and equals 6 mins and 40 seconds. Table 4.5 represents three groups of data measured in the pgACC brain region and acquired at 7T. The results of these *in vivo* measurements is that $TR = 3$ s and $Av = 128$ are the optimized parameters in this study.

4.7 Analysis of Human Brain Data using Short and Long TE Database

Fig. 4.12 and Fig. 4.13 show the 1H -MRS human brain spectra measured in the pgACC region with the short echo time $TE = 20$ ms and the long $TE = 74$ ms, respectively. The *in vivo* data was analyzed using LCModel of the basis sets using

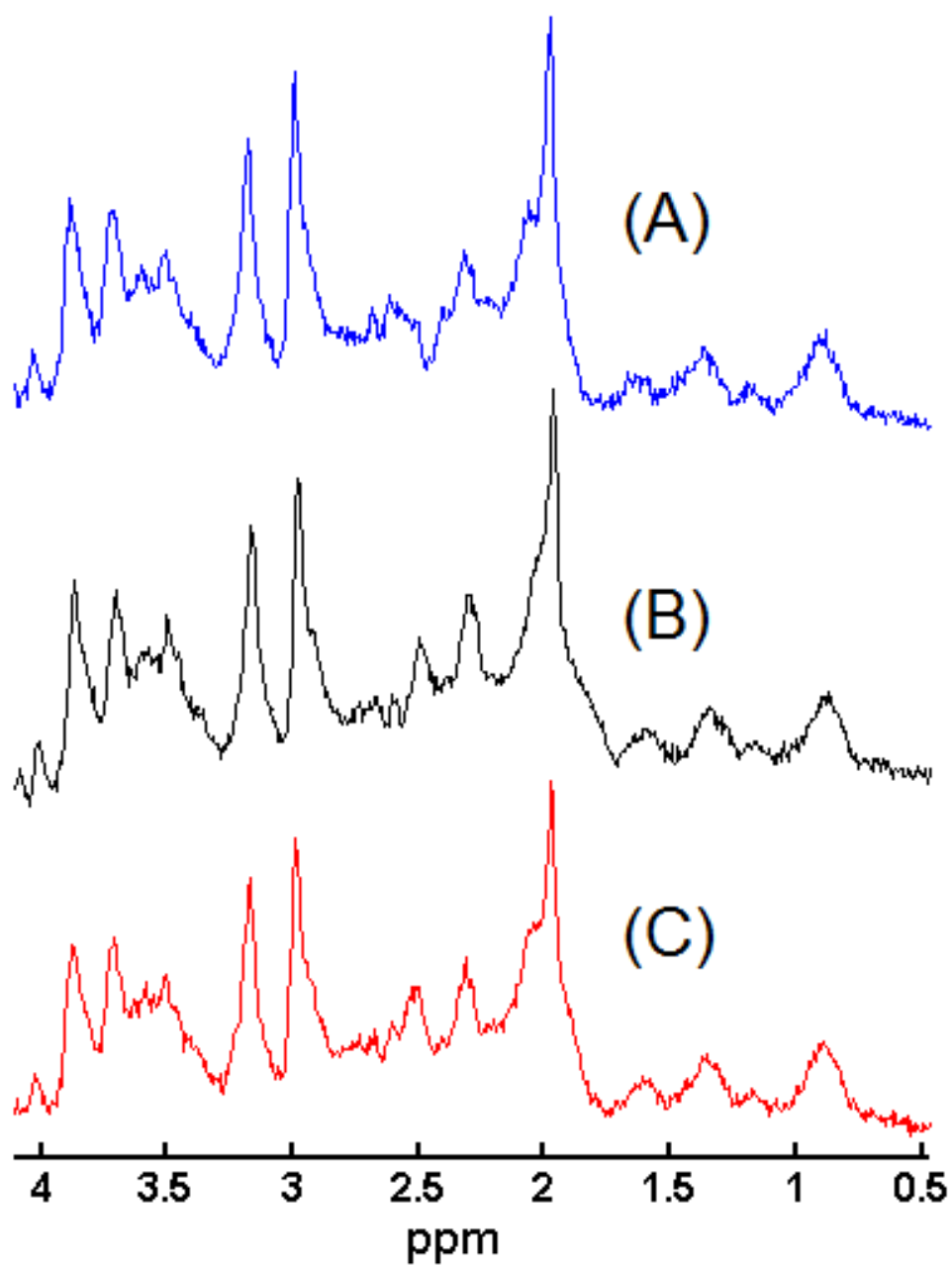


Figure 4.11: Three human brain spectra measured in the pgACC region with different number of averages and TR of the same healthy subjects. (A) TR = 3000 ms, averages = 128 (B) TR = 2500 ms, averages = 152 (C) TR = 2000 ms, averages = 192.

Table 4.5: Three groups of spectra measured in the pgACC brain region of five healthy subjects at 7T.

Group	TR (s)	Averages	At (min)	S/N
A	3	128	6.4	310.52 ± 43.82
B	2.5	152	6.4	283.85 ± 44.54
C	2	192	6.4	263.72 ± 42.13

short and long TE. The SNR and full width at half maximum (FWHM) of NAA metabolite using short TE are $\text{FWHM} = 0.032$ ppm and $\text{S/N} = 28$. However, with long TE = 74 ms are $\text{FWHM} = 0.032$ ppm and $\text{S/N} = 22$. This result conforms the previous observations of the phantom measurements. Also, the LCModel fit at TE = 74 ms illustrates the signal decay of the macromolecules (MM) and lipids, especially in the range from 0.2 ppm to 2 ppm.

4.8 Comparison between the 3T and 7T Human Spectra

4.8.1 Using PRESS at 3T and STEAM with VERSE Pulses at 7T

All measurements were done using healthy volunteers. The volume of interest (VOI) was selected according to the anatomical dimensions of the pgACC target regions. Fig. 4.14 (A and B) shows the human brain spectra measured in the pgACC region with 128 averages at 7T using STEAM with VERSE ($\text{TR/TE/TM} = 3000/20/15$ ms, $V_f = 1.4$) and at 3T [69] PRESS with $\text{TR/TE} = 2000/35$ ms and 256 of averages were used

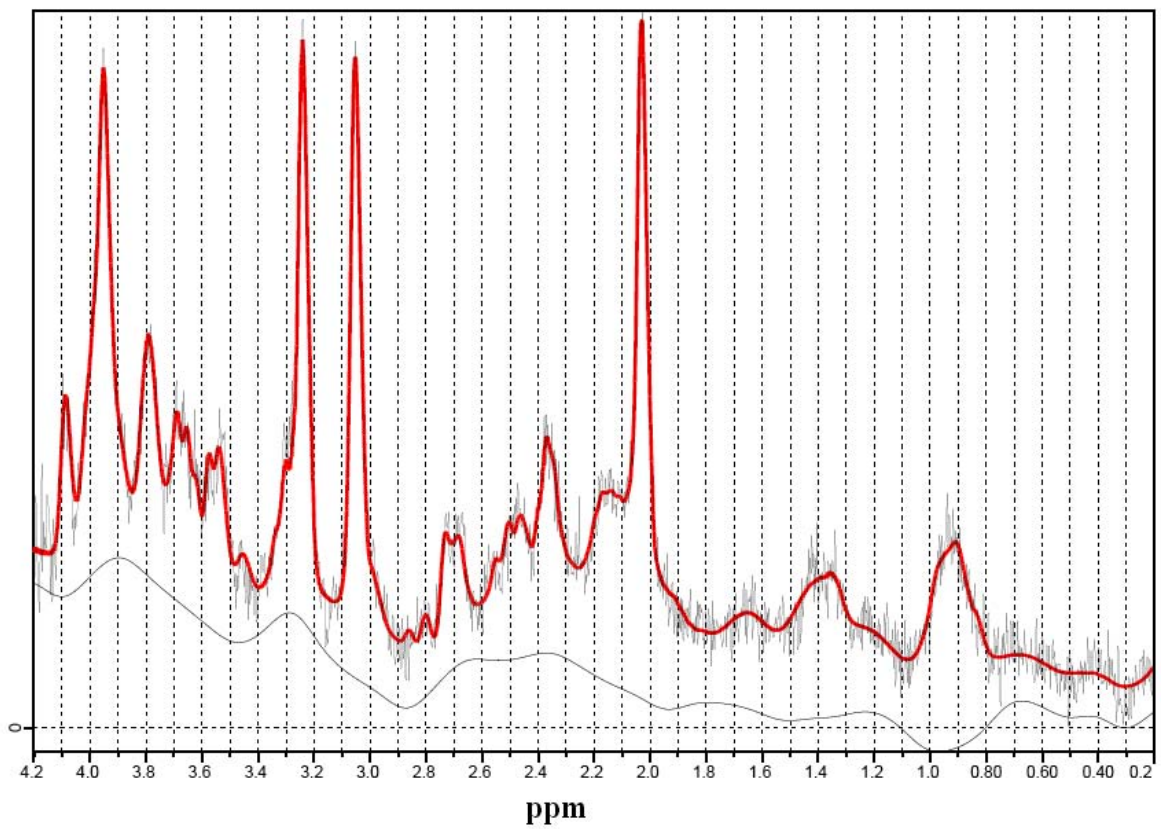


Figure 4.12: LCModel fit spectrum of the human brain data measured in the pgACC region using the simulated basis set of $TR=3000$ ms, $TE = 20$ ms and $TM = 15$ ms at $7T$

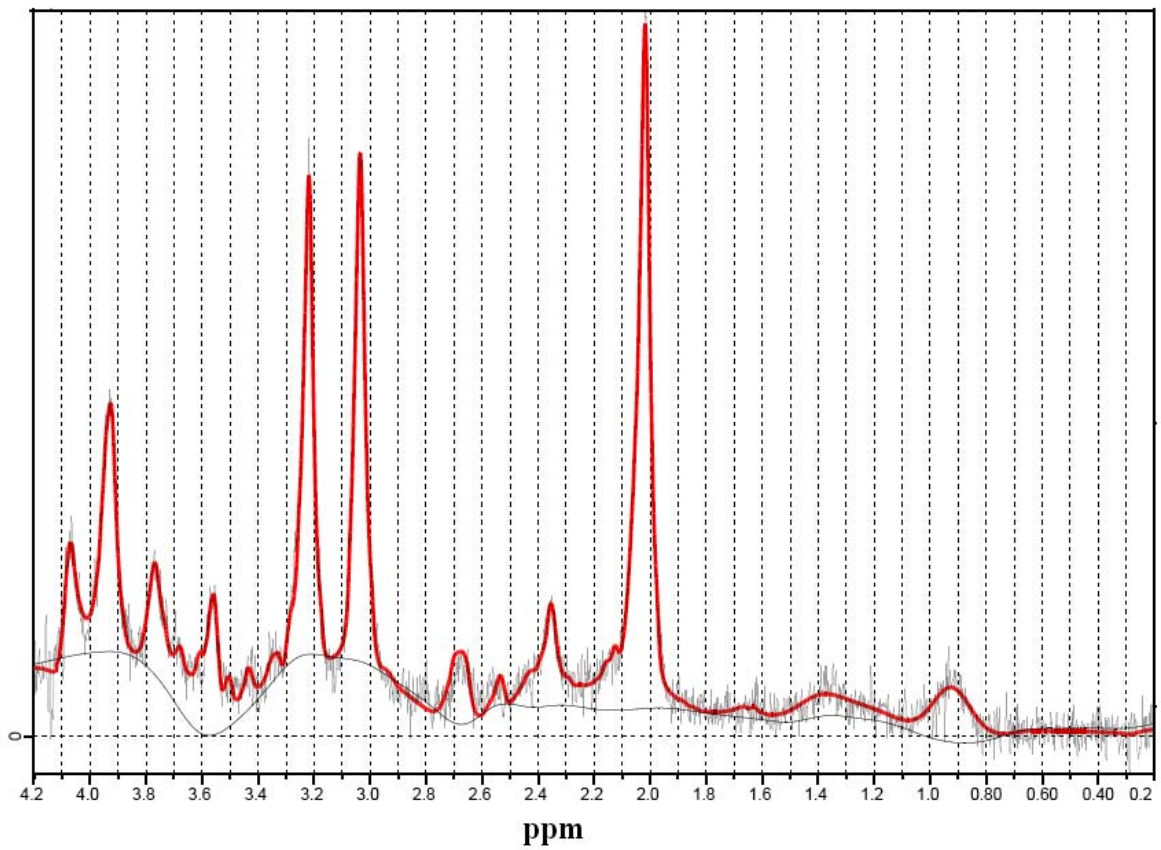


Figure 4.13: LCMODEL fit spectrum of human brain data measured in the pgACC region using the simulated basis set of $TR=3000$ ms, $TE = 74$ ms and $TM = 68$ ms at 7T

4.8.2 Using STEAM with VERSE Pulses at 7T and JPRESS at 3T

A comparison was done between the quantitative metabolite concentrations of glutamine, glutamate, N-acetylaspartate, gamma-aminobutyric at 3T [70] and their concentrations at 7T (in this study). The spectra were measured in the pgACC region. Table 4.6 shows the metabolite concentrations that are given relative to creatine as published in the corresponding study [70]. The results of our measurements at 7T concur well with this study that used J-resolved PRESS (JPRESS) spectroscopy with rather long scan times of 16 mins and a large voxel size of approximately 17 mL compared with 1.75 mL in our 7T data. A further advantage is that, although JPRESS provides encoding of the J-coupling, thus improving the specificity in detecting the J-coupled metabolites and alleviating the major limitation of 1D MRS [71], using the STEAM adapted with VERSE at 7T has proved sufficient to detect J-coupled human brain metabolites such as Gln, Glu and GABA in a shorter scan time relative to the corresponding study.

Table 4.6: Comparison between the relative concentration levels of metabolites in pgACC at 7T using STEAM with VERSE at 7T and PRESS at 3T (3 subjects) relative to JPRESS at 3T.

Metabolites	STEAM with VERSE	PRESS	JPRESS
	at 7T	at 3T	at 3T [70]
	Mean \pm SD	Mean \pm SD	Mean \pm SD
Cr (mM/kg)	5.45 \pm 0.85	7.51 \pm 0.77	6.30 \pm 0.96
GABA/Cr	0.25 \pm 0.07	0.18 \pm 0.13	0.21 \pm 0.07
Gln/Cr	0.29 \pm 0.12	0.25 \pm 0.43	0.34 \pm 0.15
Glu/Cr	1.42 \pm 0.26	1.03 \pm 0.63	1.35 \pm 0.13
NAA/Cr	1.56 \pm 0.17	1.53 \pm 0.35	1.50 \pm 0.15

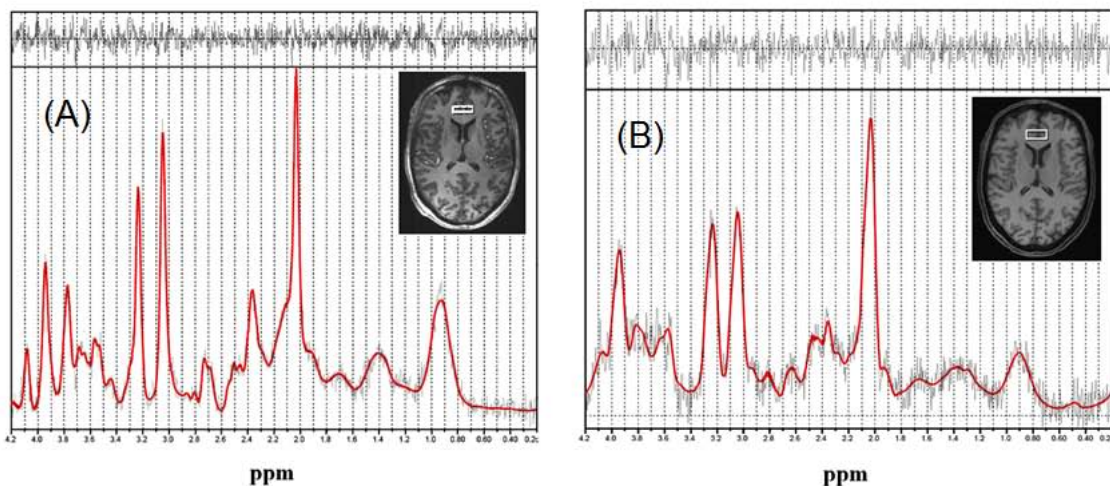


Figure 4.14: Human brain NMR spectra were acquired from the pgACC region in one volunteer a) at 7T using STEAM with VERSE, 128 averages, TR/TE/TM = 3000/20/15 ms, and voxel volume = 1.8 mL and b) at 3T using PRESS, 256 averages, TR/TE = 2000/35 ms, voxel volume = 2.5 mL, together with the LCMoDel fitting curve.

4.9 Human Brain Spectra Measured in Five Different Locations

Study of the human brain metabolism non-invasively can be done using 1H -MRS method which can be used markers for specific diseases [1, 2]. Clinical magnetic resonance spectroscopy MRS has attracted much attention in recent years [72]. As the proton is the most sensitive stable nucleus, and as almost all the metabolites contain hydrogen atoms, this study focused on the proton excitation method 1H -MRS. STEAM with VERSE pulses was used to perform a noninvasive chemical analysis on tissues the deep within the human brain of the subjects. Moreover, short echo time and reproducible water suppression increased the number of metabolites which can be detected and identified [73]. Roland Kreis in 1991 [74] used the Localized 1H MR spectroscopy technique with short echo TE = 30 ms to acquire human brain spectra from an area in the parietal cortex of three patients suffering from chronic hepatic encephalopathy and compared them with the equivalent spectra obtained from healthy control subjects at 1.5T. Also, in 2011 MRS was used in clinical diabetes, a disease where the increase in Intramyocellular acetylcarnitine associated with moderate aerobic

exercise in individuals with type 1 diabetes was significantly higher in euglycemia than in hyperglycemia. Moreover, Boss and Kreis at 1.5T [72] have used the localized volume of 2.4 mL, PRESS spectroscopy localization with TR of 3 s, TE of 20 ms. Spectra were analyzed using time and frequency domains (TDFDFit) [75]. In this work, a linear combination model (LCModel) has been used to analyze the *in vivo* data. The LCModel is working in the frequency domain, where the metabolite peak area is used in absolute concentration calculations.

4.9.1 Parietal Region

Fig. 4.15 shows analyses of a phase-corrected spectrum measured at 7T in the parietal brain region using the single volume spectroscopy technique. Fig. 4.15 (A) indicates the volume of interest in the reference image. The thin line indicates the raw data while the solid line shows the LCModel fit (red color) as seen in Fig. 4.15 (B and C), respectively. The narrow line width $\text{FWHM} = 0.027$ ppm of NAA indicates a good field homogeneity at 7T. Besides, the human brain metabolites (Glu and Gln), (Cr and PCr) and (NAA and NAAG) can be separated and detected at 7T, which normally does not separate at a lower magnetic field strength [15, 76].

Table 4.7 shows the absolute concentration values of 15 human brain metabolite measured in a white matter (WM) parietal region of 8 healthy volunteers age 25 - 45 years. In addition to the CRLB values of the quantification. The concentrations and CRLB values have been obtain from LCModel analyses. All the metabolites show CRLB values less than 20 % except for Gln, which has a value of 22.25 ± 1.92 . This CRLB value of Gln is acceptable in the WM regions. Moreover, in this region NAAG can be resolved from NAA at 7T and also in various other brain regions as will be discussed further on.

4.9.2 Pregenual Anterior Cingulate Cortex (pgACC)

Functional imaging studies suggest a specific role of the anterior brain regions in the pathogenesis of major depression. Auer et al. in 1999 [77] evaluated the possible neurochemical alterations in the frontomesial cortex in patients with a major depressive episode using $^1\text{H-MRS}$ with PRESS of $\text{TR/TE} = 2000/35$ at 1.5 T. Further, Glu

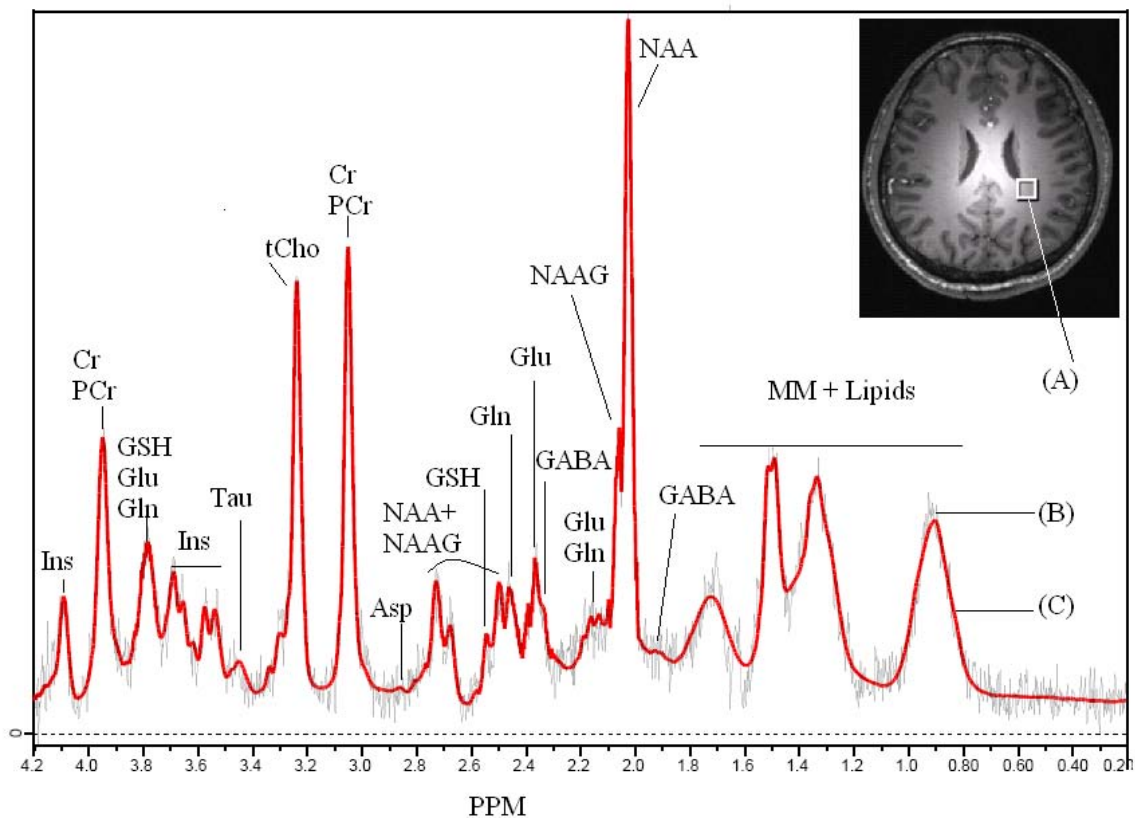


Figure 4.15: *In vivo* ^1H - NMR spectrum acquired from the parietal white matter at 7T. STEAM with VERSE ($V_f = 1.4$), $\text{TR}/\text{TE}/\text{TM} = 3000/20/15$ ms, voxel volume = 151515 mm^3 , $\text{BW} = 3600$ Hz, acquisition size = 2048, and averages = 128. (A) VOI location (B) measured data (C) LCMoDel fit of the spectrum

Table 4.7: Concentration levels of human brain metabolites of 8 healthy volunteers in the parietal region.

VOI = 3.38 mL (parietal region (WM))		
Metabolites	Concentrations Mean \pm SD (mM/kg)	CRLB \pm SD (%)
Asp	2.42 \pm 0.25	17.00 \pm 4.42
Cr	4.67 \pm 0.93	2.25 \pm 0.43
GABA	1.23 \pm 0.24	17.50 \pm 6.02
Gln	1.17 \pm 0.31	22.25 \pm 1.92
Glu	6.45 \pm 1.19	5.50 \pm 1.12
GPC	1.31 \pm 0.29	7.25 \pm 1.48
GSH	1.38 \pm 0.19	12 \pm 3
Ins	2.58 \pm 0.36	7.25 \pm 1.48
NAA	10.82 \pm 1.54	2.00 \pm 0.00
NAAG	0.90 \pm 0.27	7.75 \pm 1.30
PCr	2.91 \pm 0.64	9 \pm 2
PE	2.46 \pm 0.89	13 \pm 6
Tau	1.2 \pm 0.35	19 \pm 8
GPC + Cho	2.75 \pm 0.43	3.1 \pm 0.04
Ins + Gly	3.28 \pm 0.31	6.75 \pm 1.64

and Gln peaks cannot be successfully resolved using PRESS at 1.5 T because of the overlapping of the metabolite peaks of Glu, Gln and GABA [23, 24]. Moreover, Glu and Gln were often indistinguishable at lower field strengths [78]. Also, the Glx (Glu and Gln) signal is primarily dominated by Glu [79, 80]. As the majority of the available studies suggests higher Glx levels in bipolar patients in the frontal lobe, the direction of change in the Glx levels appears to be opposite in bipolar and unipolar affective disorders [81, 82]. All those studies demonstrate that determining the Glu/Gln concentration is vitally important for patients who suffering from Major Depressive Disorder (MDD).

Fig. 4.16 shows the LCModel fit of the human brain spectrum acquired from the grey matter (GM) pgACC region at 7T. Fifteen human brain metabolites have been detected and quantified with CRLB values less than 20 %, except for NAAG which has a CRLB value greater than 20 %. It is not mean that there is no NAAG in pgACC

region but only means that with the scan parameters TR=3 s, TE=20 ms and TM=15 ms were not the best.

Table 4.8: Concentration levels of the human brain metabolites of 8 healthy volunteers in the pgACC region.

VOI = 3.5 mL (pgACC region)		
Metabolites	Concentrations Mean \pm SD (mM/kg)	CRLB \pm SD (%)
Asp	2.08 \pm 0.98	16.67 \pm 8.08
Cr	5.44 \pm 0.85	2.83 \pm 0.37
GABA	1.36 \pm 0.06	16.50 \pm 3.25
Gln	1.59 \pm 0.10	12.08 \pm 10.40
Glu	7.74 \pm 0.22	5.00 \pm 1.15
GPC	1.46 \pm 0.16	6.50 \pm 2.22
GSH	0.74 \pm 0.16	13 \pm 3
Ins	2.98 \pm 0.86	7.00 \pm 2.16
NAA	8.51 \pm 0.15	2.83 \pm 0.13
NAAG	0.19 \pm 0.06	31.73 \pm 4.45
PCr	1.79 \pm 0.18	5.00 \pm 1.80
PE	1.44 \pm 0.10	11 \pm 1
Tau	1.32 \pm 0.32	13 \pm 3.26
GPC + Cho	1.72 \pm 0.16	2.67 \pm 0.47
Ins + Gly	3.95 \pm 1.37	6.83 \pm 1.57

Table 4.8 illustrates the absolute concentration and the CRLB values plus or minus the standard deviation. The VOI is selected as the grey matter (GM) in the pgACC region. All the 15 metabolites have a CRLB value less than 20 %. Gln and Glu can be detected and quantified in this region at 7T.

Also, Taurine (2-aminoethanesulfonic acid) has two methylene groups with nonequivalent protons, and at higher magnetic fields, it can be regarded as two triplets centered at 3.25 and 3.42 ppm [83]. The 3.43 ppm Taurine multiplet is relatively clear from the overlapping metabolites and is clearly seen in the *in vitro* 1H spectrum, at 3.27 ppm; the Taurine multiplet disappearing because of the CH myo-inositol multiplet at 3.28 ppm.

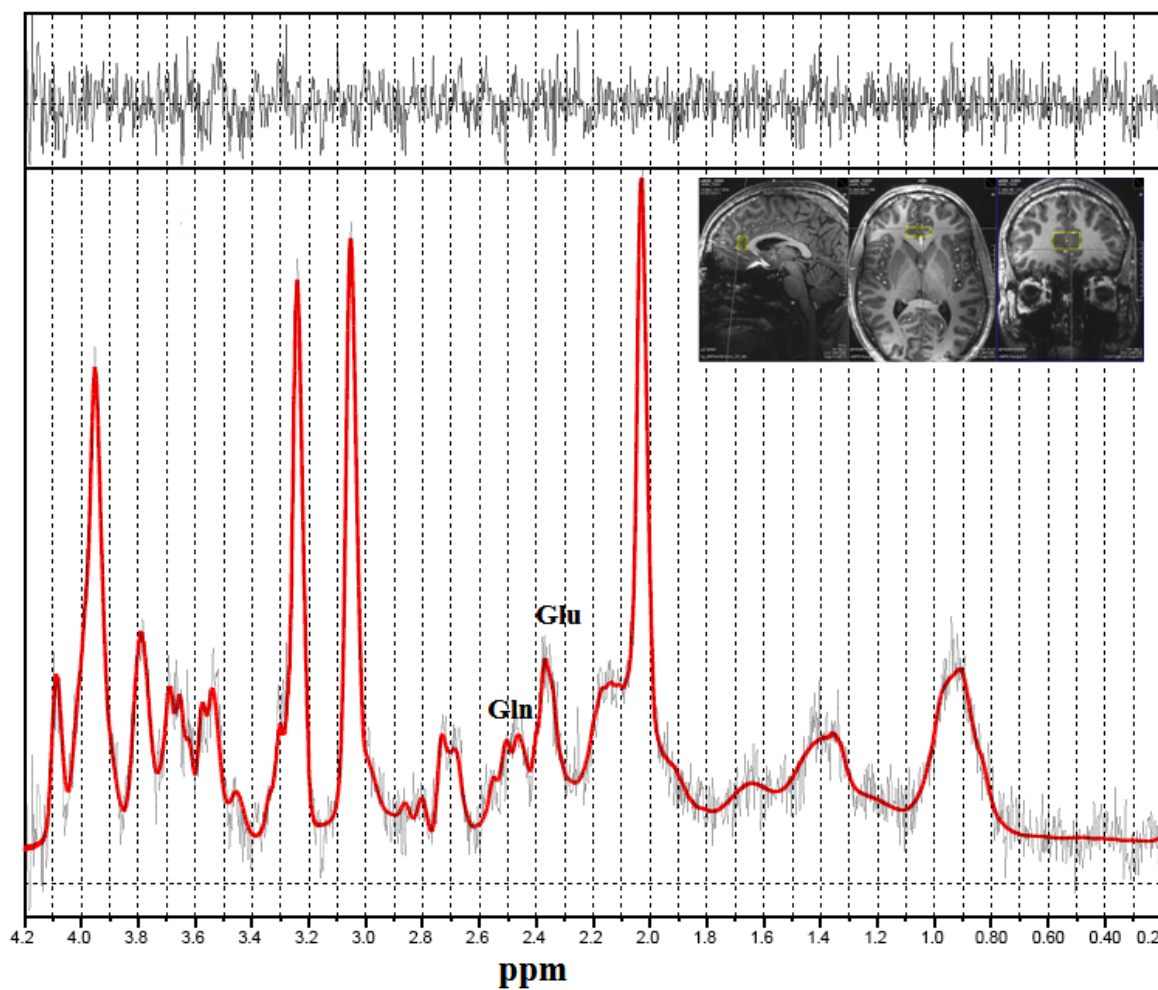


Figure 4.16: The *in vivo* ^1H -MRS spectrum acquired from the pgACC GM at 7T. STEAM with VERSE factor = 1.4, TR/TE/TM = 3000/20/15 ms, voxel volume = 3.8 mL, BW = 3600 Hz, vector size = 2048, and averages = 128

4.9.2.1 NAAG Detection using Simulated Database with Long TE

It is important to mention that the detection of 15 metabolites including Glu and Gln in a deep region such as pgACC indicates the ability of using this MRS method as a routine method, particularly for Gln/Glu separation and moreover GABA and Tau detection at 7T.

Further, the NAAG concentration in this location with short TE shows higher CRLB values than 20%, but with long TE = 74 ms it can be detected with CRLB less than 20%. However, it was observed that NAAG could be undetected in all human brain spectra measured in the pgACC area using short TE = 20 ms, but the macromolecule MM20 could be quantified using the same echo time.

There is a negative correlation between the CRLB values of the macromolecule MM20 and that of NAAG with short TE = 20 ms, as shown in Fig. 4.17 (A). However, Fig. 4.17 (B) also shows a negative correlation between the CRLB values of NAAG vs. that of MM20 using the long TE = 74 ms and TM = 64 ms. The (mean \pm SD) of concentrations and CRLB values of nine healthy volunteers are illustrated in Table 4.17.

Table 4.9: NAAG, MM20 levels of human brain metabolites of 6 healthy volunteers in the pgACC region using the long TE = 74 ms.

Metabolites	Concentrations	CRLB
	Mean \pm SD (mM/kg)	Mean \pm SD (%)
NAA	10.89 \pm 2.25	2.78 \pm 1.09
NAAG	1.01 \pm 0.40	14.44 \pm 4.30
MM20	2.75 \pm 1.56	41.33 \pm 41.45

In brief, as seen in Table 4.9 (A and B), NAAG can be detected and quantified with CRLB less than 20 % with TE = 74 ms and TM = 68 ms used. Where the MM20 signal full relaxed with long TE.

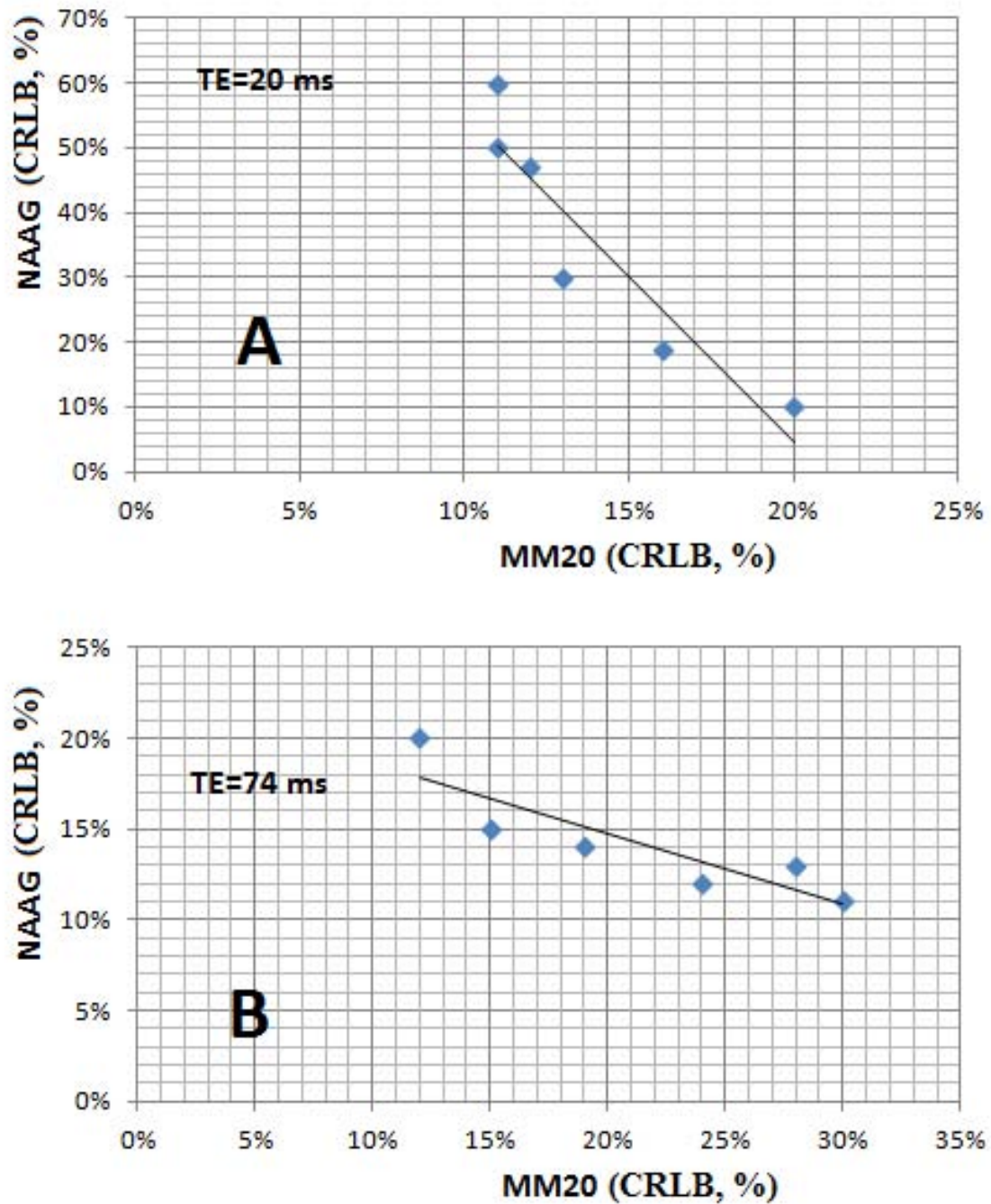


Figure 4.17: 1H -MRS spectrum acquired from the pgACC grey matter (GM) of 6 healthy subjects at 7T. STEAM with VERSE factor = 1.4, voxel size = 3.8 mL, BW = 2800 Hz, vector size = 2048, and averages = 128. A) negative relationship between CRLB of MM20 vs NAAG using TR/TE/TM = 3000/20/15 ms. B) A relation between CRLB of NAAG vs MM20 using TR/TE/TM = 3000/74/68 ms

4.9.3 Posterior Cingulate Cortex (PCC)

Fig. 4.18 shows the human brain spectrum of a healthy subject acquired from the PCC brain region at 7T.

Table 4.10: Concentration levels of the human brain metabolites of 6 healthy subjects acquired from the PCC area at 7T

VOI = 3.8 mL (pcc region)		
Metabolites	Concentrations Mean \pm SD (mM/kg)	CRLB \pm SD (%)
Asp	1.99 \pm 0.66	18 \pm 0.06
Cho	0.15 \pm 0.09	15 \pm 0.04
Cr	6.55 \pm 0.11	2 \pm 0.00
GABA	1.45 \pm 0.21	12 \pm 0.03
Gln	1.97 \pm 0.56	10 \pm 0.02
Glu	9.59 \pm 0.20	4 \pm 0.01
Gly	0.47 \pm 0.25	18 \pm 0.03
Ins	1.94 \pm 0.23	7 \pm 0.02
NAA	12.25 \pm 0.85	2 \pm 0.01
NAAG	0.38 \pm 0.16	16 \pm 0.04
GPC	1.17 \pm 0.20	6 \pm 0.02
GSH	0.83 \pm 0.23	14 \pm 0.04
PCr	2.76 \pm 0.34	6 \pm 0.03
PE	2.65 \pm 0.09	6 \pm 0.01
Tau	0.67 \pm 0.04	18 \pm 0.04
MM20	7.27 \pm 1.64	24.83 \pm 4.17

Table 4.10 gives the information of brain metabolites of 6 healthy subjects. The importance of this section is that this study involved the positions around the corpus callosum, which is located between the two brain hemispheres, i.e. deeply in the brain, therefore a volume coil is needed.

In this location, the CRLB value of the Gln metabolite is reduced by 20 % compared with that of the pgACC. According to the data in the Table, the metabolite concentration varied in different locations in the brain. Therefore, in the PCC area, GABA and Tau metabolites can be detected better than in the pgACC area.

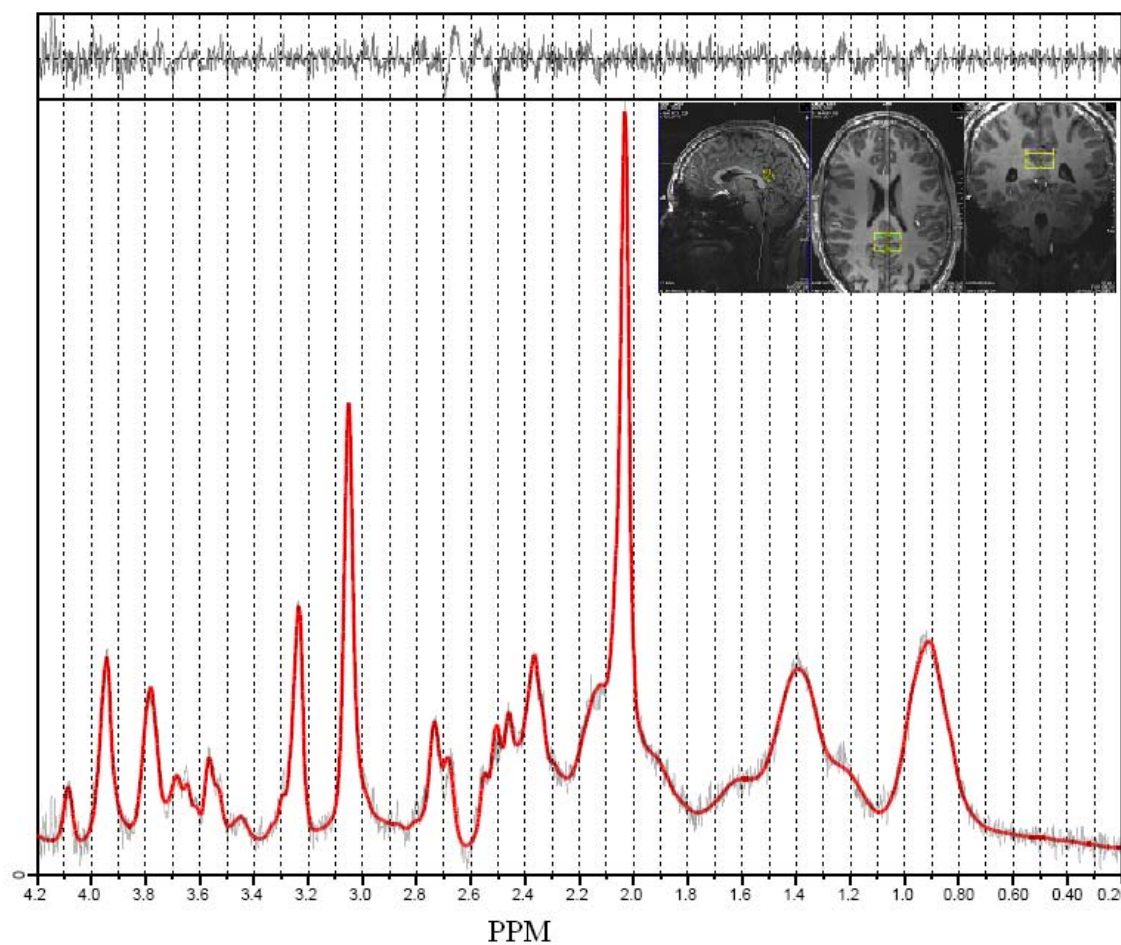


Figure 4.18: The *in vivo* ^1H NMR spectrum acquired from the PCC grey matter at 7T. STEAM with VERSE factor = 1.4, TR/TE/TM = 3000/20/15 ms, voxel size = 3.8 mL, BW = 2800 Hz, vector size = 2048, and average = 128

4.9.4 Anterior Middle Cingulate Cortex (AMCC)

In this experiment, another brain area was selected using the STEAM with VERSE pulses with TR/TE/TM = 3000/20/15 ms, average = 128, spectral B.W = 2800 Hz. Fig. 4.19 shows the human brain spectrum of a healthy subject which was acquired from the AMCC brain region at 7T. Table 4.11 demonstrates the 15 metabolites of a human brain, the data acquired from 6 volunteers in the AMCC region at 7T.

Table 4.11: Concentration levels of the human brain metabolites of 6 healthy subjects acquired from the AMCC area at 7T

VOI = 3.8 mL (AMCC region)		
Metabolites	Concentrations Mean \pm SD (mM/kg)	CRLB \pm SD (%)
Asp	2.51 \pm 1.37	13.75 \pm 5.87
Cho	0.28 \pm 0.36	11.25 \pm 12.08
Cr	6.30 \pm 0.72	2.85 \pm 0.86
GABA	1.61 \pm 0.85	12.85 \pm 7.73
Gln	1.58 \pm 0.87	17.80 \pm 8.38
Glu	9.15 \pm 1.26	4.90 \pm 1.18
Gly	0.45 \pm 0.38	19.55 \pm 16.01
GPC	1.28 \pm 0.46	6.85 \pm 3.32
GSH	1.00 \pm 0.50	17.60 \pm 9.38
Ins	2.43 \pm 0.70	9.05 \pm 7.79
NAA	9.60 \pm 2.01	3.20 \pm 1.38
NAAG	0.24 \pm 0.21	13.20 \pm 2.85
PCr	2.28 \pm 0.60	14.15 \pm 8.88
PE	2.48 \pm 0.76	8.45 \pm 2.60
Tau	0.68 \pm 0.35	21.10 \pm 9.34
MM20	6.58 \pm 1.47	18.76 \pm 5.55

Table 4.11 also illustrates that GABA can be clearly detected in this AMCC location with lower CRLB value. Moreover, Tau was not quantified as well as in the PCC and pgACC regions.

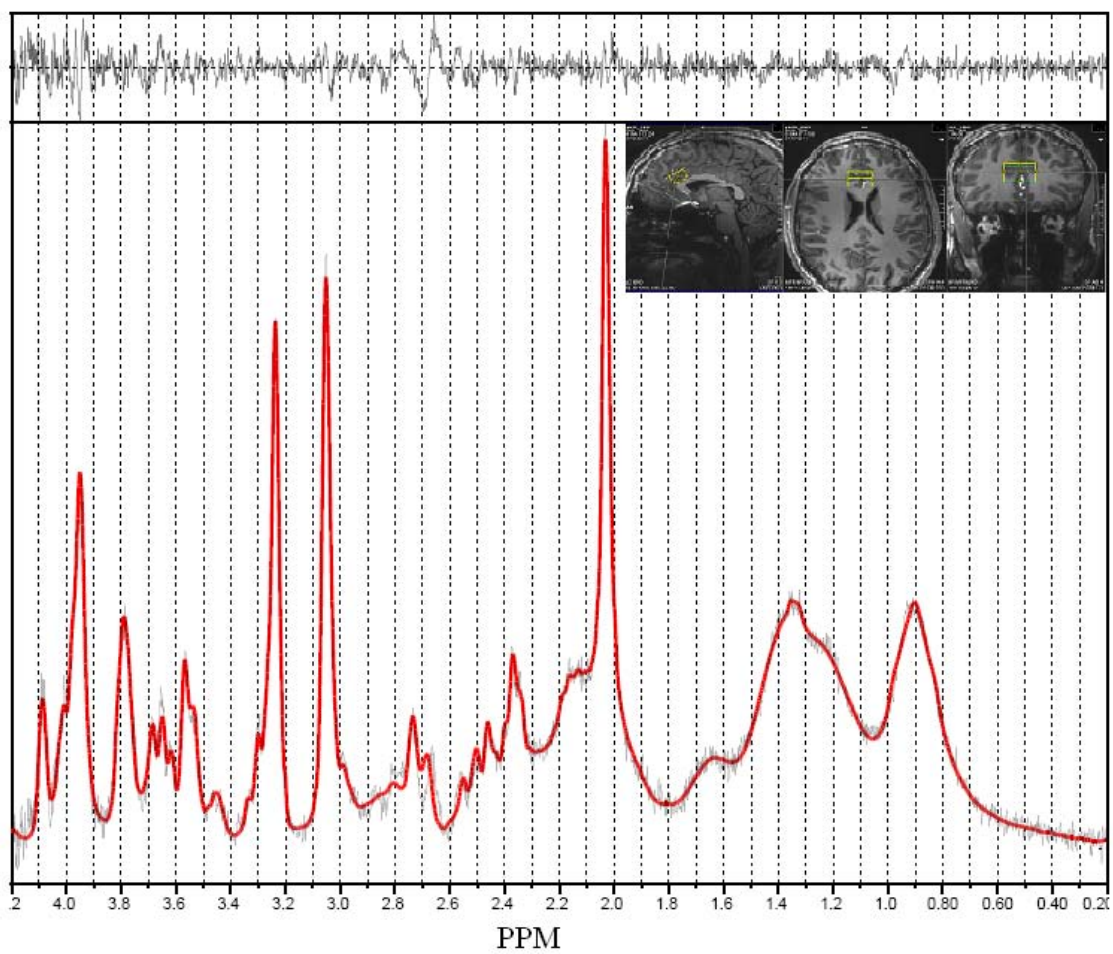


Figure 4.19: LCMoel fit of ^1H -MRS spectrum acquired from the AMCC region at 7T. STEAM with VERSE factor = 1.4, TR/TE/TM = 3000/20/15 ms, voxel size = 3.8 mL, BW = 2800 Hz, vector size = 2048, and average = 128

4.9.5 Brodmann 23C region (23C)

Fig. 4.20 shows the human brain spectrum of a healthy subject acquired from the Brodmann 23C region of the brain at 7T, including the reference image of the 23C location. The small fit residual indicates a good match between the raw data and the LCModel fit. The Gln/Glu metabolites clearly resolved in this region, as shown in Fig. 4.20. Further, Table 4.12 shows that all the 15 metabolites can be detected as in the earlier Tables. Moreover, the CRLB values of all the metabolites were less than 20 %.

Table 4.12: Concentration levels of the human brain metabolites of 6 healthy subjects acquired from the 23c area at 7T

VOI = 3.8 mL (32c region)		
Metabolites	Concentrations Mean \pm SD (mM/kg)	CRLB \pm SD (%)
Asp	2.11 \pm 1.17	14.67 \pm 8.16
Cho	0.24 \pm 0.21	16.67 \pm 13.53
Cr	6.26 \pm 0.84	3.00 \pm 0.89
GABA	1.35 \pm 0.42	18.17 \pm 9.09
Gln	2.14 \pm 0.86	15.17 \pm 6.24
Glu	8.96 \pm 0.84	5.67 \pm 1.03
Gly	0.23 \pm 0.40	7.50 \pm 12.13
GPC	1.23 \pm 0.36	8.83 \pm 4.02
GSH	0.86 \pm 0.25	18.67 \pm 3.67
Ins	2.66 \pm 0.32	7.83 \pm 1.17
NAA	11.05 \pm 1.07	2.83 \pm 0.75
NAAG	0.34 \pm 0.20	17.67 \pm 6.47
PCr	2.72 \pm 0.17	9.67 \pm 2.16
PE	2.73 \pm 0.30	8.83 \pm 1.33
Tau	0.81 \pm 0.17	14.50 \pm 2.43
MM20	6.76 \pm 1.54	25.00 \pm 4.69

At the end of this section, the detection and quantification of 15 metabolites in the different brain regions proves that the current 1H -MRS method is reliable to use at 7T. Moreover, using the 24-channel volume coil leads to the acquisition of the data from the deep brain regions such as around the corpus callosum area. Some metabolites

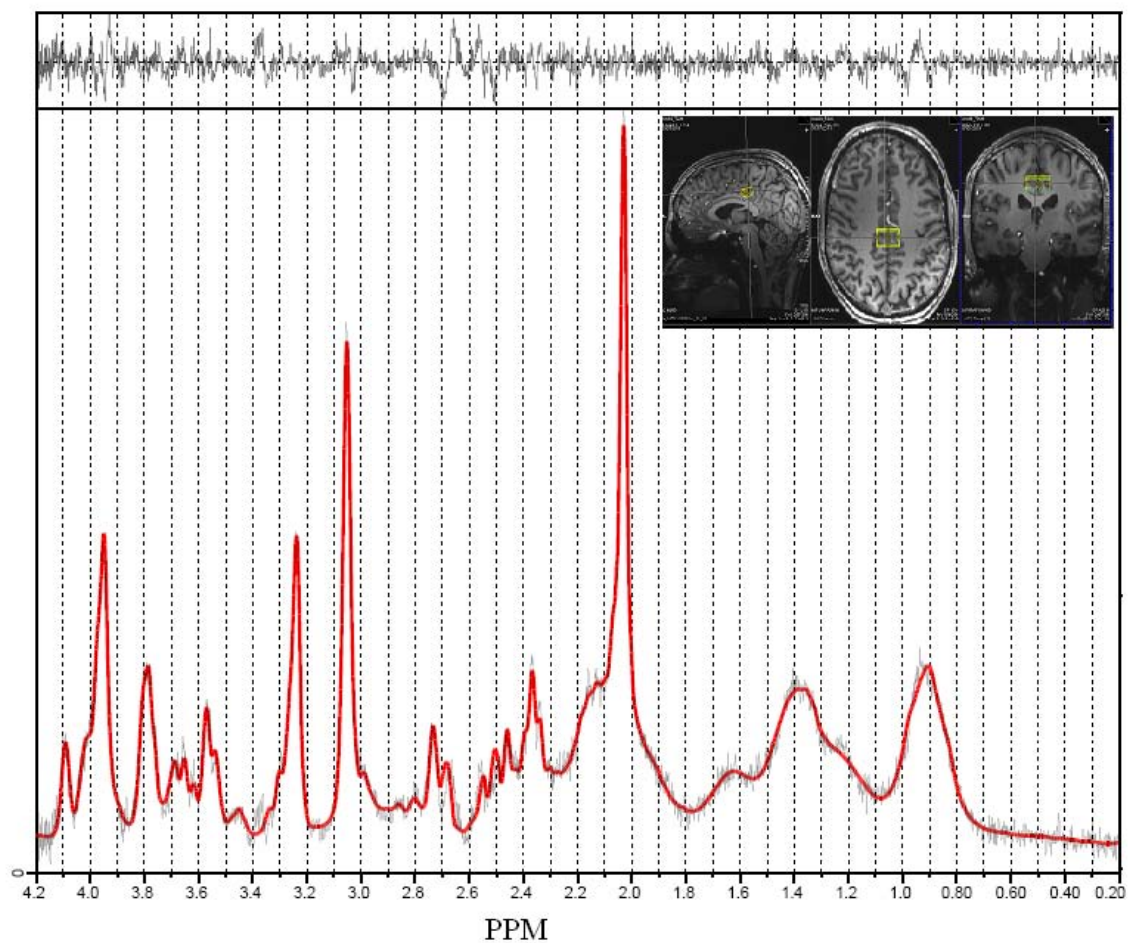


Figure 4.20: The LCMoDel fit of ^1H NMR spectrum acquired from the 23C at 7T. STEAM with VERSE factor = 1.4, TR/TE/TM = 3000/20/15 ms, voxel size = 3.8 mL, BW = 2800 Hz, vector size = 2048, and average = 128

such as Gln/Glu, NAAG/NAA and Tau/Ins can be detected and resolved very well using the current method at 7T.

4.10 Human Brain Metabolites Correlation

Some metabolites such as Gln and Glu, may overlap with other metabolites due to the low field strengths other than 7T. Other metabolites have the same resonance peaks such as PCr and Cr have the same resonance peaks at 3.01 ppm and 3.9 ppm. Therefore, the peak overlapping occurs.

4.10.1 Grey Matter and Glutamine Concentrations Correlation

Fig. 4.21 indicates a relationship between the amount of grey matter in human brain tissues and the absolute concentrations of the Gln metabolite in the partial and pgACC regions. The positive correlation ($r=0.881$, $p=0.00076$) shows the high significance of the probability of the existence of a linear relationship between the GM (partial volume) contents and the Gln concentration in different brain regions.

Table 4.7 indicates that the CRLB value of Gln is 22.25 ± 1.92 which is greater than 20 %. The reason for this increase can be interpreted because the voxel volume in parietal regions contains a high amount of WM and a low amount of GM; therefore, the Gln concentration is minimal. However, most of the other positions, pgACC, AMCC, PCC and 23C are contained GM which means that the CRLB of Gln should be less than 20 %.

4.10.2 Gln and Glu Correlation using Short and Long TE

Fig. 4.22 (A and B) shows the correlation between the Glutamine and Glutamate metabolites with a short echo time $TE = 20$ ms and with long echo times $TE = 74$ ms. The metabolite concentrations have been evaluated by the LCModel as absolute values. Significantly, a positive correlation was found between the Gln values and Glu values in the pgACC brain region at 7T using the short and long TE. As seen in Fig. 4.22 the short TE illustrates a higher significance ($r=0.71$, $p=0.03$) than long TE ($r=0.45$, $p=0.00076$).

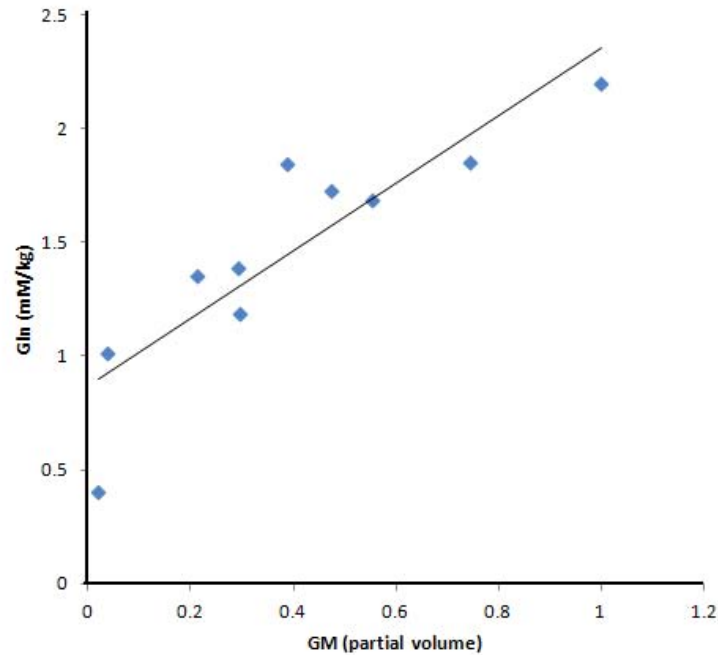


Figure 4.21: The statistical correlation between GM and Gln using the LCModel fit spectrum of human brain data of 10 healthy subjects measured in the parietal and pgACC brain regions with TR/TE/TM = 3000/20/15 ms at 7T

$r=0.67$, $p=0.05$), respectively. The two correlations show that the Glu/Gln can be detected with TE = 20 ms and also with TE = 74 ms.

4.11 Fifteen Human Brain Metabolites Detection in the Different Brain Areas

In the end, the human brain metabolites of healthy volunteers in five locations can be detected at 7T and quantified using the LCModel. The parietal, pgACC, AMCC, 23C, and PCC are the five regions examined. Some of these voxels showed the presence of more white matter (WM), while others contained more of GM; mixed WM with GM voxels were measured also.

In this study it is established that 15 metabolites could be detected and quantified using the current 1H -MRS method. All these metabolites can be quantified using the LCModel with experimental and simulated basis sets. A CRLB value below

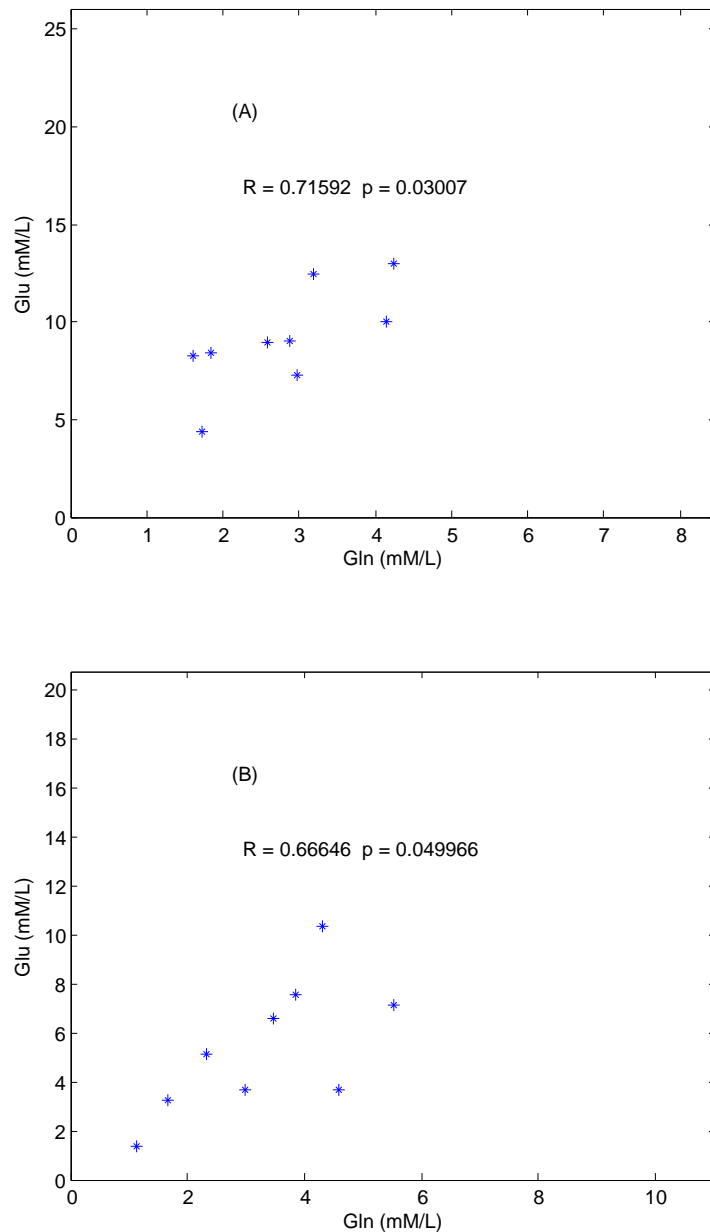


Figure 4.22: Human metabolites correlation between Gln and Glu using LCModel fit spectrum of human brain data measured in pgACC region (A) with short TE = 20 ms and (B) with long TE = 74 ms at 7T

20% has been accepted as the standard value for metabolite quantification. Absolute concentrations and CRLBs values are given as mean values \pm SDs for 30 healthy volunteers. To calculate the absolute concentrations, the value of 8 mM/kg was considered as the mean concentration of total creatine (PCr+Cr).

In this work, the 15 metabolites can be classified into two groups depending on

their WM and GM locations.

4.11.1 Metabolites Detection in WM and GM using TE = 20 ms

NAA, GABA, GSH, GPC, Glu, Asp, Cr, PCr, PE, Tau, and Ins are metabolites which can be detected and quantized with CRLB values less than 10 % in all the five locations (WM and GM) which were measured using short TE = 20 ms, TR = 3 s and TM = 15 ms.

4.11.2 Human Brain Metabolites Detected in GM using Short and Long TE

In GM structures, Gln and GABA can be reliably detected using short TE. NAAG, however, needs long TE for quantification in the GM pgACC locations. The (mean and SD) CRLB values of the Gln of eight healthy volunteers are 22.25 ± 1.92 in the parietal area. The increase in the CRLB value is because most of the parietal voxel consists of more of WM. In the middle of this chapter, GM has shown a positive correlation with Gln i.e., there is little detection of Gln in a region with large quantity of WM, such as in parietal regions. Therefore, by enlarging the voxel size to include some of GM, the Gln can be detected. However, the long TE = 74 ms and TM = 68 ms are the best parameters to detect NAAG in the GM region such as pgACC, which contains more GM than WM.

Finally, the results provide a powerful non-invasive tool for routine proton magnetic resonance spectroscopy of the human brain at a high magnetic field of 7T using a 24-channel volume head coil and a combination of *RF* sequence with the STEAM with VERSE pulses, automatic 3D shim, water suppression adjustment and single volume spectroscopy localization technique.

Chapter 5

Discussion

In this chapter, some results of this study will be discussed. The main objectives of this work are to develop a suitable $^1H - MRS$ method and to use this method at 7T to detect the human brain metabolites from different deep brain regions such as pgACC, PCC, AMCC and the Brodmann (23C) area.

5.1 Optimization of 90° Flip Angle

The true 90° flip angle depends on the VOI position in the sample and may lead to a reduced *MRS* signal. The local variation of the flip angle in the sample has occurred due to the inhomogeneity of B_1 in the sample.

Within the adjustment in volume, additional steps like water suppression adjustment are required to optimize the flip angle for the selection sequence. These procedures are time consuming and increase the scan time for the patient. In this work, the desired flip angle can be achieved using Equation 4.1. The experimental results demonstrated that the best transmitter voltage can be calculated based on the local water suppression adjustment. Therefore, the flip angle for MR spectroscopy can be optimized without additional scan time and thus the signal received from the VOI in the sample can be improved.

5.2 Reduction of the Applied Voltage of 90° Flip Angle

Determination of the required voltage was done in order to obtain a true 90° flip angle, and the method was used to make a comparison between STEAM and STEAM with VERSE pulses. In short, the experimental result shows that the required voltage decreased by 28 % using STEAM with VERSE pulses.

5.3 SNR Increase at 7T Compared to 3T

Hill et al. in 1968 showed that the signal to noise ratio is affected by different factors, like magnetization in the VOI, filling factor, sample permeability, Larmor frequency, and volume of the *RF* coil. Also, in another method of SNR calculation [65], the SNR was found to be proportional to B_0 in the sample, besides the aforementioned factors. All these factors make the dependency of SNR on the magnetic field strength a difficult issue [8].

Theoretically, increasing the static magnetic field B_0 leads to increases in the SNR [65]. For a comparison between the 3T and 7T, the SNR increases by a factor of 2.3 at 7T relative to 3T when all the other experimental parameters are similar.

In this work, a STEAM sequence was used at 7T and a PRESS sequence at 3T. Even though the STEAM sequence results in a 50 % signal loss compared with PRESS due to the stimulated echo signal generation, the SNR increases by a factor of 1.94 from 3T to 7T. Further, the MRS data of three volunteers measured at 3T and 7T have been corrected for the number of average, the voxel volume, and the line width differences. If the STEAM signal loss is considered this leads to a factor of 3.88, while this is higher than the expected; therefore, a number of additional factors may contribute to this gain. The echo time is shorter with the STEAM sequence and the receiving coil may be significantly more sensitive at 7T due to the higher number of channels. Thus, the high sensitivity and increased chemical dispersion at 7T make it possible to resolve even metabolites with very low concentrations, such as Gln, GABA and NAAG.

Moreover, it has been earlier published that SNR depends on the chemical shift displacement of the VOI [38]. In this work, two molecules (water and NAA) have

a displacement of $\Delta x = 0.15$ cm for a 1 cm slice thickness. Also, the measurement should avoid any signal acquired from outside the volume of interest. Therefore, the gradient spoiling of unwanted signals is a tool used to avoid signal contaminations. In the *in vivo* human brain 1H -MRS measurements, fat is one of the unwanted signals in spectroscopy. Therefore, strong spoiling is especially necessary [84]. Another source of unwanted signal contributions arises from the fact that *RF* pulses cannot excite a rectangular slice profile as required. Also, the water signal, which is large, compared with the metabolites is another source of signal contamination which can be avoided by the application of water suppression pulses such as CHESS [38]. Indeed, the line width broadening is caused by the magnetic field inhomogeneity. Added to this, the line width is the result of the shimming process.

5.4 GABA, Gln and Glu Quantification using Short *TE* at 7T

Kreis et al. in 1991 [74] explained that glutamine, myo-Inositol and the choline metabolites are important markers in medicine. Moreover, Hasler in 2007 [1] showed a positive correlation between the GABA and Glx pools in two voxels in the prefrontal regions at 3T.

In this thesis, at a high magnetic field strength of 7T, there is a reliability to detect each of the GABA, Gln and Glu separately with CRLB values $< 20\%$ as illustrated in the chapter on Results. Therefore, in all the regions Glu can be detected and quantified using the LCModel. In the parietal WM location Glu and GABA were found to be clearly detected with CRLB values less than 20%. Also, in the GM locations, Glu, Gln and GABA can be detected and their concentrations evaluated with CRLB values $< 20\%$. Statistical correlations between Glu and Gln have been evaluated at 7T using short $TE = 20$ ms and long $TE=74$ ms. This demonstrates that Glu and Gln can be detected and quantified with either short or long TE in all the five examined regions. However, NAA and NAAG in the GM pgACC can be only quantified using long TE .

5.5 Comparison between GM pgACC and WM Parietal Regions

Differentiation of metabolic concentration between grey matter (GM) and white matter (WM) in a human study using $TR=3$ s and $TE=20$ ms revealed that Gln concentration was 42 % higher in the GM pgACC than in the WM parietal. This has been demonstrated by the positive correlation between the GM (partial volume) and Gln absolute concentrations in the Results chapter.

As shown in Tables 4.7 and 4.8, tCr, GABA, Glu, Gln, GPC, Ins and Tau have higher concentrations in the GM pgACC than in the WM parietal locations. On the other hand, Asp, GSH, NAA, NAAG, PE and total choline show higher concentrations in the WM parietal than in the GM pgACC locations.

5.6 Human Brain Metabolites Quantification

The LCMoDel has been used to analyze human spectra acquired from five brain locations (pgACC, AMCC, Brodmann 23C region and PCC) in the WM or GM. The small fit residuals of their spectra certified that the fit matches the raw data well.

Previous studies showed that at low fields some metabolites such as NAAG, Gln, GABA, and Tau cannot be resolved due to the overlap between them and the other metabolites such as NAA, Glu, and Ins. Obviously, the detection of 15 human brain metabolites in the different brain regions either superficial or deep brain locations, gives the current method reliability to be used in medical applications.

Moreover, metabolites such as glutamine and glutamate can be separated using the long echo time [85, 86]. As, the RF pulses, the gradients, and the interpulse timings TR , TE and TM are essential elements of an MRS optimization. In this work, STEAM with VERSE pulses of 2.5 ms pulse duration and experimental parameters $TR/TE/TM = 3000/20/15$ ms were used to detect the same metabolites in the deep brain regions.

In fact, the Glutamine and Glutamate peaks can be separated in all the five locations either in the GM or in WM structures at 7T. Further, Glu can be detected in all the areas examined with CRLB less than 5 % as the mean value while Gln too can

be detected in all the regions with CRLB values $< 20\%$ except in the parietal areas with 22.15 %.

However, NAAG could not be detected at lower than 7T [15] unless specialized techniques and shimming were used [87]. In the current study, standard STEAM adapted with VERSE pulses was used to detect NAAG besides NAA in four deep brain regions with CRLB values less than 20 % except in the GM pgACC area where NAAG was detected with long $TE = 74$ ms.

Moreover, in this study, Asp can be detected in different deep brain regions. Meikle et al. in 2009 [14] showed that Asp could be detected at 7T with mean concentration of (2.9 ± 0.5) , which concurs with this study (2.452 ± 0.46) .

Furthermore, the mean of the total creatine concentration (creatine, Cr, phosphocreatine, PCr and other creatine compounds) along the five brain locations is (8.336 ± 11.35) mM/kg, which is also in agreement with the reports [47, 14].

Finally, the 7 Tesla ultrahigh field strength, 24-channel volume coil, STEAM with VERSE pulses and automatic 3D shimming are tools that have been used to detect 15 human brain metabolites in different brain regions. Moreover, we have succeeded in detecting and quantifying Gln, GABA and NAAG human brain metabolites by using 1H -MRS at 7T, which could not be separated at the lower field strengths using the standard MRS sequences (STEAM or PRESS). It is tempting to conclude that separating Gln and Glu may be useful for patients who suffer from Major Depressive Disorder (MDD).

Chapter 6

Conclusions

Ultrahigh magnetic field (7 Tesla) can provide spectra from the human brain with high signal to noise ratio. The measured data at 3T and 7T field strengths (STEAM has been used at 7T and PRESS at 3T) show that SNR increases at 7T by a factor of 1.79 compared with 3T. This gain is larger than theoretically expected and may be explained by the slightly shorter echo time for the STEAM sequence and the higher sensitivity of the 24-channel receive only coil.

The transmission voltage for the highest signal intensity can be calculated based on the local water suppression adjustment. Therefore, the flip angle for MR-spectroscopy can be optimized without the additional scan time and thus improve the signal received from the VOI in the sample.

Variable rate selective excitation (VERSE) has been applied to the standard spectroscopy sequence (STEAM) to reduce the required RF peak power. Therefore, the required voltage for true 90° flip angle was reduced by 28 % allowing it to reach this target flip angle in all parts of the brain.

This optimized method has been applied to in vivo $^1H - MRS$ measurements. Two different parameter sets have been used: (i) $TR/TE/TM = 3000/20/15$ ms and (ii) $TR/TE/TM = 3000/74/68$ ms.

For quantification of the spectra, 20 human brain metabolite solutions were prepared and measured at 7T. These experimental basis spectra were processed for use in the LCModel. Twenty simulated spectra were calculated using the NMR-SIM software to form a simulated basis set. The concentration of these brain metabolites

has been determined from the in vivo spectra using both the LCModel basis sets at 7T.

This study shows that, not only Gln, GABA and NAAG can be detected using the current MRS method with short or long echo times, but also that this $^1H - MRS$ method can be used to determine 15 human brain metabolites.

The results show that the proposed method can be employed at 7T in the deep brain structures (pgACC, AMCC, PCC or Brodmann 23 C) and allows the determination of absolute and relative concentrations of the human brain metabolites with low error levels.

In the GM structures, Gln and GABA can be reliably detected using short TE . Moreover, NAAG can be quantified using long TE for detection in the GM areas. The partial volume of GM was shown to have a positive correlation with the Gln concentration, permitting the separation of the different Gln concentrations between the grey and white matter. On the other hand, long $TE = 74$ ms and $TM = 68$ ms are the best parameters to detect NAAG in the GM regions such as pgACC.

The current MRS method has been successful in the detection and quantification of 15 human brain metabolites at 7T. This allows employing MR spectroscopy in patients. Moreover, separating the Gln and Glu can be useful for scanning patients who suffer from Major Depressive Disorder (MDD).

Appendix A

Model Spectra Database: The current basis set consists of twenty *in vitro* spectra; Act, Ala, Asp, Cit, Cr, GABA, Glc, Gln, Glu, Gly, GPC, GSH, Ins, Lac, NAA, PCh, PCr, PE, Suc, and Tau of different concentrations. All the measured spectra are processed by LCModel.

In this work, experimental basis set has been done using STEAM with VERSE pulses. The pulse duration = 2.5 ms, TR=3 s, TE=20 ms and TM=15 ms have been used. All the measured data of these 20 human brain model metabolites have been analyzed using LCModel.

Table A.1 shows the chemical shift and J-coupling values of human brain metabolites. TMSP is considered as a singlet resonance at 0 ppm and all the chemical shifts are related to it. Multiplicity shows the number of peaks in the spectrum, and also refers to the number of neighbors protons. The symbols of multiplicity are s (singlet), d (doublet), t (triplet), q (quartet) and m, multiplet [88].

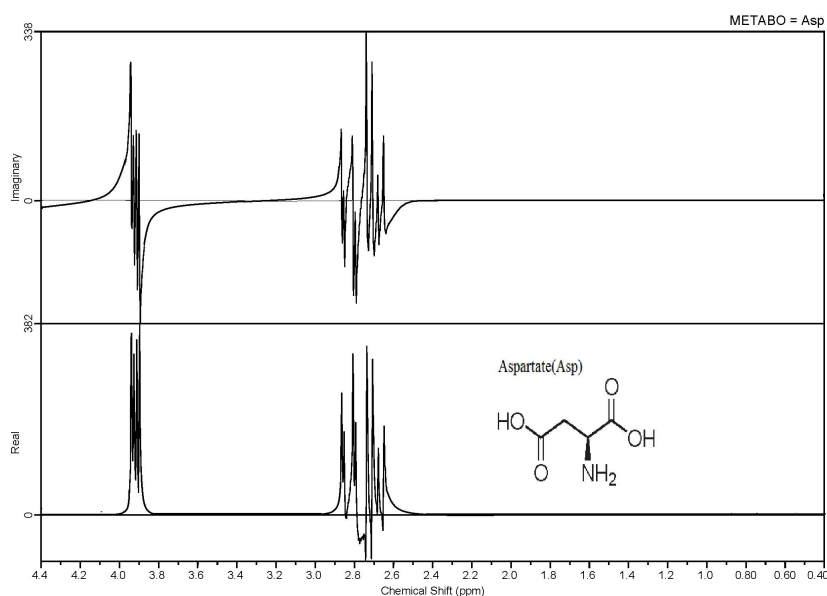


Figure A.1: *In vitro* spectra of **Aspartate** metabolite measured at 7T using STEAM with VERSE pulses, duration pulse of 2.5 ms, TR/TE/TM=3000/20/15 ms, voxel size of 3.5 mL and 2048 data points. Real and imaginary spectra in frequency domain and the chemical structure of the **Aspartate** have been demonstrated. The chemical shift range is from 0.4 ppm to 4.4 ppm.

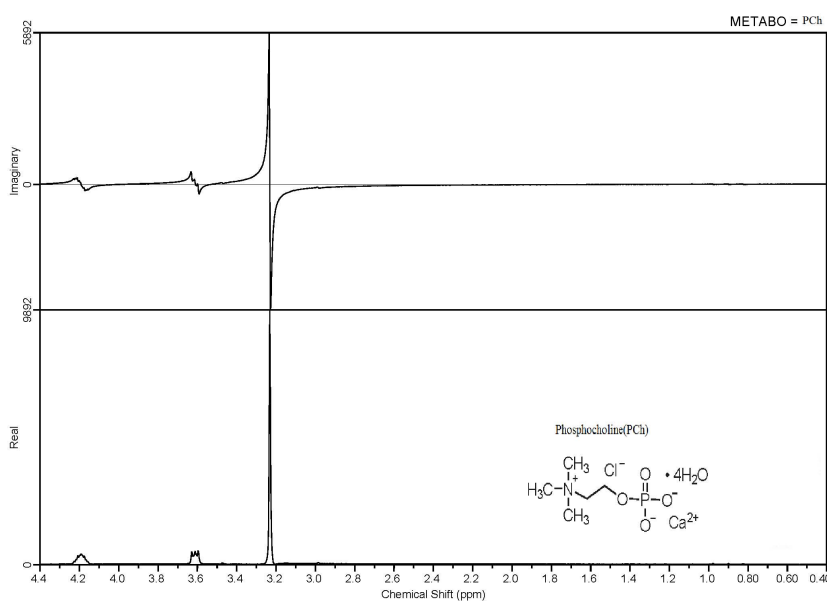


Figure A.2: *In vitro* spectra of **Phosphocholine** metabolite measured at 7T using STEAM with VERSE pulses, duration pulse of 2.5 ms, TR/TE/TM=3000/20/15 ms, voxel size of 3.5 mL and 2048 data points. Real and imaginary spectra in frequency domain and the chemical structure of the **Phosphocholine** have been demonstrated. The chemical shift range is from 0.4 ppm to 4.4 ppm.

Table A.1: Metabolite chemical structure (carbon and nitrogen groups), proton chemical shift, multiplicity and J-coupling values for human brain metabolites.

Metabolite	Group	Chemical Shift (ppm) using TMSP	Multiplicity	J (Hz)
Aspartate	2CH	3.8867	dd	3.647
	3CH ₂	2.8021	dd	9.107
Creatine	N(CH ₃)	3.0260	s	None
	2CH ₂	3.9110	s	None
	NH		s	None
γ - <i>AminobutricAcid</i>	2CH ₂	3.0082	m	5.372
	3CH ₂	1.8888	qu	10.578
	4CH ₂	2.2828	t	7.755
L-Glutamine	2CH	3.7625	t	5.847
	3CH ₂	2.1360	m	6.500
	4CH ₂	2.4350	m	9.165
Glutamate	2CH	3.7444	dd	7.331
	3CH ₂	2.0424	m	4.651
	4CH ₂	2.3354	m	8.406
Glycine	2CH ₂	3.5450	s	None
Glycerophosphocholine	1CH ₂		dd	5.77
			dd	4.53
	7CH ₂	4.312	m	3.10
	8CH ₂		m	5.90
	N(CH ₃) ₃		s	6.03
	7CH		dd	7.09
	7CH ₂		dd	4.71
Gluthatione	2CH		t	6.34
	3CH ₂		m	6.36
			m	-15.48
	4CH ₂		m	6.7
			m	7.6
	1CH	3.5177	dd	2.889
	2CH	4.0488	t	9.998
myo-Inositol	3CH	3.5177	dd	3.006
	4CH	3.6114	t	9.997
	5CH	3.2652	t	9.485
	6CH	3.6114	t	9.482
	2CH	4.0908	q	6.933
	3CH ₃	1.3125	d	
N-acetylaspartate	2CH ₃	2.0050	s	
	2CH	4.3823	dd	3.861
	3CH ₂	2.6759	dd	9.821
		2.4866	dd	-15.592
	NH	7.8155	d	6.400

Table A.2: Continuous of Table A.1

Metabolite	Group	Chemical Shift (ppm) using TMSP	Multiplicity	J (Hz)
choline	N(CH ₃) ₃	3.1890	s	None
	1CH ₂	4.0500	m	3.140
	2CH ₂	3.5060	m	6.979
Phosphocreatine	N(CH ₃)	3.0280	s	None
	2CH ₂	3.9260	s	None
	NH		s	None
	NH		s	None
phosphorylethanolamine	1CH ₂	3.9825	m	3.182
Taurine	1CH ₂	3.4190	t	6.742
	2CH ₂	3.2473	t	6.464

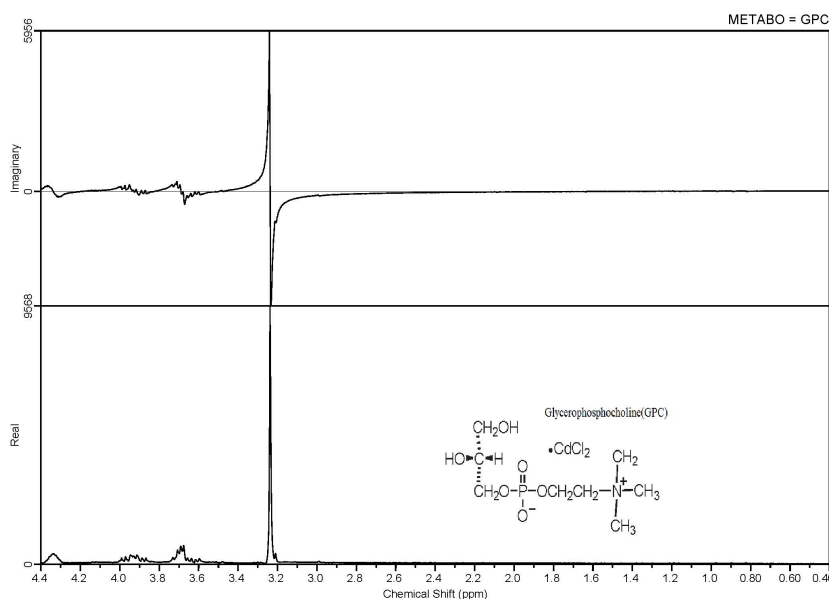


Figure A.3: *In vitro* spectra of **Glycerophosphocholine** metabolite measured at 7T using STEAM with VERSE pulses, duration pulse of 2.5 ms, TR/TE/TM=3000/20/15 ms, voxel size of 3.5 mL and 2048 data points. Real and imaginary spectra in frequency domain and the chemical structure of the **Glycerophosphocholine** have been demonstrated. The chemical shift range is from 0.4 ppm to 4.4 ppm.

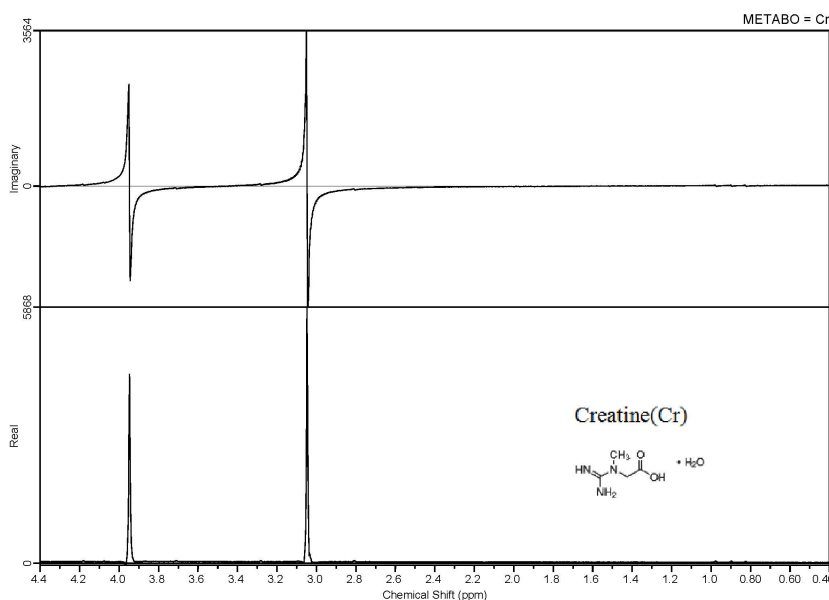


Figure A.4: *In vitro* spectra of **Creatine** metabolite measured at 7T using STEAM with VERSE pulses, duration pulse of 2.5 ms, TR/TE/TM=3000/20/15 ms, voxel size of 3.5 mL and 2048 data points. Real and imaginary spectra in frequency domain and the chemical structure of the **Creatine** have been demonstrated. The chemical shift range is from 0.4 ppm to 4.4 ppm.

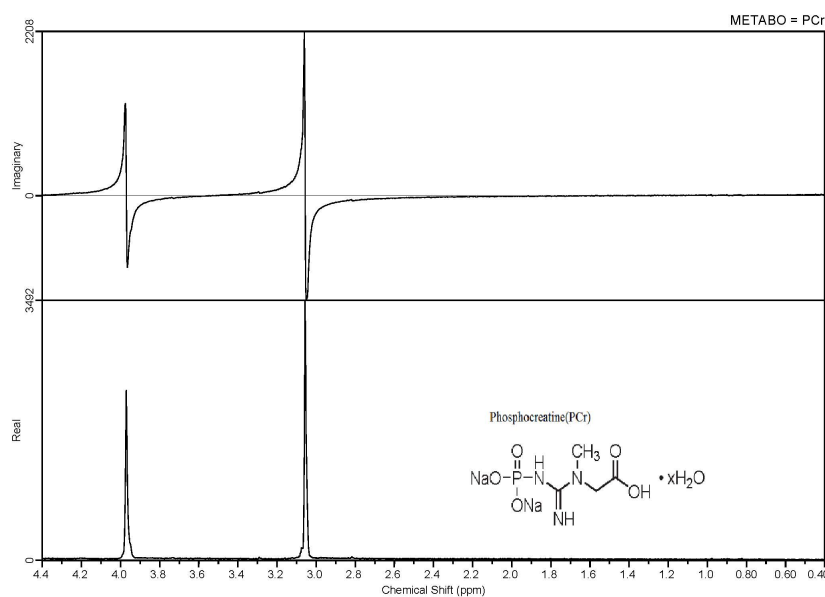


Figure A.5: *In vitro* spectra of **Phosphocreatine** metabolite measured at 7T using STEAM with VERSE pulses, duration pulse of 2.5 ms, TR/TE/TM=3000/20/15 ms, voxel size of 3.5 mL and 2048 data points. Real and imaginary spectra in frequency domain and the chemical structure of the **Phosphocreatine** have been demonstrated. The chemical shift range is from 0.4 ppm to 4.4 ppm.

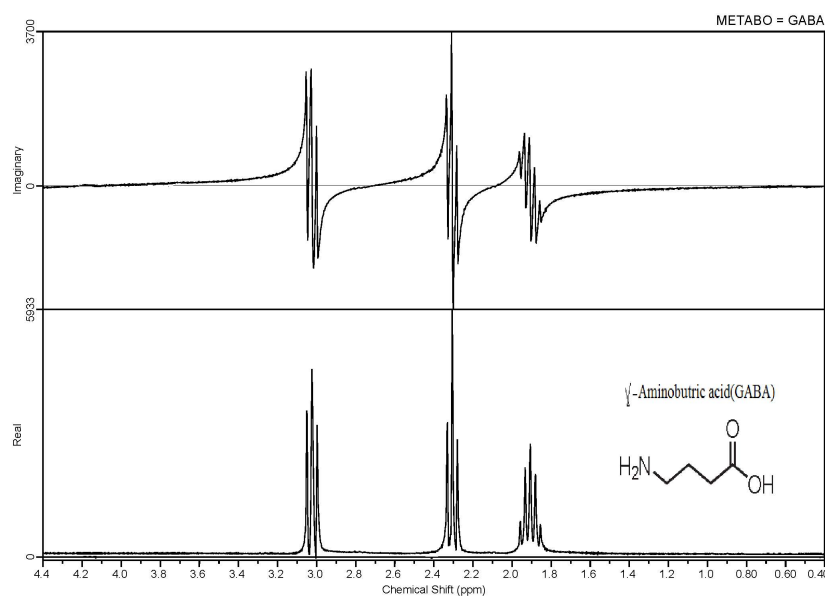


Figure A.6: *In vitro* spectra of γ -**Aminobutyric** Acid metabolite measured at 7T using STEAM with VERSE pulses, duration pulse of 2.5 ms, TR/TE/TM=3000/20/15 ms, voxel size of 3.5 mL and 2048 data points. Real and imaginary spectra in frequency domain and the chemical structure of the γ -**Aminobutyric** have been demonstrated. The chemical shift range is from 0.4 ppm to 4.4 ppm.

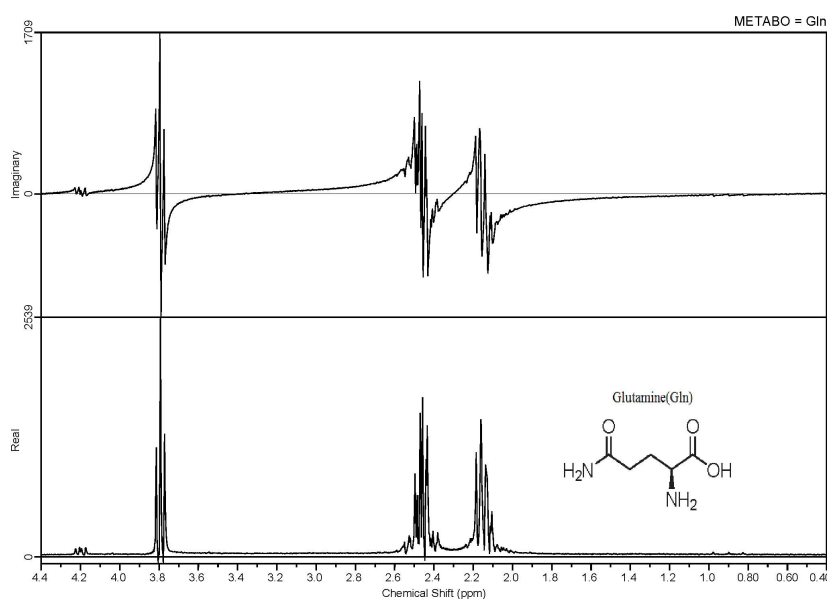


Figure A.7: *In vitro* spectra of **Glutamine** metabolite measured at 7T using STEAM with VERSE pulses, duration pulse of 2.5 ms, TR/TE/TM=3000/20/15 ms, voxel size of 3.5 mL and 2048 data points. Real and imaginary spectra in frequency domain and the chemical structure of the **Glutamine** have been demonstrated. The chemical shift range is from 0.4 ppm to 4.4 ppm.

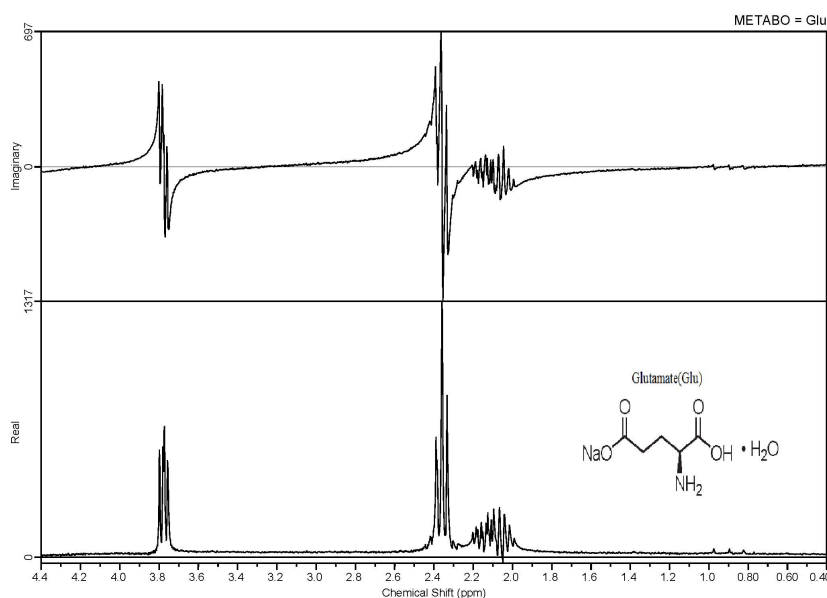


Figure A.8: *In vitro* spectra of **Glutamate** metabolite measured at 7T using STEAM with VERSE pulses, duration pulse of 2.5 ms, TR/TE/TM=3000/20/15 ms, voxel size of 3.5 mL and 2048 data points. Real and imaginary spectra in frequency domain and the chemical structure of the **Glutamate** have been demonstrated. The chemical shift range is from 0.4 ppm to 4.4 ppm.

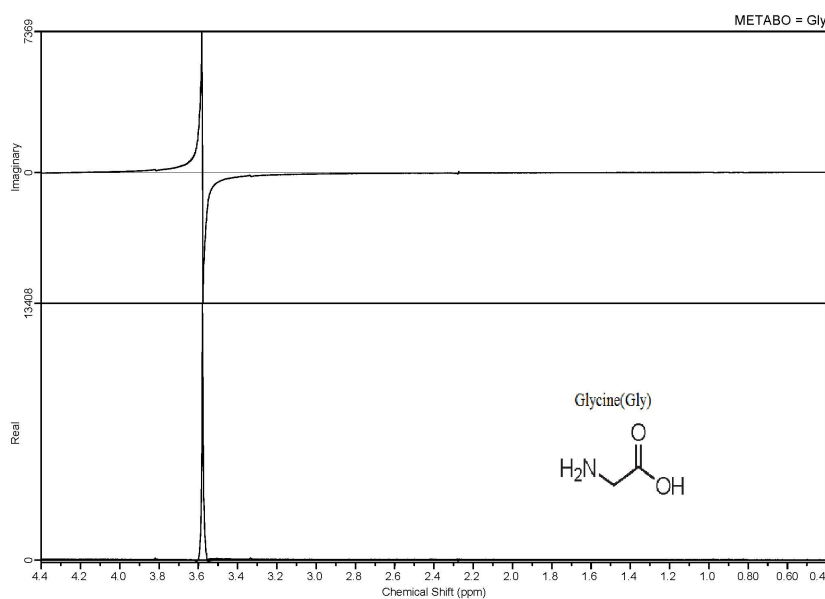


Figure A.9: *In vitro* spectra of **Glycine** metabolite measured at 7T using STEAM with VERSE pulses, duration pulse of 2.5 ms, TR/TE/TM=3000/20/15 ms, voxel size of 3.5 mL and 2048 data points. Real and imaginary spectra in frequency domain and the chemical structure of the **Glycine** have been demonstrated. The chemical shift range is from 0.4 ppm to 4.4 ppm.

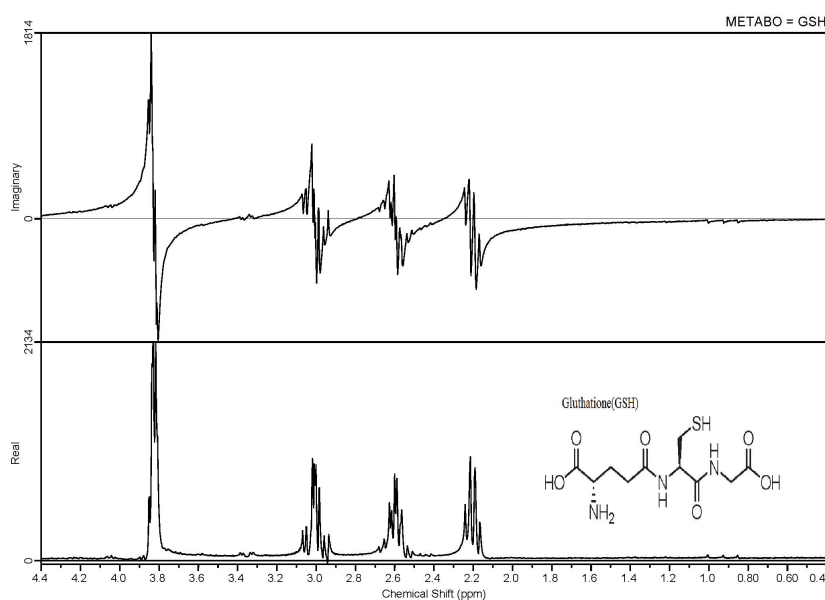


Figure A.10: *In vitro* spectra of **Glutathione** metabolite measured at 7T using STEAM with VERSE pulses, duration pulse of 2.5 ms, TR/TE/TM=3000/20/15 ms, voxel size of 3.5 mL and 2048 data points. Real and imaginary spectra in frequency domain and the chemical structure of the **Glutathione** have been demonstrated. The chemical shift range is from 0.4 ppm to 4.4 ppm.

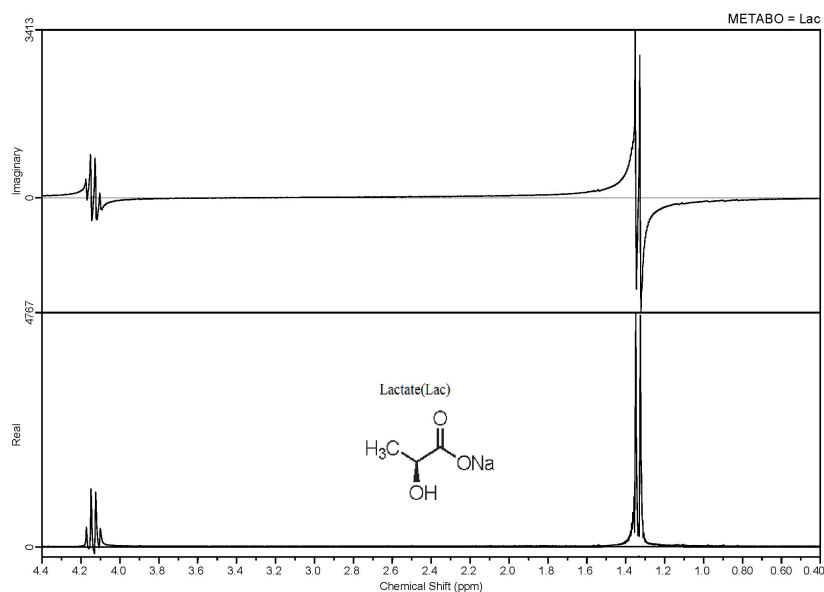


Figure A.11: *In vitro* spectra of **Lactate** metabolite measured at 7T using STEAM with VERSE pulses, duration pulse of 2.5 ms, TR/TE/TM=3000/20/15 ms, voxel size of 3.5 mL and 2048 data points. Real and imaginary spectra in frequency domain and the chemical structure of the **Lactate** have been demonstrated. The chemical shift range is from 0.4 ppm to 4.4 ppm.

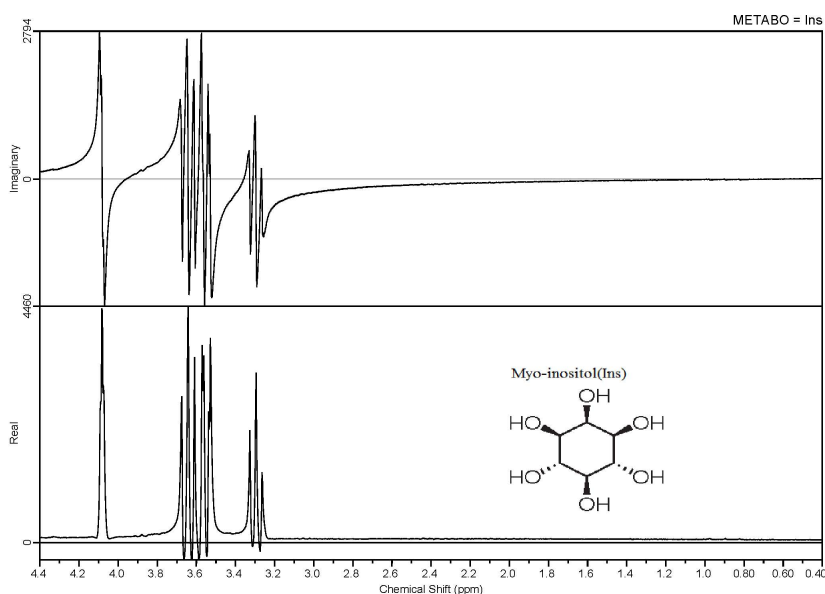


Figure A.12: *In vitro* spectra of **myo-Inositol** metabolite measured at 7T using STEAM with VERSE pulses, duration pulse of 2.5 ms, TR/TE/TM=3000/20/15 ms, voxel size of 3.5 mL and 2048 data points. Real and imaginary spectra in frequency domain and the chemical structure of the **myo-Inositol** have been demonstrated. The chemical shift range is from 0.4 ppm to 4.4 ppm.

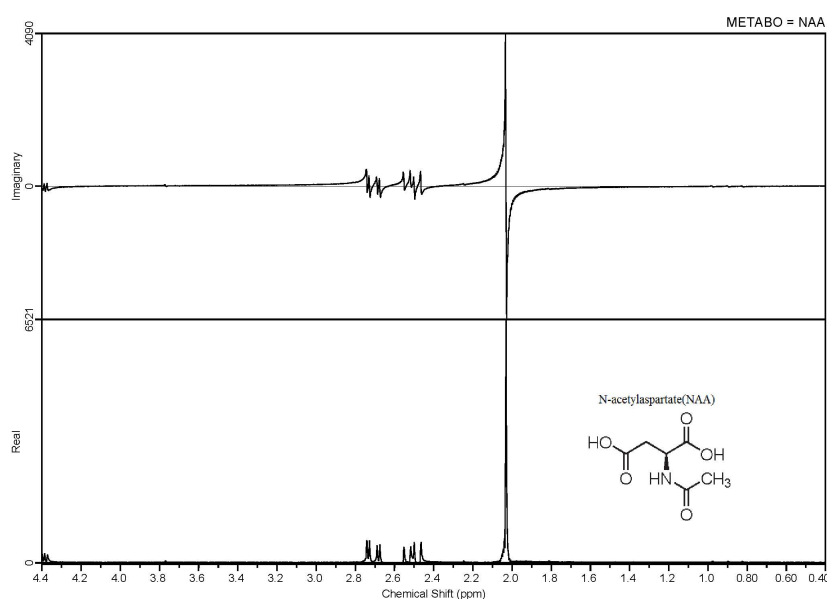


Figure A.13: *In vitro* spectra of **N-acetylaspartate** metabolite measured at 7T using STEAM with VERSE pulses, duration pulse of 2.5 ms, TR/TE/TM=3000/20/15 ms, voxel size of 3.5 mL and 2048 data points. Real and imaginary spectra in frequency domain and the chemical structure of the **N-acetylaspartate** have been demonstrated. The chemical shift range is from 0.4 ppm to 4.4 ppm.

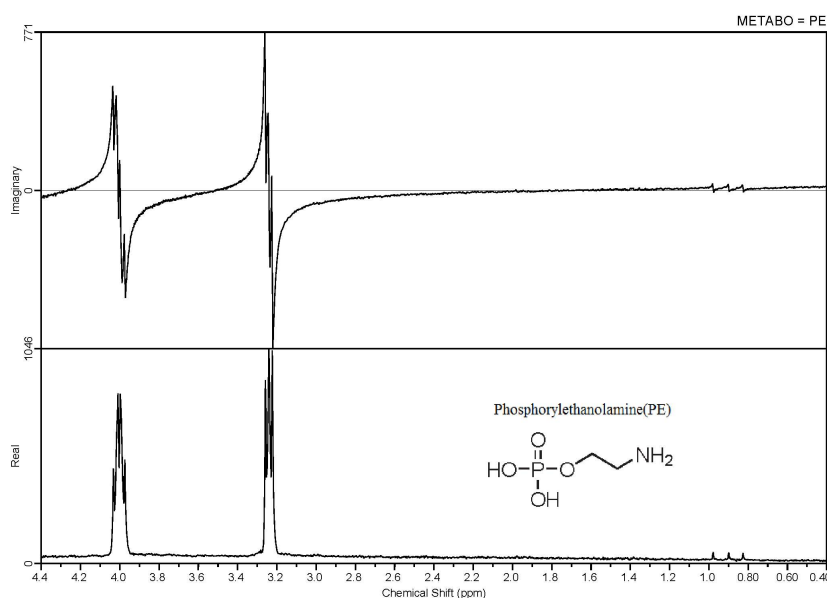


Figure A.14: *In vitro* spectra of **Phosphorylethanolamine** metabolite measured at 7T using STEAM with VERSE pulses, duration pulse of 2.5 ms, TR/TE/TM=3000/20/15 ms, voxel size of 3.5 mL and 2048 data points. Real and imaginary spectra in frequency domain and the chemical structure of the **Phosphorylethanolamine** have been demonstrated. The chemical shift range is from 0.4 ppm to 4.4 ppm.

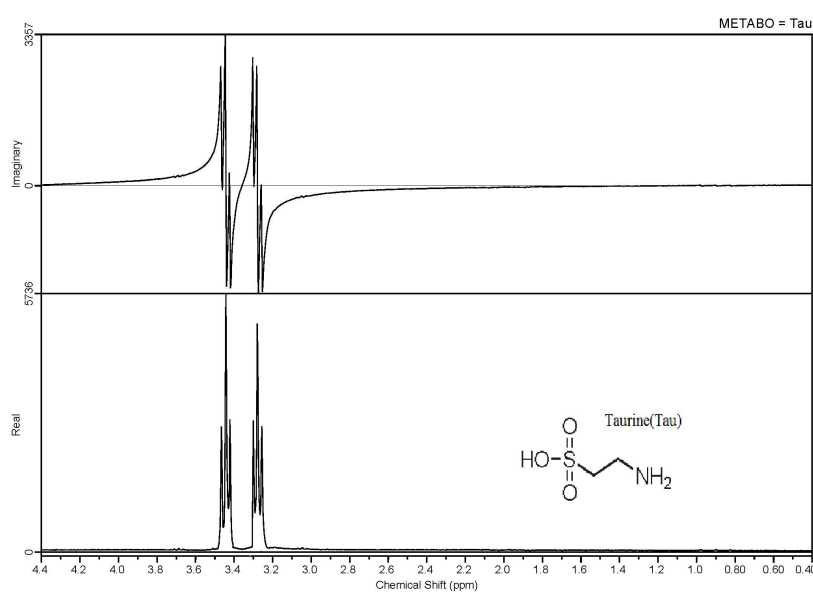


Figure A.15: *In vitro* spectra of **Taurine** metabolite measured at 7T using STEAM with VERSE pulses, duration pulse of 2.5 ms, TR/TE/TM=3000/20/15 ms, voxel size of 3.5 mL and 2048 data points. Real and imaginary spectra in frequency domain and the chemical structure of the **Taurine** have been demonstrated. The chemical shift range is from 0.4 ppm to 4.4 ppm.

Appendix B

The following metabolites did not quantified.

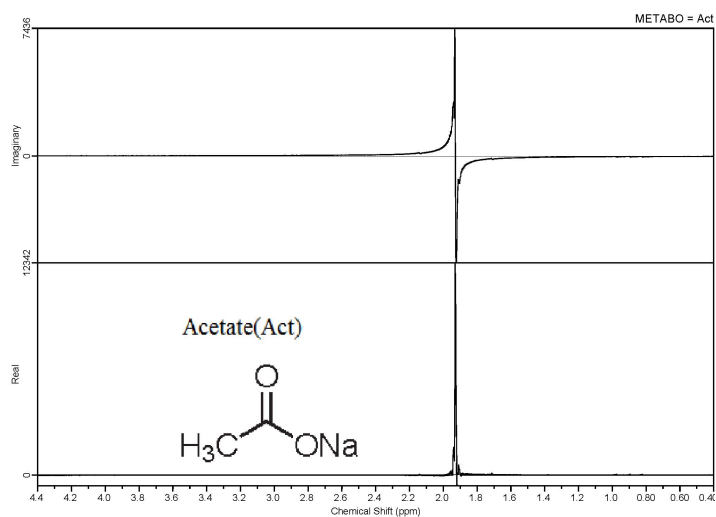


Figure B.1: *In vitro* spectra of **Acetate** metabolite measured at 7T using STEAM with VERSE pulses, duration pulse of 2.5 ms, TR/TE/TM=3000/20/15 ms, voxel size of 3.5 mL and 2048 data points. Real and imaginary spectra in frequency domain and the chemical structure of the **Acetate** have been demonstrated. The chemical shift range is from 0.4 ppm to 4.4 ppm.

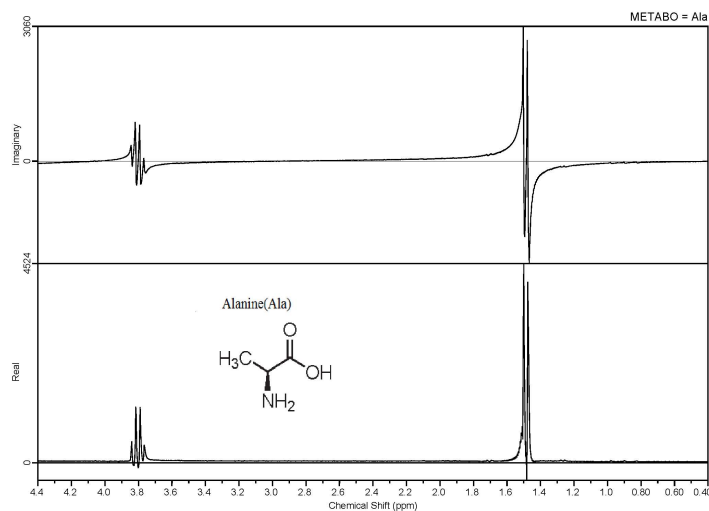


Figure B.2: *In vitro* spectra of **Alanine** metabolite measured at 7T using STEAM with VERSE pulses, duration pulse of 2.5 ms, TR/TE/TM=3000/20/15 ms, voxel size of 3.5 mL and 2048 data points. Real and imaginary spectra in frequency domain and the chemical structure of the **Alanine** have been demonstrated. The chemical shift range is from 0.4 ppm to 4.4 ppm.

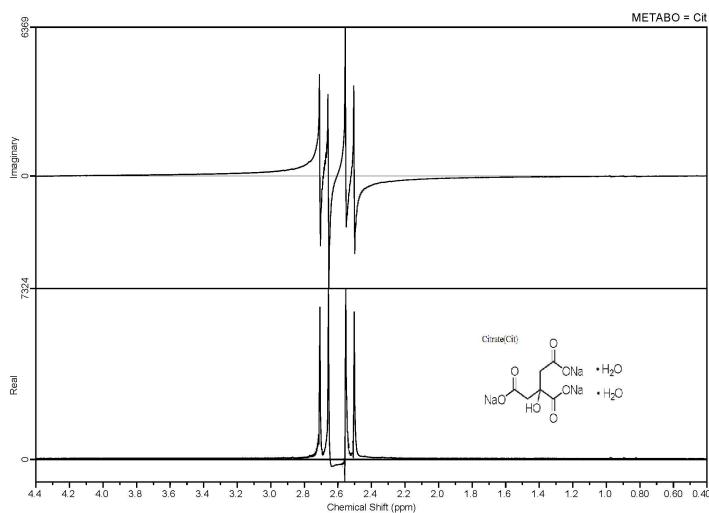


Figure B.3: *In vitro* spectra of **Citrate** metabolite measured at 7T using STEAM with VERSE pulses, duration pulse of 2.5 ms, TR/TE/TM=3000/20/15 ms, voxel size of 3.5 mL and 2048 data points. Real and imaginary spectra in frequency domain and the chemical structure of the **Citrate** have been demonstrated. The chemical shift range is from 0.4 ppm to 4.4 ppm.

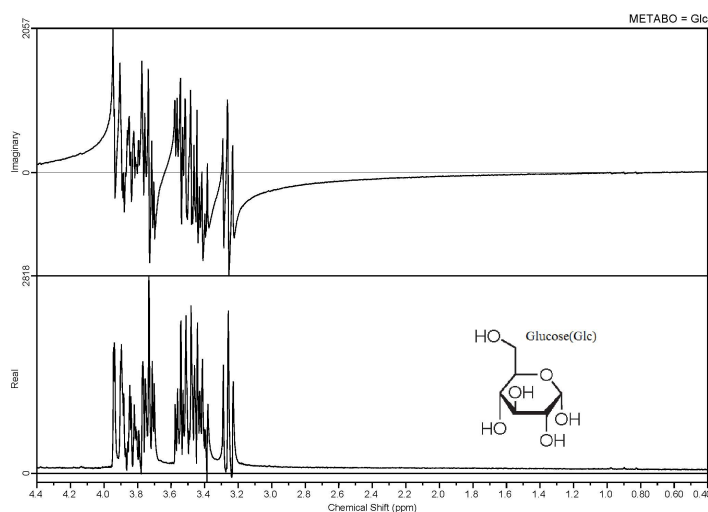


Figure B.4: *In vitro* spectra of **Glucose** metabolite measured at 7T using STEAM with VERSE pulses, duration pulse of 2.5 ms, TR/TE/TM=3000/20/15 ms, voxel size of 3.5 mL and 2048 data points. Real and imaginary spectra in frequency domain and the chemical structure of the **Glucose** have been demonstrated. The chemical shift range is from 0.4 ppm to 4.4 ppm.

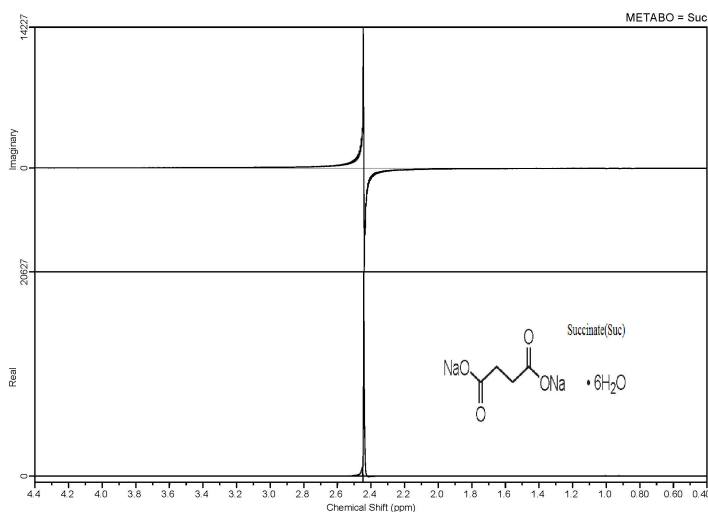


Figure B.5: *In vitro* spectra of **Succinate** metabolite measured at 7T using STEAM with VERSE pulses, duration pulse of 2.5 ms, TR/TE/TM=3000/20/15 ms, voxel size of 3.5 mL and 2048 data points. Real and imaginary spectra in frequency domain and the chemical structure of the **Succinate** have been demonstrated. The chemical shift range is from 0.4 ppm to 4.4 ppm.

Appendix C

The simulated bases set based on two parameters (1) RF pulse sequence and (2) Spin system of each metabolite. The pulse program can be written using the SIM-WIN program (teaching version) [67]. Figure C.1 demonstrates the STEAM with VERSE pulses which used in the simulation process. Figure C.2 shows the simulated spectrum of the analine (Ala) metabolite using STEAM with VERSE pulses, pulse duration of 2.5 ms, TR/TE/TM =3000/74/68 ms. The pulse program of STEAM with VERSE pulses can be described as following

; STEAM with VERSE sequence

1 ze

2 d1

p16:sp0

d2

p16:sp0

d3

p16:sp0

d4

go=2

ihc

lo to 2 times l1

wr #0

exit

Spin System Definition

Each line in the description file of spin system contains at most one command. The

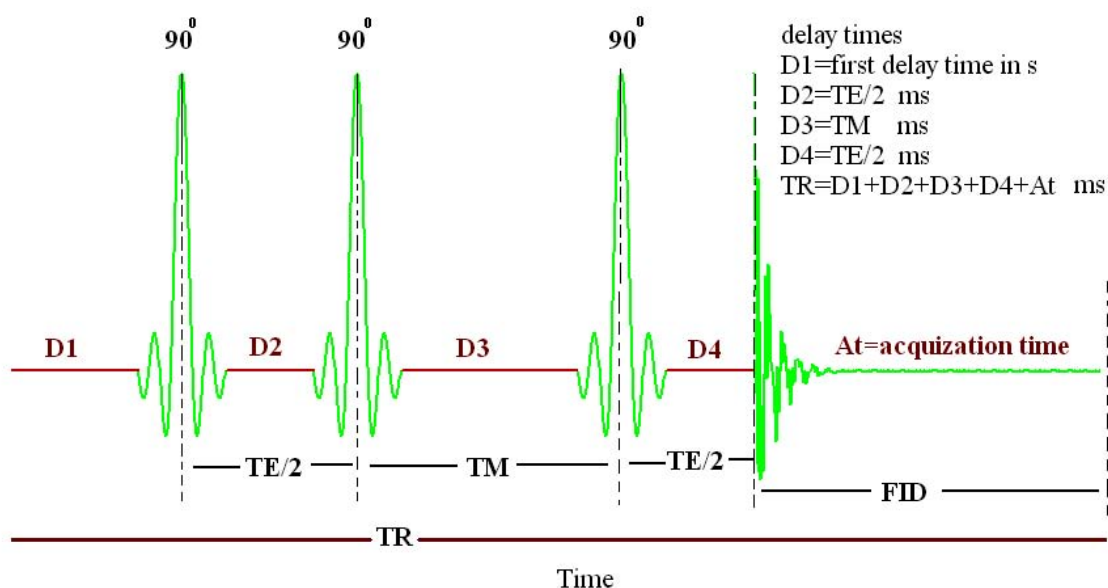


Figure C.1: STEAM pulses using the NMR simulation program. The sinc pulse matched with the same pulse used at 7T device i.e., included VERSE pulses. $TR/TE/TM=3000/74/68$ ms

lines starting with a semi-colon (;) are comments. Several molecules can be defined in one spin system description file. The molecules are completely independent, NMR-SIM calculates the resulting signal as a weighted mixture of signals from single molecules. The limitation of this method is that it is not possible to define an interaction between nuclei in different molecules. Every molecule must have a command line that is (molecule, molecule-name and the relative concentration of this molecule in the mixture) for example of alanine molecule (molecule alanine 1). The syntax of nuclei of spin (1/2) can be written as (nucleus [multiplicity *label] [chemical shift] [relax. times]), for example (proton 3*b 1.46 t1=3 t2=0.27) respectively. Moreover, the command (couple a b j) represents the j-coupling between two nuclei a and b. In the end the file ended by command (endmol).

;example of a spin system of alanine with TMSP and Na-formate molecules (Ala.ham)

; Metabolite Alanine:

molecule alanine 1

;CH-Group (c2)

proton a 3.7746 t1=3 t2=0.270

;CH-Group (C3)

proton 3*b 1.4667 t1=3 t2=0.270

;proton-proton coupling:

couple a b 7.234

;molecule tpsps

Proton y 0.00 t1=3 t2=0.270

;molecule formate 1

Proton x 8.44 t1=3 t2=0.270

endmol

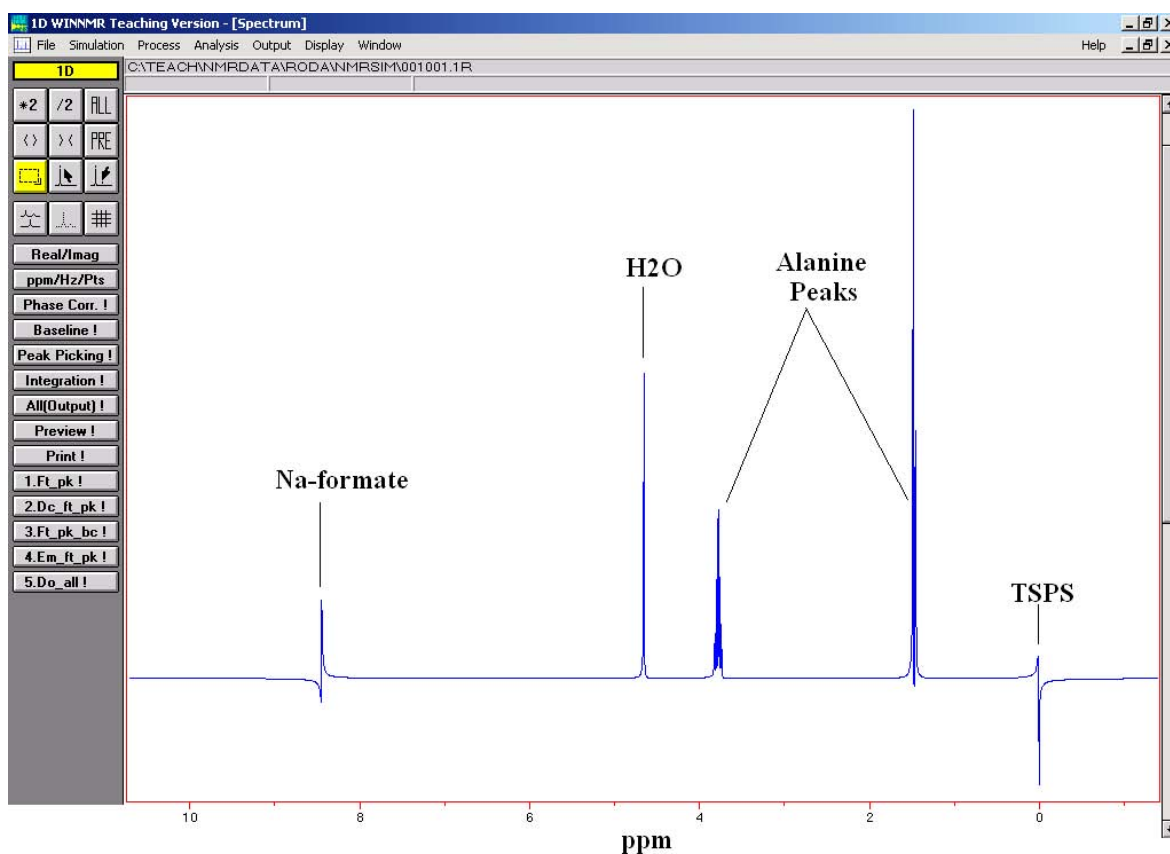


Figure C.2: Simulated *in vitro* spectrum of alanine using NMR-SIM program at 7T. The simulated spectrum includes two singlets reference peaks **TMSP** and **Na-Formate** at 0 and 8.4 ppm, respectively. Also the peak of water is included

Bibliography

- [1] G. Hasler, J. Vander-Veen, T. Tumonis, N. Meyers, J. Shen, and W. Drevets, “Reduced prefrontal glutamate/glutamine and gamma-aminobutyric acid levels in major depression determined using proton magnetic resonance spectroscopy,” *Arch Gen Psychiatry*, vol. 64, pp. 193–200, 2007.
- [2] P. Mandal, “Magnetic resonance spectroscopy (mrs) and its application in alzheimers disease,” *Concept Magnetic Res*, vol. 30, pp. 40–64, 2007.
- [3] P. Bottomley, “Spatial localization in nmr spectroscopy in vivo,” *Ann Ny Acad Sci*, vol. 508, pp. 333–348, 1987.
- [4] J. Frahm, K. D. Merfsoldt, and W. Hänicke, “Localized proton spectroscopy using stimulated echoes,” *J Magn Reson*, vol. 72, pp. 502–508, 1987.
- [5] C. Juchem, N. Logothetis, and J. Pfeuffer, “1h-mrs of the macaque monkey primary visual cortex at 7t: Strategies and pitfalls of shimming at the brain surface,” *Magn Reson Imaging*, vol. 25, pp. 902–912, 2007.
- [6] J. Kim, K. Chang, I. Song, S. Kim, B. Kwon, and M. Heehan, “Comparison of 1.5t and 3t 1h mr spectroscopy for human brain tumors,” *Korean J Radiol*, vol. 7, pp. 156–161, 2006.
- [7] K. Ugurbil, G. Adriany, P. Andersen, W. Chen, M. Garwood, and R. Gruetter, “Ultrahigh field magnetic resonance imaging and spectroscopy,” *Magn Reson Imaging*, vol. 21, pp. 1263–1281, 2003.
- [8] P. Barker, D. Hearshen, and M. Boska, “Signal - voxel proton mrs of the human brain at 1.5t and 3t,” *Magnet Reson Med*, vol. 45, pp. 765–769, 2001.

- [9] S. Michaeli, M. Garwood, X. Zhu, L. Delabarre, P. Andersen, G. Adriany, H. Merkle, K. Uğurbil, and W. Chen, “Proton t_2 relaxation study of water, n-acetylaspartate, and creatine in human brain using hahn and carr-purcell spin echoes at 4t and 7t,” *Magnet Reson Med*, vol. 47, pp. 629–633, 2002.
- [10] H. Qiao, X. Zhang, X. Zhu, F. Du, and W. Chen, “In vivo 31p mrs of human brain at high/ultrahigh field: A quantitative comparison of nmr detection sensitivity and spectral resolution between 4t and 7t,” *Magnet Reson Imaging*, vol. 24, pp. 1281–1286, 2006.
- [11] R. Gruetter, S. Weisdorf, V. Rajanayagan, M. Terpstra, H. Merkle, C. Truwit, M. Garwood, S. Nyberg, and K. Uğurbil, “Resolution improvements in in vivo 1h nmr spectra with increased magnetic field strength,” *J Magn Reson*, vol. 135, pp. 260–264, 1998.
- [12] I. Tkáč, P. Henry, P. Andersen, C. Keene, W. Low, and R. Gruetter, “Highly resolved in vivo 1h nmr spectroscopy of the mouse brain at 9.4t,” *Magnet Reson Med*, vol. 52, pp. 478–484, 2004.
- [13] I. Tkáč, R. Rao, M. Georgieff, , and R. Gruetter, “Development and determined by d regional changes in the neurochemical profile of the rat brain in vivo 1h nmr spectroscopy,” *Magnet Reson Med*, vol. 50, pp. 24–32, 2003.
- [14] R. Mekle, V. MlynaRik, G. Gambarota, M. Hergt, G. Krueger, and R. Gruetter, “. mr spectroscopy of the human brain with enhanced signal intensity at ultrashort echo times on a clinical platform at 3t and 7t,” *Magnet Reson Med*, vol. 61, pp. 1279–1285, 2009.
- [15] T. Michaelis, K. Merboldt, H. Bruhn, W. Haenicke, and J. Frahm, “Absolute concentrations of metabolites in the adult human brain in vivo: Quantification of localized proton mr spectra,” *Neuroradiology*, vol. 187, pp. 219–227, 1993.
- [16] P. Pouwels and J. Frahm, “Regional metabolite concentrations in human brain as determined by quantitative localized proton mrs,” *Mrm*, vol. 39, pp. 53–60, 1998.

- [17] P. Barker, B. Soher, S. Blackband, J. Chatham, V. Mathews, and R. Bryan, "Quantitation of proton nmr spectra of the human brain using tissue water as an internal concentration reference," *Nmr In Biomedicine*, vol. 6, pp. 89–94, 1993.
- [18] G. Jost, I. Harting, and S. Heiland, "Quantification signal-voxel spectroscopy: The reciprocity principle for receive-only head coils," *J Magn Reson Imaging*, vol. 21, pp. 66–71, 2005.
- [19] G. Adriany and R. Gruetter, "A half-volume coil for efficient proton decoupling in humans at 4 tesla," *J Magn Reson*, vol. 125, pp. 178–184, 1997.
- [20] I. Tkáč and R. Gruetter, "Methodology of 1h nmr spectroscopy of the human brain at very high magnetic fields," *Appl Magn Reson*, vol. 29, pp. 139–157, 2005.
- [21] B. Hargreaves, C. Cunningham, D. Nishimura, and S. Conolly, "Variable-rate selective excitation for rapid mri sequences," *Magnet Reson Med*, vol. 52, pp. 590–597, 2004.
- [22] O. Khorkhordin, K. Zhong, F. Godenschweger, and O. Speck, "Verse implementation for steam at 7t," in *Proc. Intl. Soc. Mag. Reson. Med.*, 2009.
- [23] A. Kumar, A. Thomas, H. Lavretsky, K. Yue, A. Huda, J. Curran, T. Venkatraman, L. Estanol, J. Mintz, M. Mega, and A. Toga, "Frontal white matter biochemical abnormalities in late-life major depression detected with proton magnetic resonance spectroscopy," *Am J Psychiatry*, vol. 4, pp. 630–636, 2002.
- [24] D. Rosenberg, F. Macmaster, Y. Mirza, J. Smith, P. Easter, S. Banerjee, R. Bhandari, C. Boyd, M. Lynch, M. Rose, J. Ivey, R. Villafuerte, G. Moore, and P. Renshaw, "Reduced anterior cingulate glutamate in pediatric major depression: A magnetic resonance spectroscopy study," *Biol Psychiatry*, vol. 58, p. 700704, 2005.
- [25] J. Frahm, H. Bruhn, M. Gyngellk, K. Merboldtw, W. HÄnicke, and R. Sauter, "Localization high-resolution proton nmr spectroscopy using stimulated echoes: Initial applications to human brain in vivo," *Magnet Reson Med*, vol. 9, pp. 79–93, 1989.

- [26] N. E. Jacobsen, *NMR Spectroscopy Explained*. Wiley, P.18, 2007.
- [27] M. H. Levitt, *Spin Dynamics: Basics of Nuclear Magnetic Resonance*. John Wiley And Sons Ltd, 2nd ed., pp. 6-7, 2007.
- [28] W. Demtröder, *Atoms, Molecules and Photons: an Introduction to Atomic-, Molecular and Quantum-Physics*. Springer, 2nd ed., pp. 7-10, 2010.
- [29] M. Balci, *Basic 1H- and 13C-NMR Spectroscopy*. Elsevier, P. 11, 2005.
- [30] J. Keeler, *Understanding NMR Spectroscopy*. Wiley, pp. 2-6, 2002.
- [31] M. Brown and C. Richard, *MRI Basic Principles and Applications*. Wiley, 3th ed., pp. 182-187, 2003.
- [32] N. E. Jacobsen, *NMR Spectroscopy Explained*. Wiley, P.34, 2007.
- [33] D. L. Pavia, G. M. Lampman, G. S. Kriz, and J. R. Vyvyan, *Introduction to Spectroscopy*,. Brooks Cole, 4th ed., pp. 109-113, 2008.
- [34] M. Brown and C. Richard, *MRI Basic Principles and Applications*. Wiley, 3th ed., pp. 21-31, 2003.
- [35] D. Weishaupt, V. Köchli, and B. Marincek, *How Does MRI Work?* Springer, 2nd ed., pp. 12-15, 2006.
- [36] R. H. Hashemi, *MRI the Basics*. Lippincott Williams, 2nd ed., pp. 49-56, 2004.
- [37] M. Balci, *Basic 1H- and 13C-NMR Spectroscopy*. Elsevier, pp. 25-30, 2005.
- [38] U. Klose, "Measurement sequences for signal-voxel proton mr spectroscopy," *European Journal of Radiology*, vol. 67, pp. 194–201, 2008.
- [39] R. De-Graaf and D. Rothman, "In vivo detection and quantification of scalar coupled 1h nmr resonances," *Concept Magnetic Res*, vol. 13, 2001.
- [40] M. Balci, *Basic 1H- and 13C-NMR Spectroscopy*. Elsevier, p. 91, 2005.
- [41] D. Pavia, G. Lampman, G. Kriz, and J. Vyvyan, *Introduction to Spectroscopy*. Brooks-Cole, 4th ed., pp. 199-201, 2008.

- [42] *Syngo MR Operator Manual*. Siemens Ag, 2006.
- [43] A. Knijn, R. De-Beer, and D. Van-Ormondt, “Frequency-selective quantitation in the time domain,” *J Magn Reson*, vol. 97, pp. 444–450, 1992.
- [44] G. Mckinnon, C. Burger, and P. Boesiger, “Spectral baseline correction using clean,” *Magn Reson Med*, vol. 13, pp. 145–149, 1990.
- [45] R. De-Beer and D. Van-Ormondt, “Analysis of nmr data using time domain fitting procedures,” *Chapter In Nmr Basic Principles And Progress*, vol. 26, pp. 202–248, 1992.
- [46] U. Klose, “In vivo proton spectroscopy in presence of eddy currents,” *Magn Reson Med*, vol. 14, pp. 26–30, 1990.
- [47] S. Provencher, “Estimation of metabolite concentrations from localized in vivo proton nmr spectra,” *Magn Reson Med*, vol. 30, pp. 672–679, 1993.
- [48] J. Keeler, *Understanding NMR Spectroscopy*. Wiley, pp. 61-62, 2002.
- [49] P. Mandal, “In vivo proton magnetic resonance spectroscopy signal processing for the absolute quantitation of brain metabolites,” *Eur J Radiol*, pp. 1–12, 2011.
- [50] A. Greiser, *Proc Scmr*, vol. 9, p. 373, 2007.
- [51] J. Schneider and P. Jezzard, in *Proc. Intl. Soc.Mag.Reson. Med*, 14, 1177, 2006.
- [52] M. S. E. Al, *Magn Reson Med*, vol. 51, pp. 799–806, 2004.
- [53] M. Schaer and E. Al, in *Proc. Intl. Soc.Mag.Reson. Med*, 14, 1735, 2002.
- [54] A. Hasse, J. Frahm, W. Hnicke, D. Matthaei, H. Bomsdorf, and W. Vollmann, “1h-nmr chemical shift selective (chess) imaging,” *Phys Med Biol*, vol. 30, pp. 341–344, 1985.
- [55] D. Matthaei, A. Haase, J. Frahm, H. Bomsdorf, and W. Vollmann, “Multiple chemical shift selective (chess) mr imaging using stimulated echoes,” *Radiology*, vol. 160, pp. 791–794, 1986.

- [56] M. Elywa, K. Zhong, and O. Speck, "Localized adjustment of radiofrequency pulses for high field mr-spectroscopy," *Arab J Nucl Sci Appl*, vol. 42, pp. 131–140, 2009.
- [57] E. Hahn, "Spin echoes," *Phys Rev*, vol. 80, pp. 580–594, 1950.
- [58] R. De-Graaf, *In Vivo NMR Spectroscopy: Principles And Techniques*. John Wiley and Sons Ltd., Usa, 2007.
- [59] C. Thomsen, K. Jensen, M. Jensen, E. Olsen, and O. Henriksen, "Mr pulse sequences for selective relaxation time measurements: A phantom study," *Magn Reson Imaging*, vol. 8, pp. 43–50, 1990.
- [60] P. Narayana, D. Johnston, and D. Flamig, "In vivo proton magnetic resonance spectroscopy studies of human brain," *Magn Reson Imaging*, vol. 9, pp. 303–308, 1991.
- [61] U. Seeger, I. Mader, T. Ngele, W. Grodd, O. Lutz, and U. Klose, "Reliable detection of macromolecules in single-volume 1h nmr spectra of the human brain," *Magnet Reson Med*, vol. 45, pp. 948–954, 2001.
- [62] U. Klose, I. Mader, W. Grodd, T. Nagele, and U. Seeger, "Parameterized evaluation of macromolecules and lipids in proton mr spectroscopy of brain diseases," *Magnet Reson Med*, vol. 49, pp. 19–28, 2003.
- [63] S. Conolly, G. Glover, D. Nishimura, and A. Macovski, "A reduced power selective adiabatic spin echo pulse sequence," *Magnet Reson Med*, vol. 18, pp. 28–38, 1991.
- [64] M. A. Bernstein, K. E. King, and X. J. Zhou, *Handbook of MRI Pulse Sequences*, 2004.
- [65] D. Hoult and R. Richards, "The signal-to-noise ratio of the nuclear magnetic resonance experiment," *J Magn Reson*, vol. 24, pp. 71–85, 1976.
- [66] F. David, "Practical aspects of birdcage coils," *J Magn Reson*, vol. 138, pp. 144–154, 1999).
- [67] C. Shorn and B. Taylor, *NMR Spectroscopy: Data Acquisition*. Wiley, 2004.

- [68] S. W. Provencher, "Automatic quantitation of localized in vivo 1h spectra with lmodel," *Nmr Biomed*, vol. 14(4), p. 260–264, 2001.
- [69] M. Kanowski, J. Kaufmann, J. Braun, J. Bernarding, and C. Tempelmann, "Quantitation of simulated short echo time 1h human brain spectra by lmodel and amares," *Magn Reson Med*, vol. 51, pp. 904–912, 2004.
- [70] M. Walter, A. Henning, S. Grimm, R. Schulte, J. Beck, U. Dydak, B. Schnepf, H. Boeker, P. Boesiger, and G. Northoff, "The relationship between aberrant neuronal activation in the pregenual anterior cingulate, altered glutamatergic metabolism, and anhedonia in major depression," *Arch Gen Psychiatry*, vol. 66, pp. 478–486, 2009.
- [71] R. Schulte, T. Lange, J. Beck, D. Meier, and P. Boesiger, "Improved two-dimensional j-resolved spectroscopy," *Nmr Biomed*, vol. 19, pp. 264–270, 2006.
- [72] A. Boss, R. Kreis, S. Jenni, J. Nuoffer, E. Christ, C. Boesch, and C. Stettler, "Non-invasive assessment of exercise-related intramyocellular acetylcarnitine in eu- and hyperglycemia in type 1 diabetic subjects using 1h-magnetic resonance spectroscopy," *Diabetes Care*, vol. 34, pp. 220–222, 2011.
- [73] B. Ross, R. Kreis, and T. Ernst, "Clinical tools for the 90s: Magnetic resonance spectroscopy and metabolite imaging," *European Journal Of Radiology*, vol. 14, pp. 128–140, 1992.
- [74] R. Kreisand, N. Farrow, and B. Ross, "Localized 1h nmr spectroscopy in patients with chronic hepatic encephalopathy analysis of changes in cerebral glutamine and choline and inositols," *Nmr Biomed*, vol. 4, pp. 109–116, 1991.
- [75] J. Slotboom, C. Boesch, and R. Kreis, "Versatile frequency domain fitting using time domain models and prior knowledge," *Magn Reson Med*, vol. 39, pp. 899–911, 1998.
- [76] J. Jansen, W. Backes, K. Nicolay, and M. Kooi, "1h mr spectroscopy of the brain: Absolute quantification of metabolites," *Radiology*, vol. 240, pp. 318–332, 2006.

- [77] D. Auer, "Reduced glutamate in the anterior cingulate cortex in depression: An in vivo proton magnetic resonance spectroscopy study," *Biol Psychiatry*, vol. 47, pp. 305–313, 2000.
- [78] A. Yesiloglu and D. Ankerst, "Review of 1h magnetic resonance spectroscopy findings in major depressive disorder: A meta-analysis," *Psychiatry Res*, vol. 147, pp. 1–25, 2006.
- [79] B. Pfeleiderer, "Effective electroconvulsive therapy reverses glutamate/glutamine deficit in the left anterior cingulum of unipolar depressed patients," *Psychiatry Res*, vol. 122, pp. 185–192, 2003.
- [80] N. Michael, "Metabolic changes within the left dorsolateral prefrontal cortex occurring with electroconvulsive therapy in patients with treatment resistant unipolar depression," *Psychol Med*, vol. 33, pp. 1277–1284, 2003.
- [81] D. Glitz, H. Manji, and G. Moore, "Mood disorders: Treatment-induced changes in brain neurochemistry and structure," *Semin Clin Neuropsychiatry*, vol. 7, pp. 269–280, 2002.
- [82] G. Malhi, M. Valenzuela, W. Wen, and P. Sachdev, "Magnetic resonance spectroscopy and its applications in psychiatry," *Aust N Z J Psychiatry*, vol. 36, pp. 31–43, 2002.
- [83] D. Hardy and T. Norwood, "Spectral editing technique for the in vitro and in vivo detection of taurine," *J Magn Reson*, vol. 133, pp. 70–78, 1998.
- [84] U. Seeger, U. Klose, O. Lutz, and W. Grodd, "Elimination of residual lipid contamination in single volume proton mr spectra of human brain," *Magn Reson Imaging*, vol. 17, p. 1926, 1999.
- [85] C. Choiand, P. Bhardwajand, P. Seresand, S. Kalra, P. Tibboand, and N. Coupland, "Measurement of glycine in human brain by triple refocusing 1h-mrs in vivo at 3.0t," *Magn Reson Med*, vol. 59, pp. 59–64, 2008.
- [86] S. Yang, J. Hu, Z. Kou, and Y. Yang, "Spectral simplification for resolved glutamate and glutamine measurement using a standard steam sequence with

- optimized timing parameters at 3, 4, 4.7, 7, and 9.4t,” *Magn Reson Med*, vol. 59, p. 236244, 2008.
- [87] I. Tkáč, G. Öz, G. Adriany, and K. U. R. Gruetter, “In vivo 1h nmr spectroscopy of the human brain at high magnetic fields: Metabolite quantification at 4t vs. 7t,” *Magn Reson Med*, vol. 62(4), p. 868879, 2009.
- [88] V. Govindaraju, K. Young, and A. Maudsley, “Proton nmr chemical shifts and coupling constants for brain metabolites,” *Nmr Biomed*, vol. 2000, pp. 129–153, 13.

List of Tables

3.1	Twenty metabolite solutions and reference substances of LCModel basis set	21
4.1	Correction factors and voltages at 3T and 7T scanners	38
4.2	The excitation voltages and the calculated voltages for different positions at 3T and 7T.	42
4.3	The resultant data at 3T and 7T.	43
4.4	Comparison between the absolute concentrations of the human brain metabolites of 6 healthy subjects at 7T using simulated and experimental basis sets	50
4.5	Three groups of spectra measured in the pgACC brain region of five healthy subjects at 7T.	52
4.6	Comparison between the relative concentration levels of metabolites in pgACC at 7T using STEAM with VERSE at 7T and PRESS at 3T (3 subjects) relative to JPRESS at 3T.	55
4.7	Concentration levels of human brain metabolites of 8 healthy volunteers in the parietal region.	59
4.8	Concentration levels of the human brain metabolites of 8 healthy volunteers in the pgACC region.	60
4.9	NAAG, MM20 levels of human brain metabolites of 6 healthy volunteers in the pgACC region using the long TE = 74 ms.	62
4.10	Concentration levels of the human brain metabolites of 6 healthy subjects acquired from the PCC area at 7T	64

4.11	Concentration levels of the human brain metabolites of 6 healthy subjects acquired from the AMCC area at 7T	66
4.12	Concentration levels of the human brain metabolites of 6 healthy subjects acquired from the 23c area at 7T	68
A.1	Metabolite chemical structure (carbon and nitrogen groups), proton chemical shift, multiplicity and J-coupling values for human brain metabolites.	83
A.2	Continuous of Table A.1	84

List of Figures

2.1	The rotational energy states of a molecule such as H ₂ O in the absence of magnetic field and on applying it.	5
2.2	The net magnetization M_0 of a sample along the magnetic field direction B_0 , at equilibrium. The coordinates (x, y and z) are right-handed. . . .	8
2.3	Applying an external magnetic field B_0 leads to the magnetization vector being tilted away from the z axis. The proton has two motion: one around its own axis that is denoted by the magnetic moment μ and a precessing motion around the direction of B_0 . The magnetic moment sweeps by a certain angle from the B_0 direction. The vector sweeps out a cone of constant angle to the magnetic field direction. This precessing frequency is known as the Larmor frequency ω_0	9
2.4	The relaxation times, the spin-lattice or longitudinal relaxation time, T_1 .	10
2.5	The relaxation times (spin-spin or transverse relaxation time, T_2). . . .	11
2.6	The chemical shift in ppm between water and the fat spectra at 7 T. . .	14
2.7	Chemical shift and J-coupling of two coupled protons H_A and H_B (spin-spin splitting). The coupling constant $^3J_{AB}$, (3) indicates the number of chemical bonds, and (AB) shows the coupled protons.	16
2.8	1H MRS spectrum of GABA solution measured at 7T. (A) The chemical structure of the compound and (B) The spectral peaks in the range 0.4 ppm to 4.4 ppm.	17
2.9	The localization techniques for MR spectroscopy applications (A) The SVS shows the intersection of three slices (VOI) (B) The CSI shows several voxels of FOV.	17

3.1	Chemical structures of (A) TMS and (B) Na-formate reference substances	22
3.2	1H -MRS spectrum represents (A) Water signal besides the metabolite signals (unsuppressed water option). (B) The metabolite signals besides the water (after water suppression was done).	26
3.3	Water suppression (CHESS) pulses.	27
3.4	Three FIDs (FID1, FID2, and FID3) achieved for spin echoes SE_{12} , SE_{13} , SE_{23} , and SE_{123} respectively. Moreover, one stimulated echo (STE) can be generated. (A) The echoes appear at distinct temporal positions, depending on the (TE) and TM periods. (B) The (ADC) of the four echoes have been shown respect to time scale.	27
3.5	PRESS sequence with three RF pulses applied simultaneously with the field gradients along the main axes of the magnet.	29
3.6	Sequence scheme for the STEAM sequence. The refocusing gradients need to be positioned before the second RF pulse and after the third RF pulse.	29
3.7	Variable-rate modification to a sinc RF pulse. (A) The original RF envelope A_0 is attenuated wherever the gradient amplitude G_0 is reduced. (B) VR-modified sinc pulse of amplitude A_{VR} with a concurrent gradient G_{VR} .	30
3.8	Pulse shape display in NMR-SIM	31
3.9	The excitation profile of the sinc 90° pulse of the STEAM with VERSE pulses.	32
3.10	The whole body 7 Tesla system	33
3.11	Volume coil setup (A) Tuning the coil at the 7T frequency circa 300MHz, (B) Connection of the coil with the scanner.	34
4.1	Different positions in a phantom sample (gray scale of the gradient echo image inverted)	37
4.2	Measured data points of one position acquired at 3T while the red line is the fit using the equation $f(x) = a * \sin(b * x)$.	39
4.3	The fitting curve using $f(x) = a * \sin^3(b * x)$ for the experimental data points of one position examined at 7T	40

4.4	The relationship between the correction factor and the fraction V_{cal}/V_{exc} at 3T B) The relationship between the correction factor and the fraction V_{cal}/V_{exc} at 7T.	41
4.5	Comparison between the STEAM and STEAM with VERSE pulses.	44
4.6	Twenty metabolite spectra of the <i>in vitro</i> database using TR = 3 s, TE = 20 ms and TM = 15 ms at 7T	45
4.7	The 20 <i>In vitro</i> spectra of metabolite solutions using long TE = 74 ms and TM = 68 ms at 7T	46
4.8	Simulated and experimental spectra of Glutamate solution using TE = 20 ms at 7T	47
4.9	LCMdel fit of 1H -MRS human brain spectrum measured in the Brodmann 23C region from a healthy volunteer using experimental basis set with TR = 3 s, TE = 20 ms and TM = 15 ms at 7T	48
4.10	1H -MRS human brain spectrum measured in the Brodmann 23C area from a healthy volunteer. The red line shows the LCModel fit using the simulated basis set (WIN-SIM) with TR = 3 s, TE = 20 ms and TM = 15 ms and at 297.14 MHz (7T)	49
4.11	Three human brain spectra measured in the pgACC region with different number of averages and TR of the same healthy subjects. (A) TR = 3000 ms, averages = 128 (B) TR = 2500 ms, averages = 152 (C) TR = 2000 ms, averages = 192.	51
4.12	LCModel fit spectrum of the human brain data measured in the pgACC region using the simulated basis set of TR=3000 ms, TE = 20 ms and TM = 15 ms at 7T	53
4.13	LCModel fit spectrum of human brain data measured in the pgACC region using the simulated basis set of TR=3000 ms, TE = 74 ms and TM = 68 ms at 7T	54
4.14	Human brain NMR spectra were acquired from the pgACC region in one volunteer a) at 7T using STEAM with VERSE, 128 averages, TR/TE/TM = 3000/20/15 ms, and voxel volume = 1.8 mL and b) at 3T using PRESS, 256 averages, TR/TE = 2000/35 ms, voxel volume = 2.5 mL, together with the LCModel fitting curve.	56

4.15	<i>In vivo</i> 1H -NMR spectrum acquired from the parietal white matter at 7T. STEAM with VERSE ($V_f = 1.4$), TR/TE/TM = 3000/20/15 ms, voxel volume = 151515 mm^3 , BW = 3600 Hz, acquisition size = 2048, and averages = 128. (A) VOI location (B) measured data (C) LCModel fit of the spectrum	58
4.16	The <i>in vivo</i> 1H -MRS spectrum acquired from the pgACC GM at 7T. STEAM with VERSE factor = 1.4, TR/TE/TM = 3000/20/15 ms, voxel volume = 3.8 mL, BW = 3600 Hz, vector size = 2048, and averages = 128	61
4.17	1H -MRS spectrum acquired from the pgACC grey matter (GM) of 6 healthy subjects at 7T. STEAM with VERSE factor = 1.4, voxel size = 3.8 mL, BW = 2800 Hz, vector size = 2048, and averages = 128. A) negative relationship between CRLB of MM20 vs NAAG using TR/TE/TM = 3000/20/15 ms. B) A relation between CRLB of NAAG vs MM20 using TR/TE/TM = 3000/74/68 ms	63
4.18	The <i>in vivo</i> 1H NMR spectrum acquired from the PCC grey matter at 7T. STEAM with VERSE factor = 1.4, TR/TE/TM = 3000/20/15 ms, voxel size = 3.8 mL, BW = 2800 Hz, vector size = 2048, and average = 128	65
4.19	LCModel fit of 1H -MRS spectrum acquired from the AMCC region at 7T. STEAM with VERSE factor = 1.4, TR/TE/TM = 3000/20/15 ms, voxel size = 3.8 mL, BW = 2800 Hz, vector size = 2048, and average = 128	67
4.20	The LCModel fit of 1H NMR spectrum acquired from the 23C at 7T. STEAM with VERSE factor = 1.4, TR/TE/TM = 3000/20/15 ms, voxel size = 3.8 mL, BW = 2800 Hz, vector size = 2048, and average = 128 .	69
4.21	The statistical correlation between GM and Gln using the LCModel fit spectrum of human brain data of 10 healthy subjects measured in the parietal and pgACC brain regions with TR/TE/TM = 3000/20/15 ms at 7T	71
4.22	Human metabolites correlation between Gln and Glu using LCModel fit spectrum of human brain data measured in pgACC region (A) with short TE = 20 ms and (B) with long TE = 74 ms at 7T	72

- A.1 *In vitro* spectra of **Aspartate** metabolite measured at 7T using STEAM with VERSE pulses, duration pulse of 2.5 ms, TR/TE/TM=3000/20/15 ms, voxel size of 3.5 mL and 2048 data points. Real and imaginary spectra in frequency domain and the chemical structure of the **Aspartate** have been demonstrated. The chemical shift range is from 0.4 ppm to 4.4 ppm. 82
- A.2 *In vitro* spectra of **Phosphocholine** metabolite measured at 7T using STEAM with VERSE pulses, duration pulse of 2.5 ms, TR/TE/TM=3000/20/15 ms, voxel size of 3.5 mL and 2048 data points. Real and imaginary spectra in frequency domain and the chemical structure of the **Phosphocholine** have been demonstrated. The chemical shift range is from 0.4 ppm to 4.4 ppm. 82
- A.3 *In vitro* spectra of **Glycerophosphocholine** metabolite measured at 7T using STEAM with VERSE pulses, duration pulse of 2.5 ms, TR/TE/TM=3000/20/15 ms, voxel size of 3.5 mL and 2048 data points. Real and imaginary spectra in frequency domain and the chemical structure of the **Glycerophosphocholine** have been demonstrated. The chemical shift range is from 0.4 ppm to 4.4 ppm. 85
- A.4 *In vitro* spectra of **Creatine** metabolite measured at 7T using STEAM with VERSE pulses, duration pulse of 2.5 ms, TR/TE/TM=3000/20/15 ms, voxel size of 3.5 mL and 2048 data points. Real and imaginary spectra in frequency domain and the chemical structure of the **Creatine** have been demonstrated. The chemical shift range is from 0.4 ppm to 4.4 ppm. 85
- A.5 *In vitro* spectra of **Phosphocreatine** metabolite measured at 7T using STEAM with VERSE pulses, duration pulse of 2.5 ms, TR/TE/TM=3000/20/15 ms, voxel size of 3.5 mL and 2048 data points. Real and imaginary spectra in frequency domain and the chemical structure of the **Phosphocreatine** have been demonstrated. The chemical shift range is from 0.4 ppm to 4.4 ppm. 86

- A.6 *In vitro* spectra of γ -**Aminobutric** Acid metabolite measured at 7T using STEAM with VERSE pulses, duration pulse of 2.5 ms, TR/TE/TM=3000/20/15 ms, voxel size of 3.5 mL and 2048 data points. Real and imaginary spectra in frequency domain and the chemical structure of the γ -**Aminobutric** have been demonstrated. The chemical shift range is from 0.4 ppm to 4.4 ppm. 86
- A.7 *In vitro* spectra of **Glutamine** metabolite measured at 7T using STEAM with VERSE pulses, duration pulse of 2.5 ms, TR/TE/TM=3000/20/15 ms, voxel size of 3.5 mL and 2048 data points. Real and imaginary spectra in frequency domain and the chemical structure of the **Glutamine** have been demonstrated. The chemical shift range is from 0.4 ppm to 4.4 ppm. 87
- A.8 *In vitro* spectra of **Glutamate** metabolite measured at 7T using STEAM with VERSE pulses, duration pulse of 2.5 ms, TR/TE/TM=3000/20/15 ms, voxel size of 3.5 mL and 2048 data points. Real and imaginary spectra in frequency domain and the chemical structure of the **Glutamate** have been demonstrated. The chemical shift range is from 0.4 ppm to 4.4 ppm. 87
- A.9 *In vitro* spectra of **Glycine** metabolite measured at 7T using STEAM with VERSE pulses, duration pulse of 2.5 ms, TR/TE/TM=3000/20/15 ms, voxel size of 3.5 mL and 2048 data points. Real and imaginary spectra in frequency domain and the chemical structure of the **Glycine** have been demonstrated. The chemical shift range is from 0.4 ppm to 4.4 ppm. 88
- A.10 *In vitro* spectra of **Gluthatione** metabolite measured at 7T using STEAM with VERSE pulses, duration pulse of 2.5 ms, TR/TE/TM=3000/20/15 ms, voxel size of 3.5 mL and 2048 data points. Real and imaginary spectra in frequency domain and the chemical structure of the **Gluthatione** have been demonstrated. The chemical shift range is from 0.4 ppm to 4.4 ppm. 88

- A.11 *In vitro* spectra of **Lactate** metabolite measured at 7T using STEAM with VERSE pulses, duration pulse of 2.5 ms, TR/TE/TM=3000/20/15 ms, voxel size of 3.5 mL and 2048 data points. Real and imaginary spectra in frequency domain and the chemical structure of the **Lactate** have been demonstrated. The chemical shift range is from 0.4 ppm to 4.4 ppm. 89
- A.12 *In vitro* spectra of **myo-Inositol** metabolite measured at 7T using STEAM with VERSE pulses, duration pulse of 2.5 ms, TR/TE/TM=3000/20/15 ms, voxel size of 3.5 mL and 2048 data points. Real and imaginary spectra in frequency domain and the chemical structure of the **myo-Inositol** have been demonstrated. The chemical shift range is from 0.4 ppm to 4.4 ppm. 89
- A.13 *In vitro* spectra of **N-acetylaspartate** metabolite measured at 7T using STEAM with VERSE pulses, duration pulse of 2.5 ms, TR/TE/TM=3000/20/15 ms, voxel size of 3.5 mL and 2048 data points. Real and imaginary spectra in frequency domain and the chemical structure of the **N-acetylaspartate** have been demonstrated. The chemical shift range is from 0.4 ppm to 4.4 ppm. 90
- A.14 *In vitro* spectra of **Phosphorylethanolamine** metabolite measured at 7T using STEAM with VERSE pulses, duration pulse of 2.5 ms, TR/TE/TM=3000/20/15 ms, voxel size of 3.5 mL and 2048 data points. Real and imaginary spectra in frequency domain and the chemical structure of the **Phosphorylethanolamine** have been demonstrated. The chemical shift range is from 0.4 ppm to 4.4 ppm. 90
- A.15 *In vitro* spectra of **Taurine** metabolite measured at 7T using STEAM with VERSE pulses, duration pulse of 2.5 ms, TR/TE/TM=3000/20/15 ms, voxel size of 3.5 mL and 2048 data points. Real and imaginary spectra in frequency domain and the chemical structure of the **Taurine** have been demonstrated. The chemical shift range is from 0.4 ppm to 4.4 ppm. 91

- B.1 *In vitro* spectra of **Acetate** metabolite measured at 7T using STEAM with VERSE pulses, duration pulse of 2.5 ms, TR/TE/TM=3000/20/15 ms, voxel size of 3.5 mL and 2048 data points. Real and imaginary spectra in frequency domain and the chemical structure of the **Acetate** have been demonstrated. The chemical shift range is from 0.4 ppm to 4.4 ppm. 92
- B.2 *In vitro* spectra of **Alanine** metabolite measured at 7T using STEAM with VERSE pulses, duration pulse of 2.5 ms, TR/TE/TM=3000/20/15 ms, voxel size of 3.5 mL and 2048 data points. Real and imaginary spectra in frequency domain and the chemical structure of the **Alanine** have been demonstrated. The chemical shift range is from 0.4 ppm to 4.4 ppm. 93
- B.3 *In vitro* spectra of **Citrate** metabolite measured at 7T using STEAM with VERSE pulses, duration pulse of 2.5 ms, TR/TE/TM=3000/20/15 ms, voxel size of 3.5 mL and 2048 data points. Real and imaginary spectra in frequency domain and the chemical structure of the **Citrate** have been demonstrated. The chemical shift range is from 0.4 ppm to 4.4 ppm. 93
- B.4 *In vitro* spectra of **Glucose** metabolite measured at 7T using STEAM with VERSE pulses, duration pulse of 2.5 ms, TR/TE/TM=3000/20/15 ms, voxel size of 3.5 mL and 2048 data points. Real and imaginary spectra in frequency domain and the chemical structure of the **Glucose** have been demonstrated. The chemical shift range is from 0.4 ppm to 4.4 ppm. 94
- B.5 *In vitro* spectra of **Succinate** metabolite measured at 7T using STEAM with VERSE pulses, duration pulse of 2.5 ms, TR/TE/TM=3000/20/15 ms, voxel size of 3.5 mL and 2048 data points. Real and imaginary spectra in frequency domain and the chemical structure of the **Succinate** have been demonstrated. The chemical shift range is from 0.4 ppm to 4.4 ppm. 94

-
- C.1 STEAM pulses using the NMR simulation program. The sinc pulse matched with the same pulse used at 7T device i.e., included VERSE pulses. TR/TE/TM=3000/74/68 ms 96
- C.2 Simulated *in vitro* spectrum of alanine using NMR-SIM program at 7T. The simulated spectrum includes two singlets reference peaks **TMSP** and **Na-Formate** at 0 and 8.4 ppm, respectively. Also the peak of water is included 97

Erklärung

Ich erkläre, dass ich die der Naturwissenschaftlichen Fakultät der Otto-von-Guericke-Universität zur Promotion eingereichten Dissertation mit dem Titel

STUDY OF HUMAN BRAIN METABOLITES USING MAGNETIC RESONANCE SPECTROSCOPY METHODS AT 7 TESLA

im Institut für Experimentelle Physik und die Abteilung biomedizinische Magnetresonanz (BMMR), der Otto-von-Guericke-Universität Magdeburg, mit Betreuung durch Prof. Dr. rer. nat. Oliver Speck ohne sonstige Hilfe durchgeführt und bei der Abfassung der Dissertation keine anderen als die dort aufgeführten Hilfsmittel benutzt habe. Bei der Abfassung der Dissertation sind Rechte Dritter nicht verletzt worden. Ich habe diese Dissertation bisher an keiner in- oder ausländischen Hochschule zur Promotion eingereicht. Ich übertrage der Naturwissenschaftlichen Fakultät das Recht, weitere Kopien meiner Dissertation herzustellen und zu vertreiben.

M.Sc. Mohammed Elywa

Curriculum Vitae

PERSONAL INFORMATION:

Name	Mohammed Abdelsalam Mohammed Elywa
First name	Mohammed
Family name	Elywa
Date of birth	27-03-73
Nationality	Egyptian
Gender	Male
Marital Status	Married (two children)
Occupation	Ph.D. Student
Affiliation	Otto-von-Guericke-University Magdeburg, Institute of Experimental Physics (IEP)
Work Address	Leipziger Str. 44, H65-ZENIT, 39120, Magdeburg
Home Address	Walter Rathenau Str 19, WNr. 0117, 39106 , Magdeburg
Phone No.	+49 391 6117117
Fax No.	+49 391 6117115
E-mail	mohamed.elywa@st.ovgu.de
WWW:	http://www.bmmr.uni-magdeburg.de

EDUCATION:

2007 – <i>now</i>	Ph.D. Student, Otto-von-Guericke University, Magdeburg, Germany.
2000 – 2003	Master in Radiation Protection Physics, Physics Department, Faculty of Science, Zagazig university and Egyptian Atomic Energy Authority (EAEA), Biophysics and Radiation Protection Department. Thesis Title: <i>Thermoluminescence of Semiconducting Materials</i>
1997 – 1999	Nuclear Physics, Dept. of Physics , Zagazig University, Egypt
1992 – 1996	Dept. of Physics, Zagazig University, Egypt
1989 – 1991	Secondary School, Zagazig, Egypt

EMPLOYMENT HISTORY:

2003 – 2007	Assistant Lecturer, Department of Physics, Faculty of Science, Zagazig University, Egypt
1997 – 2003	Demonstrator, Department of Physics, Faculty of Science, Zagazig University, Egypt.

List of Publications

M. Elywa, S. Mulla-Osman, F. Godenschweger and O. Speck. Proton Magnetic Resonance Spectroscopy in Deep Human Brain Structures at 7T. *Journal of Applied Spectroscopy*, 79, 120-125 (January 2012)

M. Elywa, K. Zhong, O. Speck. Localized Adjustment of Radiofrequency Pulses for High Field MR-spectroscopy. *Arab J Nucl Sci Appl*, 42, 131-140 (May 2009).

S. M. Kamal, I. I. Bashter, A. Mamoon, and **M. Elywa**. Thermoluminescent low Curve Analysis and Trap Parameters for Different Doped Semiconductor Materials. *Arab J Nucl Sci Appl*, 36, 239-245 (Sep 2003).

S. M. Kamal, I. I. Bashter, A. Mamoon, and **M. Elywa**. Semiconductor Compounds for Occupational Dosimetry. *Arab J Nucl Sci Appl*, 36, 247-251 (Sep 2003).